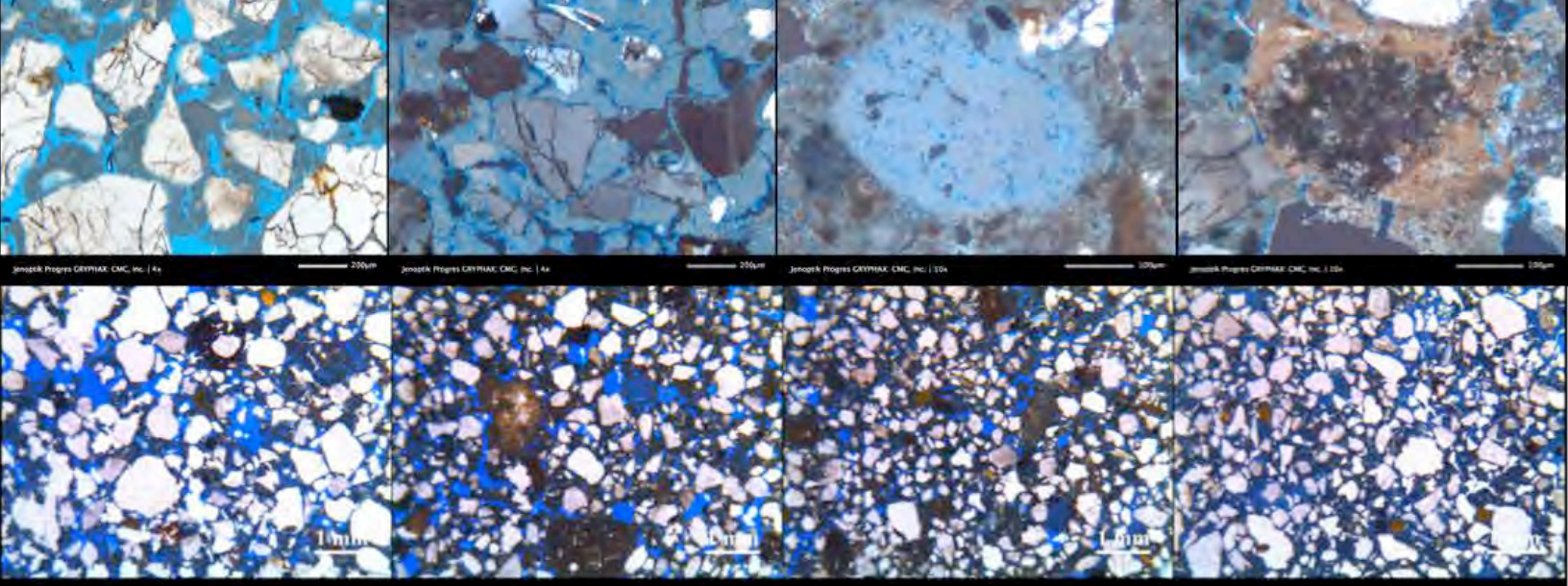

Historic Mortars From A National Historic Landmark In The Nation's Capital

Dipayan Jana

Construction Materials Consultants, Inc. and Applied Petrographic Services, Inc.

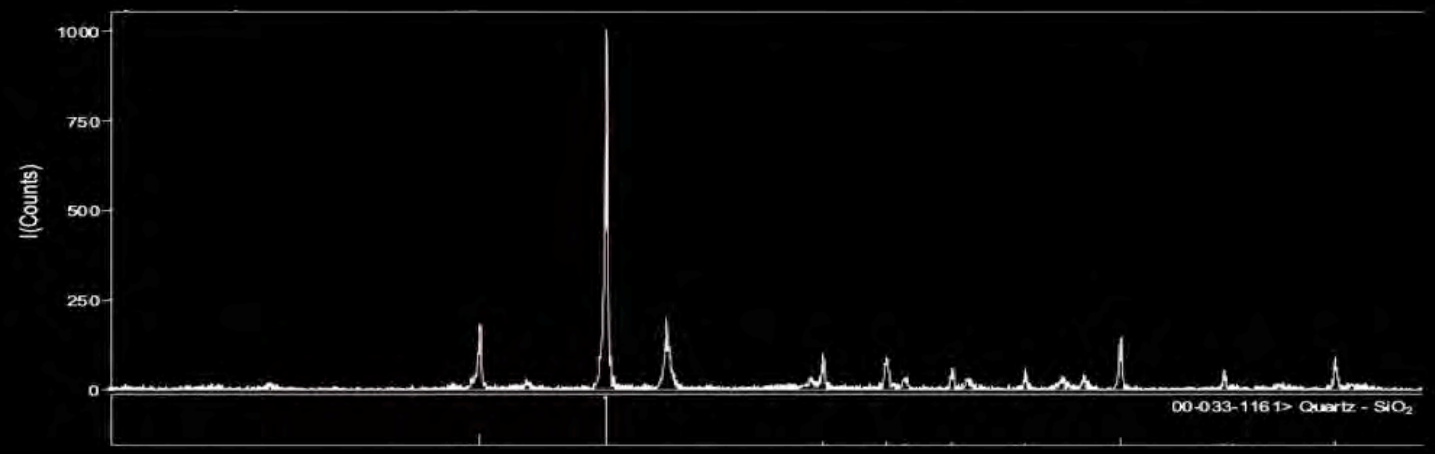

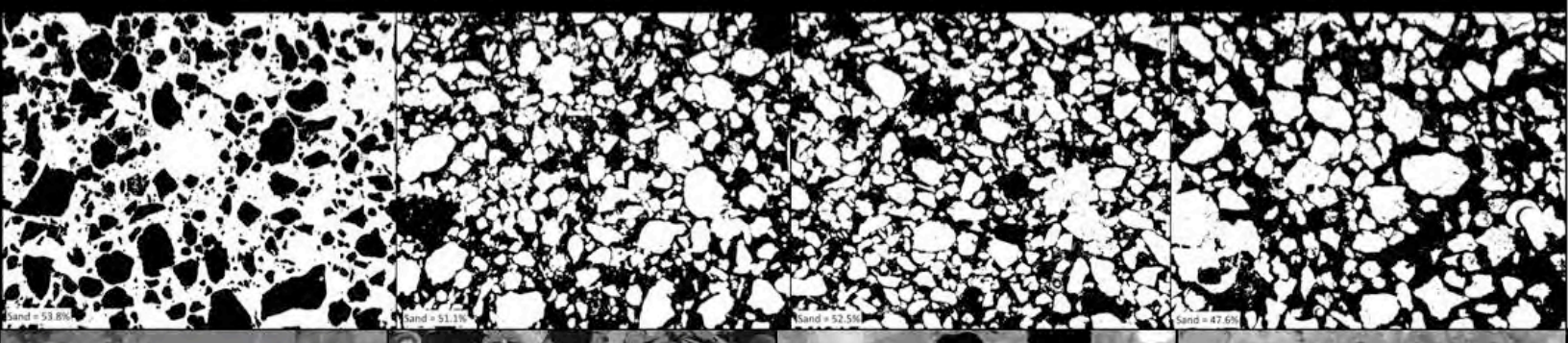

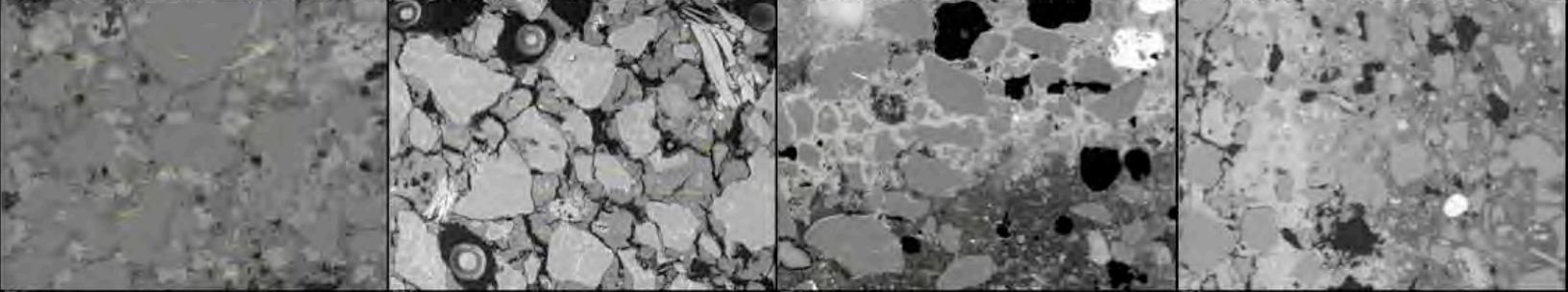

TABLE OF CONTENTS

Abbreviations:
PPL: Observations in plane polarized light mode in a petrographic microscope; XPL: Observations in crossed polarized light mode in a petrographic microscope; FW: Field width of a photomicrograph measured in millimeters
XRD: X-ray diffraction
SEM-EDS: Scanning electron microscopy and Energy-dispersive X-ray fluorescence spectroscopy
BSE: Backscatter electron image; SED: Image from a secondary electron detector
CI: Cementation Index
THIS ARTICLE CAN BE BEST VIEWED IN A PC OR TABLET WITH ZOOMING OPTIONS TO SEE THE PHOTOMICROGRAPHS BETTER.

ABSTRACT

One of the oldest known types of mortars, dating back to the 6th millennium BC and widely used in Ancient Rome and Greece, lime mortars have been used extensively as the material of choice for many masonry constructions. Lime is produced from calcination of high calcium limestone, magnesian limestone, or dolomite (dolostone) having various degrees of silica, alumina, and iron impurities as interstitial clay or silica minerals. Slaking of the calcination product i.e. quicklime with a controlled amount of water, or, with excess water produces a range of binders from dry hydrate powder (hydrated lime), to a liquid, paste, or slurry suspension of lime in water, of high-calcium, magnesian, or dolomitic lime varieties depending on their respective raw feeds. The final slaked lime could either be a high-purity non-hydraulic lime (if their feeds had negligible impurities), or, a hydraulic lime containing 'hydraulic' component(s) i.e. if the feeds contained appreciable silica from interstitial quartz/chert and/or dehydroxylated clay impurities to react with lime and form hydraulic components that set under water. Despite its widespread use in many other countries, in the United States especially during the pre-1950s constructions, use of hydraulic lime was far more limited compared to its non-hydraulic cousins i.e. limes manufactured from high purity forms of high-calcium, magnesian limestones, or dolomitic stones.

Natural cements were used extensively in the US during many 19th century constructions from structural to masonry applications, especially prior to the acceptance of Portland cement from late 19th century. In this regard, the present case study stands as a good example where a range of historic (mid-19th century) mortars of varying compositions and hydraulicity, e.g., from non-hydraulic lime mortars to blended lime-natural cement mortars of varying lime-cement proportions have been used during various phases of constructions of a national historic landmark in the nation's capital.

Brick and stone masonry mortars from eight interconnected buildings at the St. Elizabeths West Campus Center Building, a mid-19th century national historic landmark in Washington D.C. were studied by petrographic and chemical techniques. Twelve brick mortars (MA1 through MA12) contained: (i) non-hydraulic lime mortars (MA11 and MA12), and (ii) blended lime-natural cement mortars having estimated more lime than cement in most (except MA3 and MA7) mortars. The non-hydraulic lime mortars show the hallmark microstructures of many historic lime mortars, e.g., porous, fine-grained, severely carbonated lime matrix having occasional lumps of unmixed lime with sharp boundaries from the rest of the lime matrix, carbonation shrinkage microcracks in lime matrix as well as within the unmixed lumps, etc. The lime-natural cement mortars show (i) remnants of ground, variably calcined raw feed particles of natural cement, and (ii) patchy-textured paste having areas denser and richer in silica along with calcium (representing pastes from hydration and carbonation of the original hydraulic components of natural cement) adjacent to more porous, fine-grained, carbonated paste areas (representing areas contributed from carbonation of the original slaked lime component of binder). All hydraulic brick masonry mortars share both these end member compositions and microstructures at varying degrees, indicating a range of hydraulicity of the original lime-natural cement binders from varying proportions used, all mixed with compositionally similar, well-graded, well-distributed, sound, siliceous (quartz-quartzite) sand aggregates. Mix proportions are calculated to be in the range of 1-part natural cement to slightly less than 1 (in MA3 and MA7) to 5-part lime to 2 to 8-part sand for MA1 through MA10 hydraulic mortars, and 1-part lime to 3-part sand (sand volume is over-estimated for included clay) for non-hydraulic mortars MA11 and MA12. Calculation proportions, however, are dependent on the assumed composition (20% SiO_2, 40% CaO) of natural cement, which, unlike Portland cement, vary considerably. Proportions of sand relative to sums of separate volumes of cement and lime are less than the commonly recommended minimum of 2½ times sand for modern masonry mortars *a la* ASTM C 270.

Stone masonry mortars from the same set of buildings show similar compositional variations of mortars from non-hydraulic lime in one mortar to blended lime-natural cement mortars in the rest, all containing sands of similar types as those found in the brick mortars. Noticeable amongst the stone mortars (especially in the hydraulic types), however, are various degrees of weathering, alterations, and leaching of lime from the carbonated lime matrix of mortars, leaving patches of silica gel-type optically isotropic pastes, often contaminated with coarse secondary calcite crystallization, all indicating extensive moisture percolations, loss of lime from the mortars (probably provided seeds for efflorescence and secondary calcite deposits in voids), microcracking from freezing at moist conditions, or salt crystallization, and overall more altered and distressed conditions of mortars from the service environment than the relatively 'fresher' and better overall conditions of brick masonry mortars.

Suitable tuckpointing mortars for both brick and stone masonries could be similar lime-natural cement-quartz sand mortars having variable proportions of components adjusted within the acceptable limits to generate mortars giving closest match in appearances and properties to the existing mortars, along with the needed breathability of the walls and ability to withstand any wall movements.

INTRODUCTION

Lime, gypsum, and mud were the three most common types of binders used during the construction history of mankind until about two centuries ago, when their widespread use was gradually replaced by various natural cements, and eventually by Portland cements and its varieties, which is the dominant binder of choice in modern construction. The use of lime dates back to the 6th millennium BC, and was widely used in Ancient Rome and Greece, when it largely replaced the clay and gypsum mortars common to Ancient Egyptian construction. Since then, lime has been used in numerous applications, e.g., masonry mortars for brick and stone buildings, wall finishes both internally (plaster) and externally (render), floor foundations, rubble mortars for infilling of walls, casings of water conduits or jointing compounds from terracotta pipes, decoration mortars, etc. (Elsen 2006). Majority of the historic mortars in masonry structures across Europe, America, and many other parts of the world are lime-based. Romans mixed lime with a natural or artificial pozzolan (volcanic ash, or ceramic dust when ash was not available) to improve strength, durability, and to provide the Roman mortars the ability to set under water (hydraulicity).

Traditionally, *lime* is produced from calcination (at 850-1200°C, below sintering) of *high calcium limestone*, *magnesian limestone*, or *dolomite (dolostone*) having various degrees of silica, alumina, and iron impurities as interstitial clay or silica minerals. Slaking of the calcination product i.e. *quicklime* with a controlled amount of water, or, with excess water produces a range of binders from dry hydrate powder (*hydrated lime*), to a liquid, paste, or slurry suspension of lime in water (*lime putty*) of *high-calcium, magnesian, or dolomitic lime* varieties depending on their respective raw feeds. During historic constructions, slaking was done either: (a) with a surplus of water and matured for days, months, or years, or (ii) dry slaked under a layer of sand (fine quicklime was dampened with a little water and kept under sand layer to retain exothermic heat from slaking), or, (iii) burnt lime was crushed and used unslaked with sand and water, or with wet sand at the jobsite as so-called hot mixed mortar.

The final slaked lime can either be a high-purity *non-hydraulic lime* (if the feed has negligible impurity, most common in the lime putty form), or, a *hydraulic lime* (mostly in dry powder form) containing 'hydraulic' component(s) i.e. if the feed contains appreciable silica from interstitial quartz/chert and/or dehydroxylated clay impurities to react with lime and forms a dicalcium silicate hydraulic component (and some minor calcium aluminosilicates from solid-state lime-silica-alumina reactions). Unlike non-hydraulic limes, hydraulic limes can set under water i.e. in addition to the overwhelming non-hydraulic slaked lime component in both varieties that sets slowly by atmospheric carbonation. Depending on the calcination temperature reached and the duration remained at that temperature, some underburned feeds (maintaining original texture, mineralogy, and integrity of limestone), as well as overburned particles (with dead-burned refractory fabrics) can be noticed along with relict calcined products of variable hydraulicity, crystallinity, and grain size - all distributed in a cured (carbonated) matrix of slaked quicklime, which forms the skeleton of the mortar microstructure. Large variations in the resultant microstructures and characteristics of historic mortars are thus the consequences of diverse choices of raw materials used for calcination, additions of natural or artificial pozzolans, as well as such diverse processes of calcination, slaking, and mixing employed. One of the main objectives of laboratory investigations of historic mortars is to unravel the historic materials, provenance, and the construction techniques used in fabrications of these mortars.

Both non-hydraulic and variably hydraulic limes were used extensively in many historic European structures. In the United States especially during the pre-1950s constructions, however, use of hydraulic lime was far more limited (Boynton 1980) compared to its non-hydraulic cousins manufactured from carefully selected high purity forms of high-calcium, magnesian limestones, or dolomitic stones and used mostly as lime putty. During 1980s, there was only one manufacturer of hydraulic lime in the US in the State of Virginia, whereas in Europe (mainly in Italy, Germany, and France), South America (Argentina), and parts of Asia it has been produced extensively for many centuries.

Natural cement, however, was used far more extensively in the eastern US than hydraulic lime even though both required calcination of an impure limestone (having more clay impurities in the feeds for natural cements than that for hydraulic limes). Natural cements in the eastern US were traditionally produced directly from argillaceous dolostones by calcining below the sintering point, where the calcined products were ground and marketed, no slaking was required. Problems encountered with poor performance of traditional (i.e. non-hydraulic) lime mortars during construction of the Erie canal in the early 19th century, first commercial production of natural (hydraulic) cement in Europe in 1796 as Parker's Roman cement, discovery of many argillaceous dolostone formations in New York (Fayetteville) in 1818 by Canvass White, and subsequently in Rosendale, NY in 1825 (which became the hub of American natural cement productions), and discovery of similar natural 'cement rocks' (clayey limestone) in Lehigh Valley, PA, all of which could be directly calcined to a hydraulic cement to set under water with no requirement for slaking just grinding (similar to the marl deposits used in the production of Roman cements) are the series of historic events that set the foundation for large-scale production and widespread use of American natural cements that had persisted for almost 150 years from 1819 through 1970 in numerous construction projects ranging from hundreds of canals to many enduring landmarks, portions of US Capitol, bridges, aqueducts, etc. Despite such widespread use of natural cements, hydraulic lime its closest and older cousin, however, was still in limited use in the US, sometimes used in conjunction with natural cements. A number of masonry constructions during 19th century US have incorporated mixtures of natural cements and lime of variable hydraulicities.

The present case study stands as a good example where historic mortars of various hydraulic natures, from non-hydraulic lime mortars to ones having varying proportions of limes and natural cements were used during various stages of construction of a mid-19th century national historic landmark in the nation's capital where use of natural cements was already at its peak in masonry construction, and, Portland cement was not introduced. The study provides a comprehensive petrographic examination of historic mortars from traditional optical microscopy to X-ray diffraction, chemical analyses, and scanning electron microscopy with X-ray microanalyses.

ST ELIZABETHS WEST CAMPUS CENTER BUILDING: BRIEF HISTORY

A detailed understanding of the history of the building, construction practices followed, its geographic location, weather conditions, sources of raw materials used, etc. are essential for proper assessment of the data collected from laboratory investigation of masonry mortars. St. Elizabeths Hospital was established by Congress in 1855 as the Government Hospital for the Insane but was known as St. Elizabeths after the name of the land on which the hospital

was constructed (www.stelizabethsdevelopment.com, Otto, 2013, Appendix A1). The facility provided mental health facilities for the Army, Navy, and District of Columbia, and served as a hospital for Civil War soldiers. In 1916, Congress officially changed the name to St. Elizabeths Hospital.

St. Elizabeths Campus stands as a prominent example of the mid-19th century reform movement, which believed in moral treatment for the care of the mentally ill through the therapeutic blending of architecture with the natural environment. The St. Elizabeths site is located on a plateau along the Anacostia hills surrounding the core of Washington, D.C. High above the Potomac and Anacostia Rivers, St. Elizabeths offers panoramic views and unique vantage points toward Alexandria, Baileys Crossroads, Ronald Reagan National Airport, Rosslyn, the National Cathedral, the Washington Monument, the U.S. Capitol dome, the Armed Forces Retirement Home, and the Shrine of the Immaculate Conception.

Figure 1: St. Elizabeths West Campus Center Building

St. Elizabeths has two campuses. The West Campus is owned by the federal government and is under the custody and control of the U.S. General Services Administration (GSA). It is located in the Anacostia community in southeast Washington on a hill overlooking the Anacostia River with panoramic views of Washington and Virginia. The East Campus, owned by the District of Columbia, is located across Martin Luther King, Jr. Avenue from the West Campus and is still in use as a mental health facility.

West Campus Facts:

- Located at 2700 Martin Luther King Jr. Avenue, SE, Washington, D.C.
- The project site is bounded by Martin Luther King, Jr. Blvd to the East, Interstate 295 to the West, Barry Farm Dwellings to the North, and Shepherd Park/Congress Heights to the South.
- Constructed between the 1850s and the 1960s.
- Consists of 176 acres and 61 buildings with approximately 1.1 million gross square feet of space.
- National Historic Landmark.

When St. Elizabeths was designated a National Historic Landmark, there were 70 buildings located on the 176-acre West Campus, 62 of which were identified as contributing to the landmark. Of those 62 buildings, 52 will be reused in the development of the site. Eight of those approved for demolition are greenhouses in significant disrepair that cannot be adaptively reused. One of the oldest buildings on campus, the Center Building, was designed by Dr. Nichols and Thomas U. Walter (Architect of the Capitol) in a modified Kirkbride Plan (architectural design specific to mental asylums). The Gothic Revival style structure is truly native to the West Campus. The clay for the bricks was dug from the grounds of St. Elizabeths and fired in ovens on site. Presently, building conditions are being studied to determine their physical condition, evaluate architectural integrity, identify significant spaces, and determine the

potential for reuse. Since approval of the Final Master Plan in January 2009, seven buildings have been demolished in preparation for the construction of a new U.S. Coast Guard headquarters.

MORTAR SAMPLES

A total of twelve (12) mortar samples were collected from the brick masonry walls, and, a second set of five (5) mortar samples were collected from stone masonry walls, all of which are shown in Appendix A2 in as-received conditions.

Brick masonry mortars were identified as: 8-69-MA1, 4-85-MA2, $^{1}/_{2}$-121-MA3, 3-142-MA4, 5-1-MA5, 5-5-MA6, 3-16-MA7, 2-31-MA8, 1-34-MA9, 4-41-MA10, 6-56-MA11, and, 6-64-MA12. Stone masonry mortars are identified as: Building 1 North Stone Joint Mortar 1-94-SMA1, Building 1 North Top of Foundation Brownstone 1-94-SMA2, Building 3 North Stone Joint Mortar 3-138-SMA3, Building 3 Stone Joint Mortar 3-142-SMA4, Building 6 North Brownstone Joint Mortar 6-81-SMA5. Due to the complexity of sample identifications, in some photographs the samples are described following the suffixes, in the same order, e.g., MA1 through MA12 for brick masonry mortars, and SMA1 through SMA5 for stone masonry mortars, respectively. Figure 2 and Appendixes A3 through A10 show individual pieces of all mortar samples, as received, after removing from their respective separate plastic bags, and scanned in a flatbed scanner. All seventeen (17) samples were, reportedly, collected from eight (8) interconnected buildings, reportedly constructed at different time periods from late 19th to early 20th centuries.

Features that are apparent from the conditions and appearances of as-received samples are listed below:

1. Brick masonry mortars are light grey to beige in color, moderately soft to moderately hard; earthy-textured; individual fragments are intact, with some variations in hardness/softness amongst the samples. Samples MA11 and MA12 appear softer (with more dusts on individual fragments) than the rest, samples MA2, MA3, MA7, and MA8 appear firmer and harder, and samples MA1 and MA4 appear somewhat intermediate in softness.
2. A number of fragments in various samples contain lumps of white unmixed lime, many are marked. These white lime lumps are characteristic of many historic lime mortars that are indicative of unmixed lime in the lime binder or use of lime putty left over as clumps after mixing of lime and sand. Samples MA7 and MA8 show somewhat lesser abundance of such lumps (none are boxed in the figure) than the rest.
3. Stone masonry mortar fragments are more weathered, darker in color for SMA1, SMA2, and SMA4 than all other mortars, having green algal deposits in SMA1 and SMA4, compared to the overall 'fresher' appearance of brick masonry mortars. Such visual observation of weathering and algal deposits on stone fragments are indicative of the presence of moisture for prolonged periods and hence possible moisture activities and migration through these mortars, which became evident in subsequent microscopical examinations, showing leaching of lime from many areas of pastes in many stone mortars.

The purposes of the present examination are to determine: (a) the types of aggregates and binders present in the brick and stone masonry mortars; (b) compositions, qualities, and conditions of mortars from the chemistry, mineralogy, and microstructure of aggregates and binders; (c) estimations of mix proportions, and types of mortars used (from the contents of aggregate, and components of binder added, pozzolans, additives, pigments, and polymers, if any, etc.); and, (d) based on determined compositions of the mortars, suggestions for suitable tuckpointing mortars that can be compatible with the existing mortars.

From each sample, representative fragments were selected for: (a) optical microscopy, (b) scanning electron microscopy and x-ray microanalyses, (c) x-ray diffraction, and (d) chemical analysis.

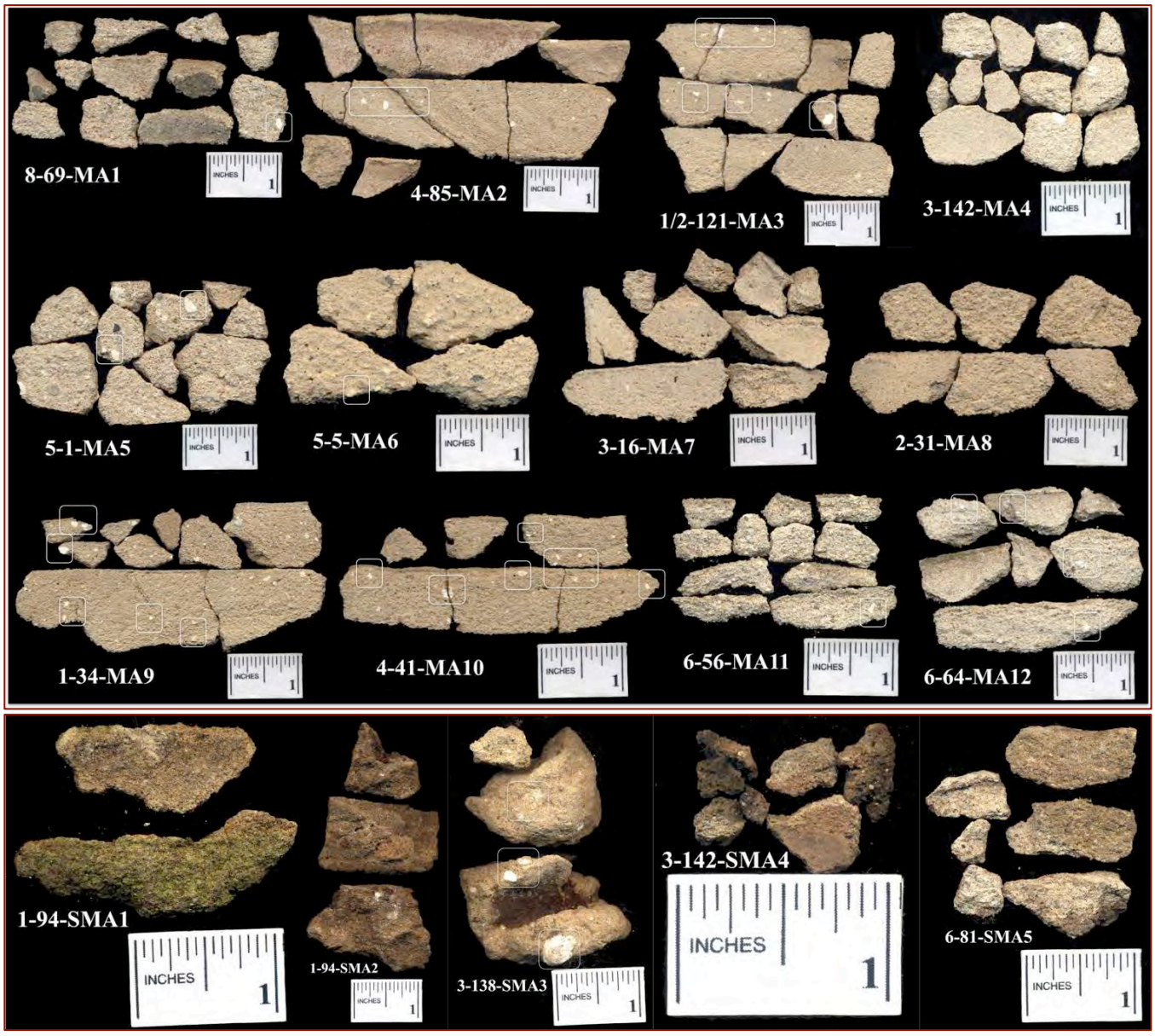

Figure 2: Intact fragments of twelve (12) brick masonry mortar samples (top), and, five (5) stone masonry mortar samples (bottom), as received. Individual pieces of each sample are scanned in a flatbed scanner. Boxes in many of these pieces enclose white unmixed lime lumps. These fragments were removed from bags that also contained an appreciable amount of powdery, disintegrated mortars that may have lost the integrity during collection and/or

subsequent transportation to our laboratory. Enlarged views of each sample are shown in the Appendix A2 through A10.

METHODOLOGIES

The mortar samples were tested by following the methods of ASTM C 1324 "Standard Test Method for Examination and Analysis of Hardened Masonry Mortar," along with various analytical methods to test historic mortars as described in various literatures, e.g., Erlin and Hime 1987, Doebley and Spitzer 1996, Chiari et al. 1996, Middendorf et al. 2005 a and b, Elsen 2006, Bartos et al. 2000, Valek et al. 2012, and Goins 2001 and 2004.

SAMPLE SELECTION & SAMPLE PREPARATION

From all fragments of each mortar, 'representative' subset fragment(s) were selected for optical and electron microscopy, X-ray diffraction, and chemical analyses. Any piece that appeared 'unusual' in visual examinations from the rest is not included, since the piece may represent a tuckpointing mortar. Figures 5 and 6 show the typical flow charts for laboratory investigation of masonry mortars that are followed in the author's laboratories.

OPTICAL MICROSCOPY

Fragments selected for microscopical examinations were photographed with a digital camera, a flatbed scanner, and, a low-power stereomicroscope. A fragment was placed in a flexible (molded silicone) sample holder, and encapsulated with a blue dye-mixed low-viscosity epoxy under vacuum to impregnate the pore spaces by epoxy. The epoxy-encapsulated cured solid block of sample is then de-molded and processed through fine grinding, lapping, attachment of the lapped surface to a frosted large-area (50 × 75 mm) glass slide, precision sectioning, precision grinding, and final polishing steps to prepare a polished thin section. Sample preparation steps are described in detail in Jana 2006.

Steps followed during light optical microscopical examinations of mortar samples include:

- Visual examinations of mortar fragments, as received, to select fragments for optical microscopy;
- Low-power stereomicroscopic examinations of saw-cut and freshly fractured sections of the samples for evaluation of textures, compositions, and appearances;
- Examinations of oil immersion mounts for special features and materials from the mortars in a petrographic microscope (Jana 2005);
- Image analyses of photomicrographs of blue dye-mixed epoxy-impregnated thin sections of mortar fragments for estimations of pores, voids, intergranular open spaces, and shrinkage microcracks (i.e. areas that were impregnated by blue dye-mixed epoxy and highlighted in image analysis) by using Image J, a Java-based image processing program developed by National Institute of Health;

- Examinations of blue dye-mixed epoxy-impregnated polished thin sections of mortar fragments in a petrographic microscope for detailed compositional and microstructural analyses of aggregates and binders in mortars, along with diagnoses of evidences of any deleterious processes.

SCANNING ELECTRON MICROSCOPY AND ENERGY-DISPERSIVE X-RAY SPECTROSCOPY (SEM-EDS)

Portions of thin sections used for optical microscopy were coated with conductive gold film for SEM-EDS studies. Polished and coated thin sections (or solid encapsulated blocks) of mortar fragments were examined in SEM to determine the chemical compositions of binder and to determine if a calcitic or a dolomitic lime was used in the binder, possible hydraulic phases present and compositions, and spatial variations in compositions of binders across the section. Usually, the same thin sections used for optical microscopy were polished and partially coated with a conductive gold film for SEM (Figure 12) so that both optical and electron microscopy could be done interchangeably. Procedures for SEM examinations are described in ASTM C 1723.

X-RAY DIFFRACTION

In order to determine mineralogical compositions of bulk mortars, including dominant mineralogies of aggregates, mineralogies of binder phases, and the presence of any potentially deleterious constituents, X-ray diffraction of: (i) pulverized portions of bulk mortars as well as (ii) sands extracted from mortars were done.

X-ray diffraction was carried out in a Siemens D5000 Powder diffractometer employing a long line focus Cu X-ray tube, divergent and anti-scatter slits fixed at 1 mm, a receiving slit (0.6 mm), diffracted and incident beam Soller slits (0.04 rad), a curved graphite diffracted beam monochromator, and a sealed proportional counter. Generator settings used were 45 kV and 30mA. A dry, finely ground sample pulverized to pass US 325 sieve (44-μm) was placed in a 1-in. diameter circular sample holder and excited with the copper radiation of 1.54 angstroms. Tests were performed at a 2-theta range from 4° to 64° with a step of 0.02° and a dwell time of one second.

The resulting diffraction patterns were collected by using DataScan 4 software of Materials Data, Inc. (MDI), analyzed by using Jade 9.0 software of MDI with ICDD PDF-4 (Minerals 2014) diffraction data, and, phase identification plus quantitative analyses were carried out with MDI's Search/Match and Easy Quant modules, respectively. Steps followed during sample preparation for XRD are provided in Figure 3. For the present sets of brick and stone masonry mortars, pulverized (to minus US 325 sieve) portions of representative fragments of bulk mortar samples (Step 2 in Figure 3) were analyzed.

CHEMICAL ANALYSES

Chemical analyses of the mortars were done to determine the: (a) hydrochloride acid-insoluble residue contents, (b) loss on ignition, (c) soluble silica contents, (d) calcium and magnesium oxide contents, and (e) the presence of magnesium hydroxide, if any (i.e. if dolomitic lime was used) by using various chemical methods outlined in ASTM C 1324 and Middendorf et al. 2005a, e.g., by wet chemistry, atomic absorption spectroscopy, energy-dispersive x-

ray spectroscopy, thermal analysis, and x-ray diffraction. Steps followed during chemical analyses of mortars are described in ASTM C 1324, which are summarized in Figure 4.

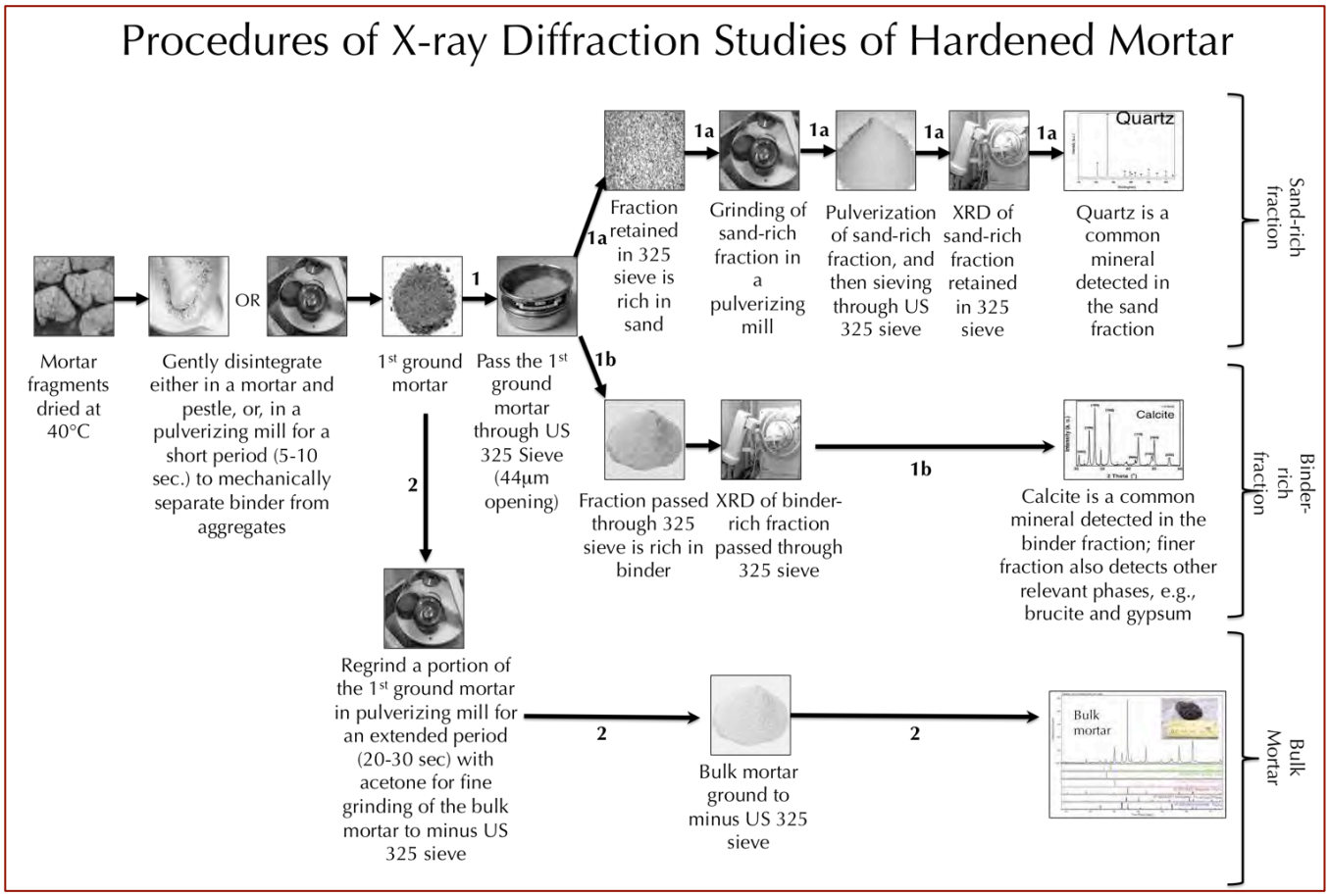

Figure 3: Steps followed during sample preparation for X-ray diffraction studies.

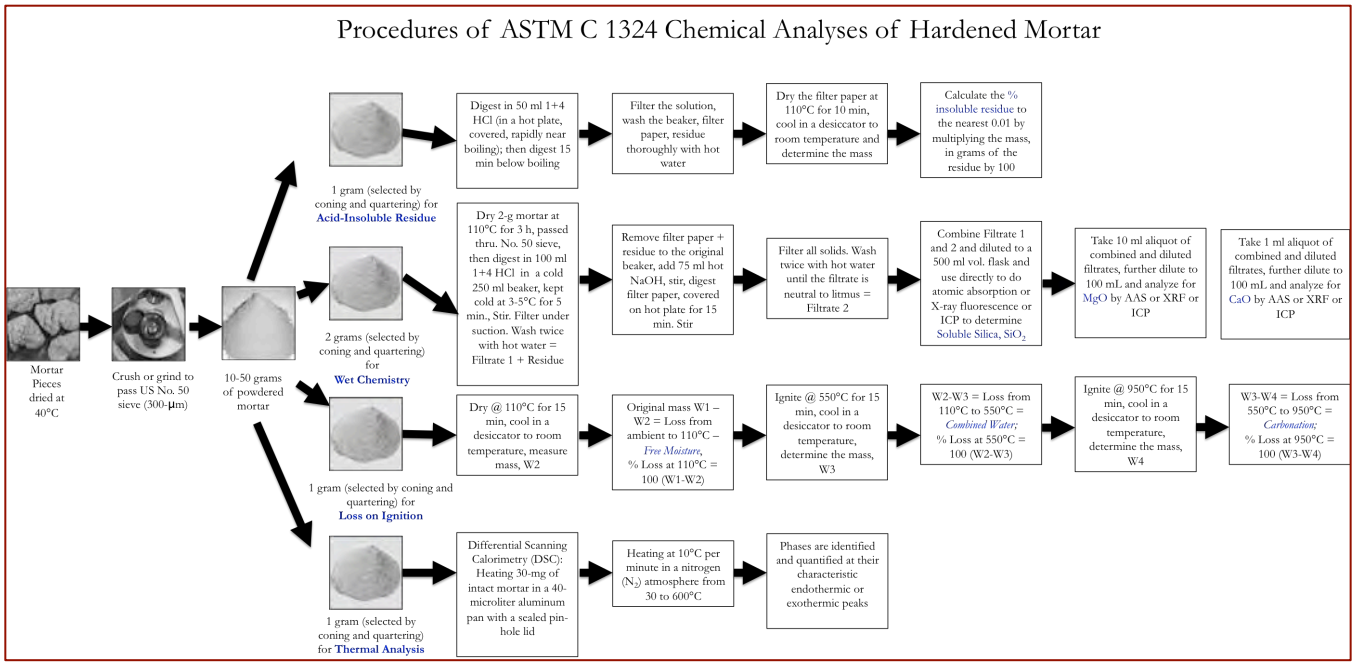

Figure 4: Steps followed during various chemical analyses of mortars.

The hydrochloride acid-insoluble residue content provides the siliceous (non-soluble) content of mortar, which corresponds to the siliceous components of sand. The soluble silica content corresponds to the silica mostly contributed from the binder components (and a minor amount from any soluble silica component in the aggregates). The loss in weight by ignition of a pulverized portion of bulk mortar in a muffle furnace from ambient to 110°C corresponds to the free water content of mortar, whereas, further weight loss from 110°C to 550°C corresponds to the structurally bound hydrate water content, which is proportionate to the amount of hydrated component in the mortar. Finally, the loss of weight by calcination to 950°C corresponds to the degree of carbonation of lime binder of mortar. Oxide compositions determined from wet chemistry or other instrumental techniques provide compositions of binder and mortar. Thermal analyses (DTA, TGA, and DSC) of mortar were done to determine the amounts of hydrates (mainly brucite to check the presence of dolomitic lime), sulfate (gypsum), hydrate water, as well as high-temperature transformations of silica polymorphs.

Figure 5 shows the four main steps followed during laboratory investigation of masonry mortars: (i) from preliminary visual examinations to petrographic examinations of mortars to determine the types of aggregates used and the binders present, based on which (ii) subsequent chemical analyses were done to determine the chemical compositions of binders and proportions of sand, water, and degree of carbonation. Information obtained from petrographic examinations is useful and form the very guidelines to devise the appropriate chemical methods to follow, and to properly interpret the results of chemical analyses. For example, detection of siliceous versus calcareous versus argillaceous natures of aggregates in mortar, or the presence of any pozzolan in the binder (slag, fly ash, ceramic dusts, etc.) from petrography restricts which chemical method to follow, and how to interpret the results of such analyses, e.g., acid-insoluble residue contents. Therefore, a direct chemical analysis e.g., acid digestion of a mortar without doing a prior petrographic examination to determine the types of aggregates and binder used could lead to highly erroneous results and interpretation. Armed with petrographic and chemical data, and (iii) based on assumed compositions and bulk densities of the sand and the binder(s) similar to the ones detected from petrographic examinations (iv) volumetric proportions of sand and various binders present in the examined mortar can be calculated. The estimated mix proportions from such calculations can provide at least a rough guideline to use as a starting mix during formulation of a tuckpointing mortar to match with the existing (examined) mortar.

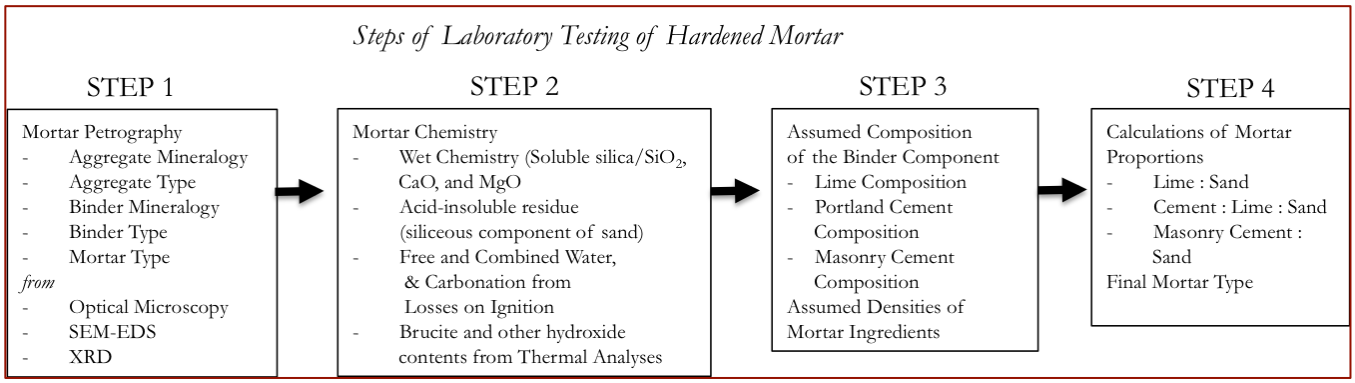

Figure 5: Steps followed during laboratory investigation of mortars.

Figure 6 shows a flow chart for various steps followed during ASTM C 1324.

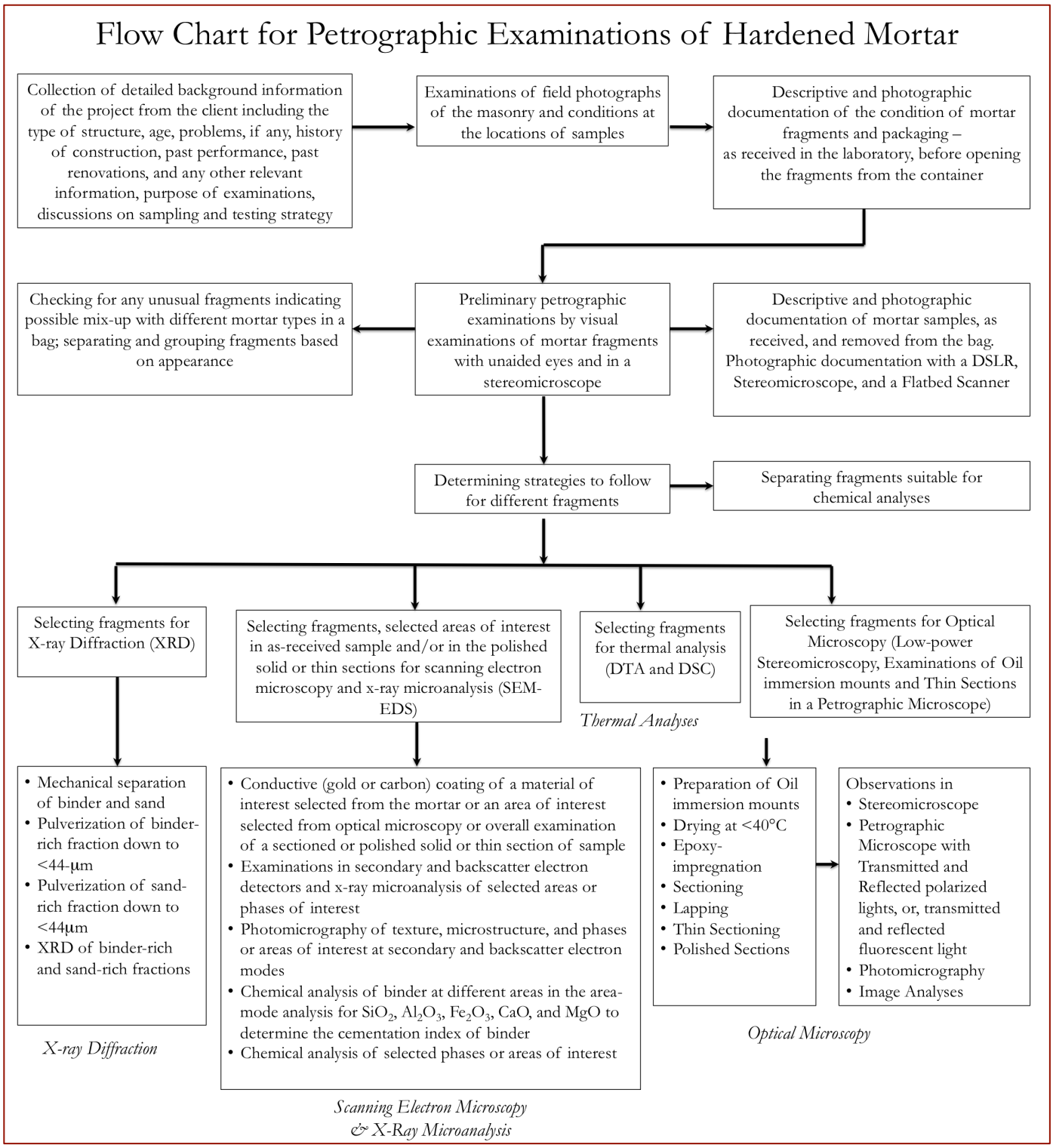

Figure 6: Flow Chart for Various steps followed during ASTM C 1324.

PETROGRAPHIC EXAMINATIONS

VISUAL EXAMINATIONS

Figure 2 and Appendix A2 through A10 show conditions and appearances of brick and stone masonry mortar samples, as received, in a great detail, prior to any sample preparation steps. The following Table summarizes overall weights in grams, dimensions (in inches) of largest fragments, appearance, and integrity of each sample:

Sample ID	Weight (grams)	Largest Piece (in.)	Appearance	Integrity
Brick Masonry Mortars				
8-69-MA1	30.6	$^{7}/_{8} \times {}^{3}/4 \times {}^{1}/4$	Beige, Moderately Hard	Intact
4-85-MA2	44.3	$1{}^{1}/2 \times 1{}^{1}/_{8} \times {}^{3}/_{16}$	Beige, Moderately Hard	Intact
$^{1}/_{2}$-121-MA3	33.5	$1{}^{3}/4 \times {}^{13}/_{16} \times {}^{1}/_{8}$	Beige, Moderately Hard	Intact
3-142-MA4	28.7	$1{}^{1}/4 \times {}^{3}/4 \times {}^{1}/_{8}$	Light Grey, Mod. Soft	Intact
5-1-MA5	50.7	$1{}^{1}/_{8} \times 1 \times {}^{1}/4$	Med. Grey, Mod. Hard	Intact
5-5-MA6	50.5	$1{}^{1}/2 \times 1 \times {}^{1}/4$	Beige, Moderately Hard	Intact
3-16-MA7	39.9	$2 \times {}^{3}/4 \times {}^{5}/_{16}$	Beige, Moderately Hard	Intact
2-31-MA8	34.2	$1{}^{1}/4 \times 1 \times {}^{3}/_{16}$	Beige, Moderately Hard	Intact
1-34-MA9	52.2	$3 \times 1{}^{1}/4 \times {}^{3}/_{8}$	Beige, Moderately Hard	Intact
4-41-MA10	29.7	$1{}^{3}/_{8} \times {}^{7}/_{8} \times {}^{1}/4$	Beige, Moderately Hard	Intact
6-56-MA11	37.1	$1½ \times {}^{1}/_{2} \times {}^{3}/_{16}$	Light Grey, Mod. Soft	Intact
6-64-MA12	36.7	$2{}^{7}/_{8} \times {}^{3}/4 \times {}^{5}/_{16}$	Light Grey, Mod. Soft	Intact
Stone Masonry Mortars				
1-94-SMA1	10.3	$2 \times {}^{1}/_{2} \times {}^{1}/4$	Beige, Moderately Hard	Weathered, Intact
1-94-SMA2	49.4	$2 \times 1 \times {}^{1}/_{2}$	Beige, Moderately Hard	Weathered, Intact
3-138-SMA3	68.3	$1{}^{3}/4 \times 1 \times 1$	Beige, Moderately Hard	Intact
3-142-SMA4	2.1	$^{1}/4 \times {}^{1}/4 \times {}^{1}/_{8}$	Light Grey, Mod. Soft	Weathered, Intact
6-81-SMA5	15.5	$1{}^{1}/_{8} \times {}^{1}/_{2} \times {}^{3}/_{8}$	Med. Grey, Mod. Hard	Micro-cracked

Table 1: Weight, dimensions of largest fragment, color, hardness/softness, and integrity of mortar samples. Despite intact fragments of all samples, plastic bags of samples contain powders indicating some disintegration during collection and transport. Notice SMA1, SMA4, and SMA5 were received in insufficient amounts to do all necessary tests.

Brick masonry mortars appeared fresh and more intact in visual examinations and received in larger quantities than the stone masonry mortars. Mortars from stone masonry are more weathered and altered.

POROSITY, SAND SIZE, & GRADING FROM IMAGE ANALYSES

Figures 7 through 10 and Appendix A11 through A16 show:

(i) Photomicrographs of blue dye-mixed epoxy-impregnated thin sections of representative fragments of brick and stone masonry mortars,

(ii) Estimated volumetric proportions of open spaces (voids, pores, microcracks) that are filled with and hence highlighted by the blue dye-mixed epoxy, along with

(iii) Variations in size, shape, angularity, and sphericity of sand aggregates in the mortars.

(iv) The black and white binary images highlighting pore spaces (corresponding to the blue areas in the thin section photomicrographs) are derived from Adobe Photoshop, and, proportions of pore spaces are

calculated from Image J, an open-source image analysis software developed by the National Institute of Health (www.imagej.nih.gov).

Results of pore spaces (and sand volumes in Figure 11) obtained from such practices are only considered as rough estimates of porosity (and sand volumes), since adequate numbers of such photomicrographs across the entire examined surface area of a mortar sample are needed for better accuracy of these parameters. Care is needed to select pore spaces and void areas that are inadequately filled with blue dyed epoxy, or of aggregate-paste gaps during the process of highlighting not only just the easily detectable pore spaces and voids but also any not so distinct voids. Selection of all voids, open spaces, microcracks, etc. are done in Adobe Photoshop in the final processed blue-dyed photomicrographs, which are then transferred to Image J to calculate the volumes of pore spaces not only from entrained and entrapped air voids but also from cracks, microcracks, and aggregate-paste separations. Shrinkage microcracks are carefully identified and separated from any sand-paste separations since they both may appear similar in the black and white binary images.

With some practice, such approach of processing a photomicrograph in Photoshop and analysis of its binary image in Image J become quick and important for rough estimation of porosities and sand volumes in the mortars, as well as size, shape, grading, and distribution of sand, a quick detection of if a mortar is over-sanded or under-sanded, and if a mortar is porous, excessively air-entrained, or dense. Stitching multiple photomicrographs (captured at an overlapping pattern) over an entire thin section of a mortar can provide meaningful information on all these aspects from such approach on image analysis.

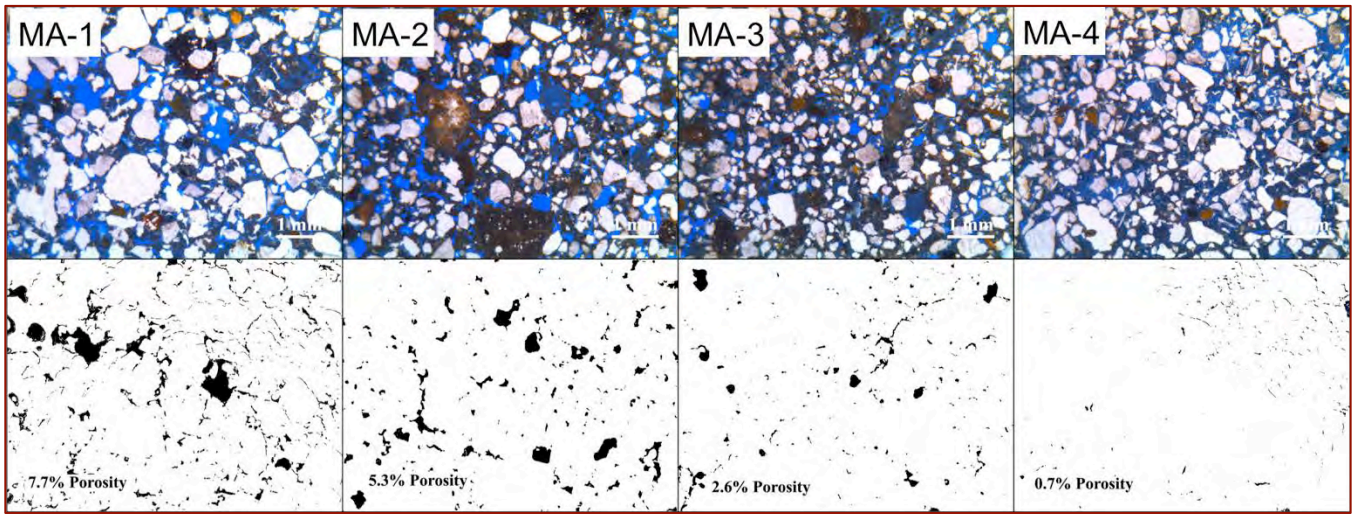

Figure 7: Photomicrographs of blue dye-mixed epoxy-impregnated thin sections of brick masonry mortars MA1 through MA4 and corresponding black and white binary images that highlight the open spaces in black and calculated percent volumes of such open areas from Image J. Short, thin, discontinuous, irregular, elongated black linear features in bottom row are shrinkage microcracks (along with some separations along sand-paste interfaces) in paste that are highlighted by dyed epoxy (appear in black). Also notice the variations in size, shape, angularity, and sphericity of sand particles in aggregates. See Appendix A11 through A14 for enlarged views.

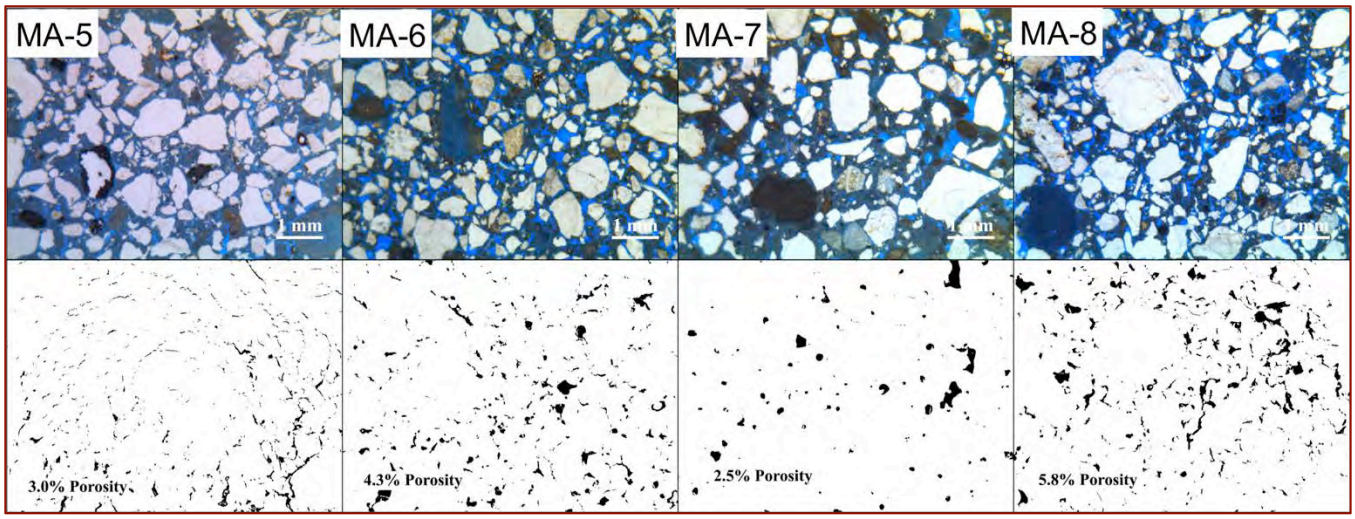

Figure 8: Photomicrographs of blue dye-mixed epoxy-impregnated thin sections of brick masonry mortars MA5 through MA8 and corresponding black and white binary images that highlight the open spaces in black and calculated percent volumes of such open areas from Image J. Short, thin, discontinuous, irregular, elongated black linear features in bottom row are shrinkage microcracks (along with some separations along sand-paste interfaces) in paste that are highlighted by dyed epoxy (appear in black). Also notice the variations in size, shape, angularity, and sphericity of sand particles in aggregates. See Appendix A11 through A14 for enlarged views.

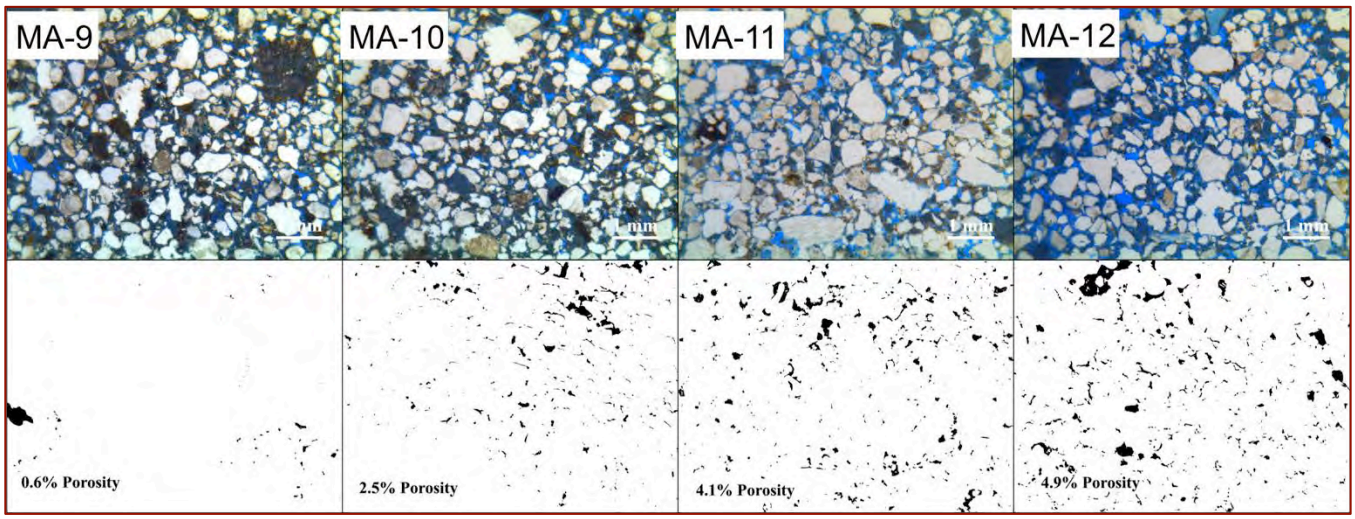

Figure 9: Photomicrographs of blue dye-mixed epoxy-impregnated thin sections of brick masonry mortars MA9 through MA12 and corresponding black and white binary images that highlight the open spaces in black and calculated percent volumes of such open areas from Image J. Short, thin, discontinuous, irregular, elongated black linear features in bottom row are shrinkage microcracks (along with some separations along sand-paste interfaces) in paste that are highlighted by dyed epoxy (appear in black). Also notice the variations in size, shape, angularity, and sphericity of sand particles in aggregates. See Appendix A11 through A14 for enlarged views.

All brick masonry mortars show similar size, shape, angularity, and size distribution of sand indicating use of sand from similar source. Shrinkage microcracks are effectively demarked by discontinuous elongated, irregular-shaped lines in binary images. Entrapped, intergranular voids are also easily highlighted by coarse black areas.

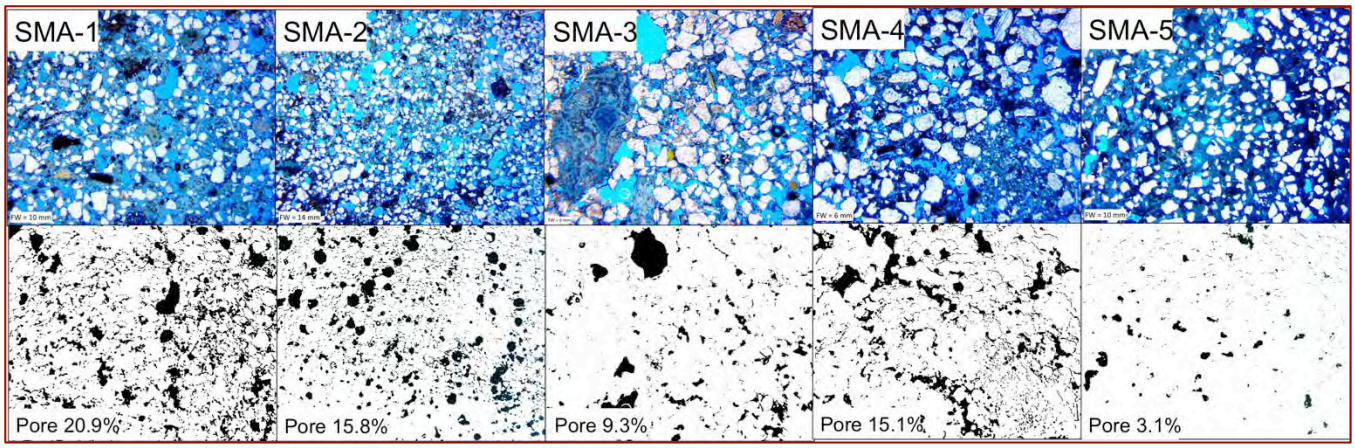

Figure 10: Photomicrographs of blue dye-mixed epoxy-impregnated thin sections of stone masonry mortars MA9 through MA12 and corresponding black and white binary images that highlight the open spaces in black and calculated percent volumes of such open areas from Image J. Short, thin, discontinuous, irregular, elongated black linear features in bottom row are shrinkage microcracks (along with some separations along sand-paste interfaces) in paste that are highlighted by dyed epoxy (appear in black). Also notice the variations in size, shape, angularity, and sphericity of sand particles in aggregates. See Appendix A15 and A16 for enlarged views. Compared to brick mortars, estimated pore volumes in most of these images (e.g., in SMA-1, 2, and 4) are very high, which is determined to be due to extensive lime leaching that these mortars have experienced.

Figure 11 shows size, shape, angularity, grading, and distribution of sand particles, by highlighting all sand particles as white or black against the rest in opposite background in these black-and-white binary images (developed from the original optical photomicrographs by Adobe Photoshop) and calculating volumetric proportions of sand thus isolated from the rest by particle analysis in Image J. Appendixes A11 through A16 provide larger images of Figures 7 through 11.

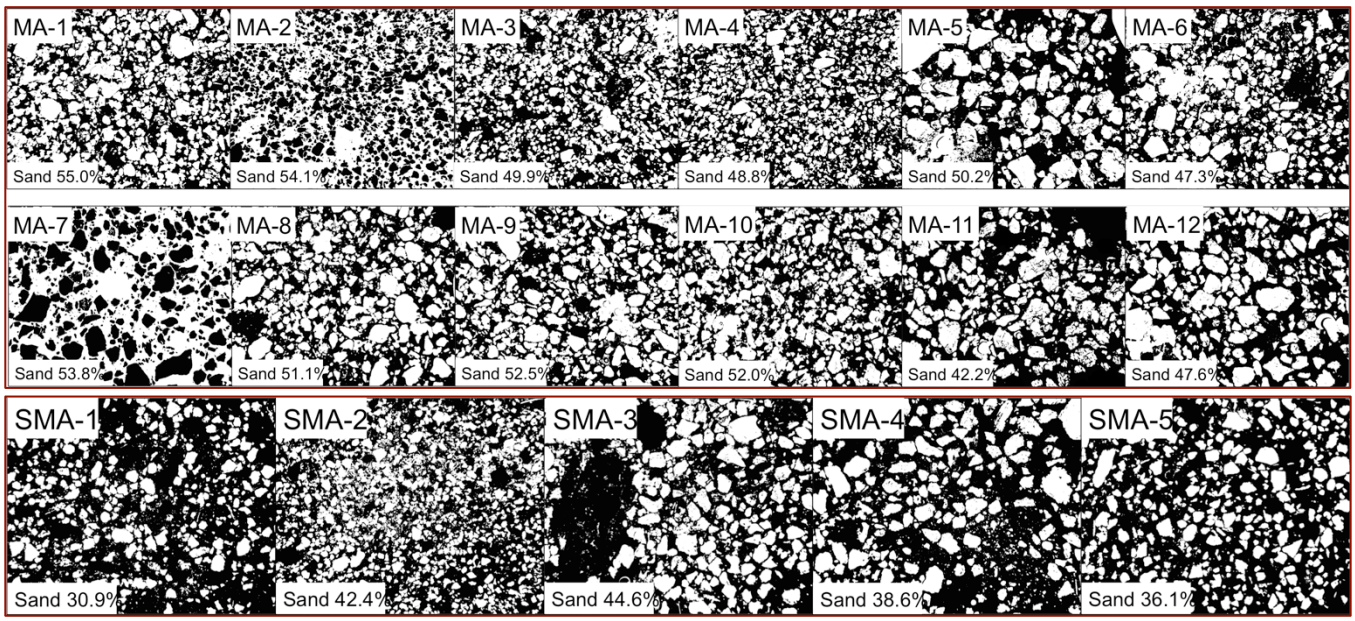

Figure 11: Size, shape, angularity, grading, and distribution of sand particles by highlighting sand as white or black against the rest in opposite background in these black-and-white binary images (volumetric proportions of sand in these images are calculated from Image J). See Appendix for enlarged views.

Table 2 summarizes the results from Figures 7 through 11, and, shows overall lower sand volumes and higher porosities in many stone masonry mortars than most of the brick masonry mortars.

Sample ID	Estimated (%) Volumes of Voids and Microcracks	Proportion of Irregular Voids	Proportion of Shrinkage Microcracks	Total Volume is Contributed From:	Sand Nominal Maximum Size (mm)	Sand Angularity, Grading	Estimate Sand Volumes in Images (%)
Brick Masonry Mortars							
8-69-MA1	7.7	Many	Numerous	Both	2.0	Subangular, Well-graded	55.0
4-85-MA2	5.3	Many	Few	Irregular Voids	0.5	Subangular, Well-graded	54.1
1/2-121-MA3	2.6	Moderate	Few	Irregular Voids	0.5	Subangular, Well-graded	49.9
3-142-MA4	0.7	Very Few	Few	Shrinkage Microcracks	1.0	Angular, Well-graded	48.8
5-1-MA5	3.0	Very Few	Numerous	Shrinkage Microcracks	2.0	Angular, Well-graded	50.2
5-5-MA6	4.3	Few	Many	Both	1.0	Angular, Well-graded	47.3
3-16-MA7	2.5	Many	Very Few	Irregular Voids	2.0	Angular, Well-graded	53.8
2-31-MA8	5.8	Many	Numerous	Shrinkage Microcracks	2.0	Angular, Well-graded	51.1
1-34-MA9	0.6	Very Few	Very Few	Irregular Voids	0.5	Angular, Well-graded	52.5
4-41-MA10	2.5	Moderate	Many	Both	0.5	Angular, Well-graded	52.0
6-56-MA11	4.1	Many	Moderate	Both	1.0	Angular, Well-graded	42.2
6-64-MA12	4.9	Many	Many	Both	1.0	Angular, Well-graded	47.6
Stone Masonry Mortars							
1-94-SMA1	20.9	Many	Numerous	Both	1.0	Subangular, Well-graded	30.9
1-94-SMA2	15.8	Many	Numerous	Both	0.5	Angular, Well-graded	42.4
3-138-SMA3	9.3	Moderate	Few	Irregular Voids	1.0	Angular, Well-graded	44.6
3-142-SMA4	15.1	Many	Numerous	Both	1.0	Angular, Well-graded	38.6
6-81-SMA5	3.1	Few	Few	Both	1.0	Angular, Well-graded	36.1

Table 2: Estimated porosity, types of pore spaces, nominal maximum size (determined from photomicrographs) of sand aggregates and angularity and grading of sand in brick and stone masonry mortars.

APPEARANCE FROM THIN SECTIONS OF MORTARS

Figure 12 shows blue dye-mixed epoxy-impregnated thin sections of representative pieces of mortars that were used for optical microscopy and scanning electron microscopy.

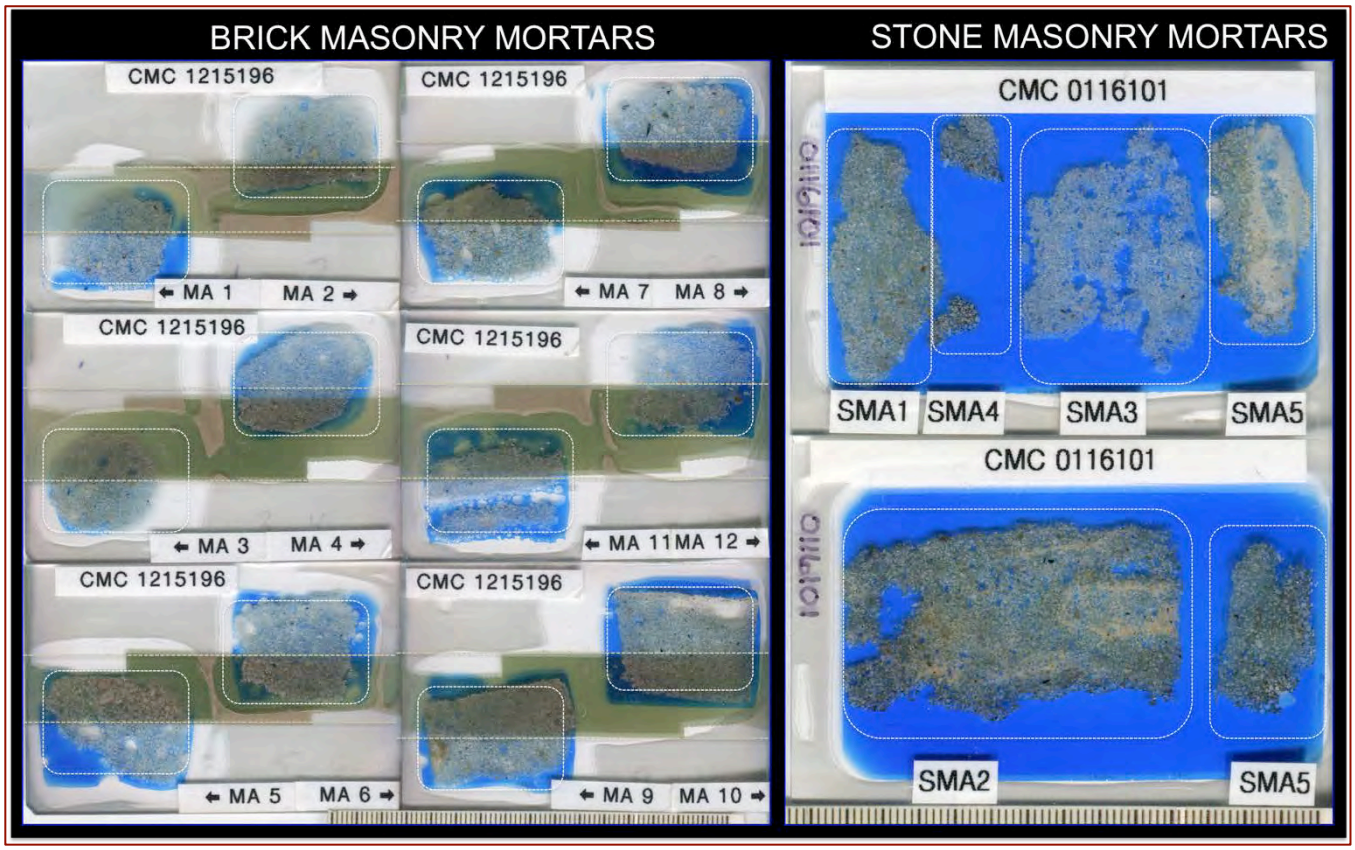

Figure 12[1]: Blue dye-mixed epoxy-impregnated polished thin sections of mortars used for optical and scanning electron microscopy. The band in the middle of each section in brick masonry mortars is conductive gold coating for electron microscopy. Stone masonry mortars also received such gold coating, but after these scans. Vertical lines in the rulers at the bottom are millimeters apart.

MINERGALOGIES, TEXTURES, AND MICROSTRUCTURES OF AGGREGATES AND BINDERS FROM OPTICAL MICROSCOPY

Appendixes A17 through A25, and, A26 through A74 provide comprehensive examinations of detailed mineralogy and microstructures of aggregates and binder phases in mortars as revealed from light-optical microscopy. Relevant features from those figures are summarized in the following sections.

AGGREGATE TYPES FROM OPTICAL MICROSCOPY

Figure 11 shows angular to subangular (crushed) sand aggregates in all mortar samples that are well-graded, and well-distributed siliceous sands having nominal maximum sizes of <1 to 2 mm containing major amounts of quartz and quartzite, subordinate to minor amounts of feldspar, mica, clay, and ferruginous constituents.

[1] Large-area photomicrographs of thin section of each mortar taken through a low-power transmitted-light stereomicroscope are shown in Appendix A17 through A25.

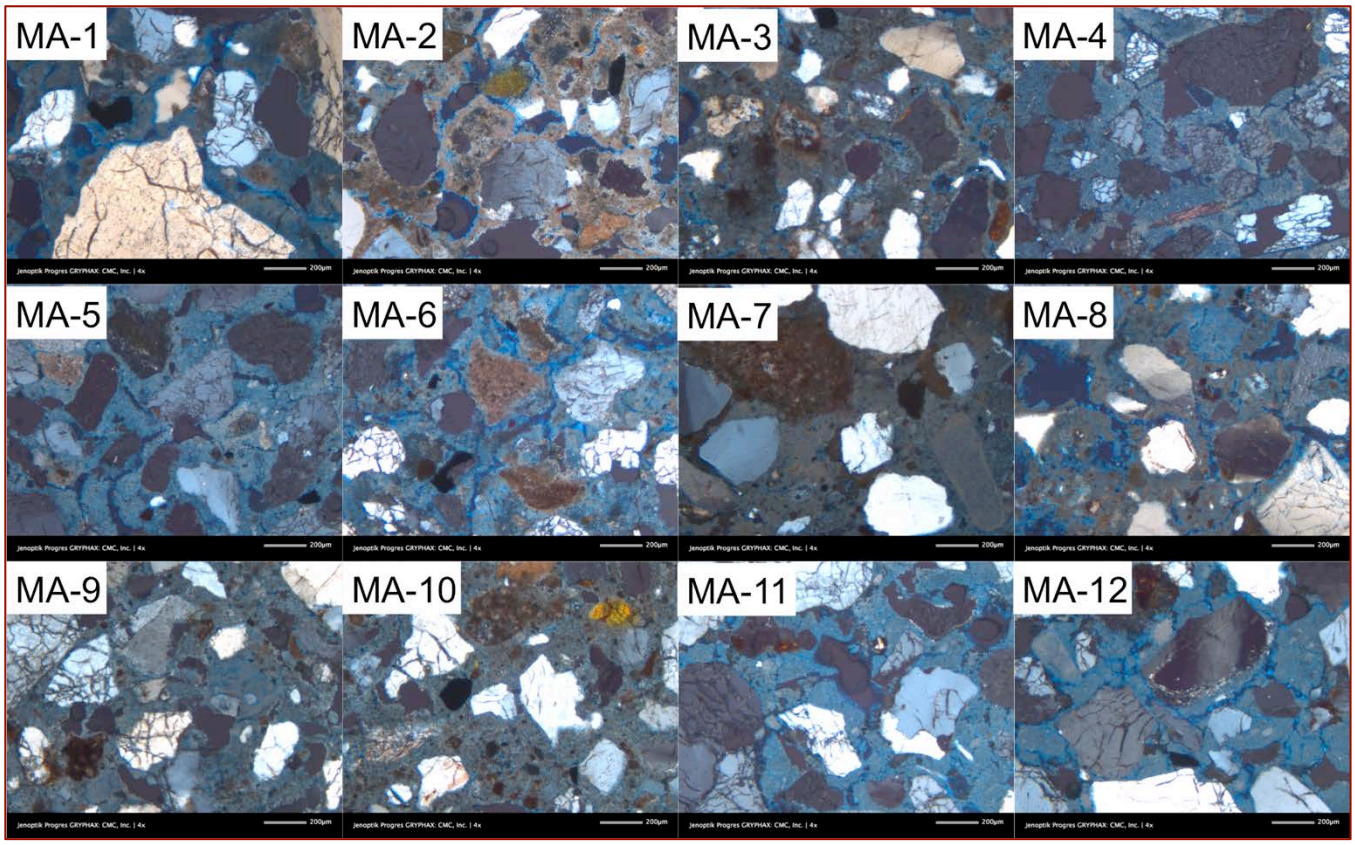

Figure 13: Photomicrographs of thin sections of brick masonry mortars viewed in XPL mode in a petrographic microscope showing angular (crushed), well-graded, well-distributed, siliceous (quartz-quartzite) sand aggregates having similar compositions and mineralogies across all samples.

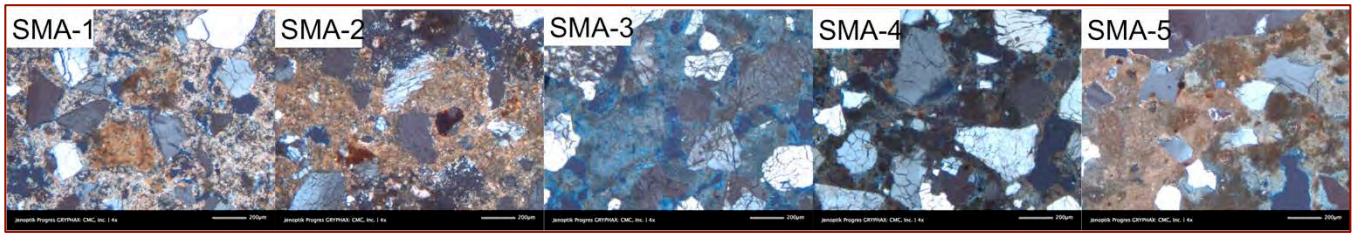

Figure 14: Photomicrographs of thin sections of stone masonry mortars viewed in XPL mode in a petrographic microscope showing angular (crushed), well-graded, well-distributed, siliceous (quartz-quartzite) sand aggregates having similar compositions and mineralogies across all samples.

Appendixes A25 through A53 for brick masonry mortars and A54 through A74 for stone masonry mortars provide more detailed photomicrographs of variations in size, shape, gradation, and angularities of quartz sand aggregates, which are all similar siliceous (quartz-quartzite) sand having some mica and clay in some extracted mortar sands, as revealed from X-ray diffraction studies (Table 6). In all samples, sand aggregates are reasonably well-graded, well-distributed, and have been sound during their services in the mortars. There is no evidence of alkali-aggregate or any other potentially deleterious reactions of sand in any mortar.

AGGREGATE GRADATION AND MINERALOGY AFTER EXTRACTION FROM MORTAR

A representative portion from each mortar sample was selected for digestion in (1+3) dilute hydrochloric acid to dissolve away all binder and extract, wash, and dry the acid-insoluble component of aggregates (which, based on optical microscopy, is determined to be the entire mass of sand since sand contains no acid-soluble components). Based on optical microscopy, a portion of residue is also expected to contain clay and silt from un-calcined (or under-calcined) raw feed.

Sieve Analyses of Sand Extracted From Mortars

Sand, thus extracted by acid digestion of intact mortar fragments (without any pulverization or fracturing of mortar to obtain the original sand used), was sieved through various size fractions to examine conformance to the standard specification of masonry sand *a la* ASTM C 144. The following Table summarizes result of sand size distributions along with specified size ranges from ASTM C 144:

Sieve Size	US Sieve No.	Percent Passing for		Percent Passing					
		Natural Sand	Manufactured Sand	MA1	MA2	MA3	MA4	MA5	MA6
4.75-mm	4	100	100	100	100	100	100	94.4*	100
2.36-mm	8	95-100	95-100	92.9*	97.0	100	100	86.8	98.2
1.18-mm	16	70-100	70-100	87.4	94.2	97.2	100	80.4	93.7
600-µm	30	40-75	40-75	67.0	87.4*	90.1*	93.4*	58.8	74.6
300-µm	50	10-35	20-40	19.9*	49.7*	49.0*	46.6*	16.5*	23.5
150-µm	100	2-15	10-25	3.3*	11.1	10.6	6.9*	3.9*	4.6*
75-µm	200	0-5	0-10	1.1	2.6	2.2	0.9	0.7	0.7

Table 3: Size distribution of sand extracted from brick masonry mortars after acid digestion and specified size fractions in various US Sieves *a la* ASTM C 144. The 3rd and 4th columns show C 144 size ranges for natural and crushed sand, respectively. Asterisks on results for various sieve sizes indicate deviations from C 144 specified ranges.

Sieve Size	US Sieve No.	Percent Passing for		Percent Passing					
		Natural Sand	Manufactured Sand	MA7	MA8	MA9	MA10	MA11	MA12
4.75-mm	4	100	100	100	100	100	100	100	100
2.36-mm	8	95-100	95-100	96.5	95.8	93.9	100	98.8	98.0
1.18-mm	16	70-100	70-100	41.4*	89.7	93.3	97.9	93.1	94.9
600-µm	30	40-75	40-75	30.0*	70.0	88.0*	93.4*	79.2*	79.1*
300-µm	50	10-35	20-40	11.0*	27.1	42.9*	49.4*	30.7	29.5
150-µm	100	2-15	10-25	3.7*	7.9*	8.4*	9.0*	2.2*	2.7*
75-µm	200	0-5	0-10	0.4	2.5	1.8	1.9	0.0	0.3

Table 4: Size distribution of sand extracted from brick masonry mortars after acid digestion and specified size fractions in various US Sieves *a la* ASTM C 144. The 3rd and 4th columns show C 144 size ranges for natural and crushed sand, respectively. Asterisks on results for various sieve sizes indicate deviations from C 144 specified ranges.

Sieve Size	US Sieve No.	Percent Passing for		Percent Passing				
		Natural Sand	Manufactured Sand	SMA1	SMA2	SMA3	SMA4	SMA5
4.75-mm	4	100	100	-	100	100	-	-
2.36-mm	8	95-100	95-100	-	100	100	-	-
1.18-mm	16	70-100	70-100	-	100	99.6	-	-
600-µm	30	40-75	40-75	-	95.9*	92.3*	-	-
300-µm	50	10-35	20-40	-	47.3*	46.7*	-	-
150-µm	100	2-15	10-25	-	11.0	9.8*	-	-
75-µm	200	0-5	0-10	-	2.9	3.3	-	-

Table 5: Size distribution of sand extracted from stone masonry mortars after acid digestion and specified size fractions in various US Sieves *a la* ASTM C 144. The 3rd and 4th columns show C 144 size ranges for natural and crushed sand, respectively. Asterisks on results for various sieve sizes indicate deviations from C 144 specified ranges. Samples SMA1, SMA4, and SMA5 did not produce sufficient residue after acid digestion for sieve analysis.

Optical microscopical examinations in Figures 7 through 11 show relatively good grading and well-distribution of sand particles. Results of sieve analyses of sands extracted after acid digestion of mortars show relatively good grading, without any major gap in a particular size, or any major deviation from the specified size ranges of ASTM C 144 (except for some small deviations from C 144 ranges that are marked with asterisks beside the results). Distribution of various particle sizes of sands in Figures 7 through 11 show a range of particles sizes to effectively fill the intergranular spaces and hence minimize the paste volumes. Additionally, angularity (crushed nature) of well-graded sands provides an effective packing efficiency to minimize the inter-particle void spaces in the mortars.

Mineralogical Compositions of Sands Extracted From Mortars

Sand extracted from the acid-digested mortar contained quartz as the major constituent, and variable amounts of mica and clay as two undesirable constituents. Substantial amounts of mica and clay in the residues are indicative of possible derivations from the argillaceous impurities of original raw feeds. Table 6 shows various mineral constituents of sands as extracted from acid-digested mortars and used in X-ray diffraction:

Sample ID	Quartz	Calcite	Gypsum	Biotite	Illite	Vaterite
Brick Masonry Mortars						
8-69-MA1	91.3	-	-	8.7	-	-
4-85-MA2	89.5	-	3.5	7.0	-	-
1/2-121-MA3	88.8	-	-	-	11.2	-
3-142-MA4	93.7	-	-	6.3	-	-
5-1-MA5	93.5	-	-	6.5	-	-
5-5-MA6	95.3	-	-	4.7	-	-
3-16-MA7	94.7	2.8	2.5	-	-	-
2-31-MA8	97.2	-	2.8	-	-	-
1-34-MA9	97.6	2.4	-	-	-	-
4-41-MA10	91.8	-	2.5	5.7	-	-
6-56-MA11	84.5	-	2.2	3.1	10.1	-
6-64-MA12	79.9	-	-	5.1	15.0	-
Stone Masonry Mortars						
1-94-SMA1	-	-	-	-	-	-
1-94-SMA2	67.6	-	-	1.3	31.2	-
3-138-SMA3	97.1	-	-	2.9	-	-

3-142-SMA4	-	-	-	-	-	-
6-81-SMA5	-	-	-	-	-	-

Table 6: X-ray diffraction studies on sand extracted from brick mortar fragments after digesting in hydrochloric acid. There weren't enough insoluble residue left to do sieve analysis of sand for SMA1, SMA4, and SMA5 due to the small sizes of fragments remained for acid digestion after all other tests.

BINDER MICROSTRUCTURE FROM OPTICAL MICROSCOPY

Imprints of Hydraulic and Non-Hydraulic Components of the Original Binders Consisting of Limes and Natural Cements in Brick Masonry Mortars

Salient features of binder microstructures in the brick masonry mortars include an intimate mixture of:

a) Major amounts of very fine-grained, porous, severely carbonated lime paste, often with characteristic fine, irregular, elongated, discontinuous, shrinkage microcracks, and, some isolated occurrences of unmixed still-carbonated lime lumps (often with shrinkage microcracks within the lumps, and, sharp boundaries from the rest of lime matrix) that define the carbonated product of the slaked lime component of the original binder;
b) Subordinate amounts of isolated patchy, denser areas of pastes distributed in the overall carbonated lime matrix (Figures 18 through 22) that often contain – (i) hydration products of original hydraulic phases in natural cements, many of which are contained within the (ii) variably calcined remains of the ground original raw feed limestone fragments containing siliceous (quartz), argillaceous (clay), and ferruginous (oxidized reddish brown stained) impurities. This second part of the binder components indicates use of natural cement in varying proportions with lime in the binder. Many authors describe this second part as residual (natural) cement (even though many of these particles may not have calcined enough to develop cementitious properties; the present author, therefore, prefers to call these as they are i.e. ground calcined raw feed particles).

Detection of remains of these ground calcined raw feed particles (Figures 18 through 22) is an important microstructural feature in many of these historic mortars, where further detection of remains of hydraulic components within these feeds, along with areas or patches of denser microstructures of pastes in many mortars indicate use of natural cements with lime at varying proportions in these historic mortars. Care is needed to separate these calcined limestone raw feed particles from any argillaceous limestone, if added in the aggregate. Usually, the following three microstructural characteristics are common in these ground calcined raw feed particles (or residual natural cement particles), which are helpful for their positive identifications:

a) Many original ground calcined raw feed limestone/dolomite particles show a near-isotropic character in XPL (Figures 18 through 22) where the near-isotropic nature is the result of formation of weekly birefringent hydraulic components (e.g., β-C_2S, and other calcium-magnesium-alumino-silicates) from calcination, and an amorphous (isotropic) aluminosilicate (possibly pozzolanic or cementitious) phase from lime-silica reactions as well as from dehydroxylation of clay impurities (fused clay).

b) SEM-EDS analyses of many of these feed particles show characteristic depletion in calcium due to decomposition of calcite, and enrichment in silica, magnesia, alumina, and iron relative to calcium-rich surrounding lime matrix (Figure 32).
c) Many feed particles are coated with a distinct rim of a dense paste layer that is still carbonated but distinctly denser than the overwhelming porous carbonated lime matrix (and have a golden yellow interface color in XPL, Figures 20 and 21) that is indicative of hydration of the inherent hydraulic components within these calcined raw feeds.

Many of these above microstructural features of ground calcined feed particles i.e. near-isotropic core from calcination and golden yellow rims of dense pastes from hydration and carbonation, are shown in great detail in Appendixes A26, A29, A33, A39, A41, A43, A44, A46, A48, A49, and A50 for the brick masonry mortars.

For most of the brick mortars, the carbonated lime matrix from the slaked lime component in the original binders far outweighs the intermixed patchy hydrated and carbonated component from the original hydraulic (natural cement) components of the binders. This indicates use of a greater proportion of non-hydraulic lime than natural cement in the original binders. All brick and stone masonry mortars examined share the common basic microstructural feature of many historic lime mortars that consists of porous, fine-grained, severely carbonated lime matrix having hallmark microstructural features, e.g., shrinkage microcracks and occasional lumps of unmixed lime. These features are more easily detectable in samples MA11, MA12 for the brick masonry mortars (Figures 16 and 17) and SMA3 (later described in Figure 25) for the stone masonry mortar, where the samples, as received, also contained white lumps of unmixed lime.

The original binders, therefore, are determined to contain: (a) slaked lime in major proportions, which is judged to be non-hydraulic lime, and, (b) a hydraulic component (consisting of di-calcium silicate, and, an interstitial amorphous phase) in subordinate proportion, which is judged to be from natural cement. These compositional and microstructural features are characteristic of many historic hydraulic mortars from the 19th century US that contained mixtures of slaked lime and natural cement, where the slaked lime component set by atmospheric carbonation, and, the natural cement component set and hardened by: (i) slow and continuous hydration of β-C_2S and other calcium-magnesium-alumino-silicates, (ii) possible pozzolanic reactions between the amorphous phase and slaked lime to produce hydrates of cementitious properties, (iii) possible cementitious property of the amorphous phase to contribute to setting and early age strength development (when β-C_2S is inactive), followed by (iv) atmospheric carbonation of the calcium silicate hydrate (CSH) and hydration/reaction products of β-C_2S and other calcium-magnesium-alumino-silicates, and the interstitial amorphous phase.

Some mortars (e.g., MA11, MA12) lack the denser hydrated (hydraulic) component, and are composed predominantly to almost entirely of the overwhelming porous, fine-grained carbonated lime matrix with little or no evidence of any hydraulic component or any ground calcined raw feed fragments, which are indicative of use of a non-hydraulic lime without any natural cement in those mortars.

The following series of photomicrographs of thin sections of mortars in Figures 15 through 22 (along with more comprehensive atlas of photomicrographs in Appendixes A26 through A74) show these above-mentioned microstructural features of binders - in *eight (8) different sets of salient features of binder microstructures*.

Photos in Figure 15 were taken in XPL mode to highlight the severely carbonated nature of the overwhelming lime matrix forming the main skeleton in which quartz sand particles are well dispersed. Figure 16, on the other hand shows images taken mostly in PPL mode to highlight the fine, discontinuous, elongated irregularly-shaped shrinkage microcracks that are the characteristic hallmark microstructural feature of many lime mortars. Figures 17 through 22 were taken at both PPL and XPL modes, depending on the mode that features the object of interest prominently.

All these photomicrographs were taken by using a Progres GRYPHAX digital camera from Jenoptik Optical Systems attached to a Nikon Eclipse 600POL Petrographic microscope having transmitted and reflected polarized-light and fluorescent-light capabilities.

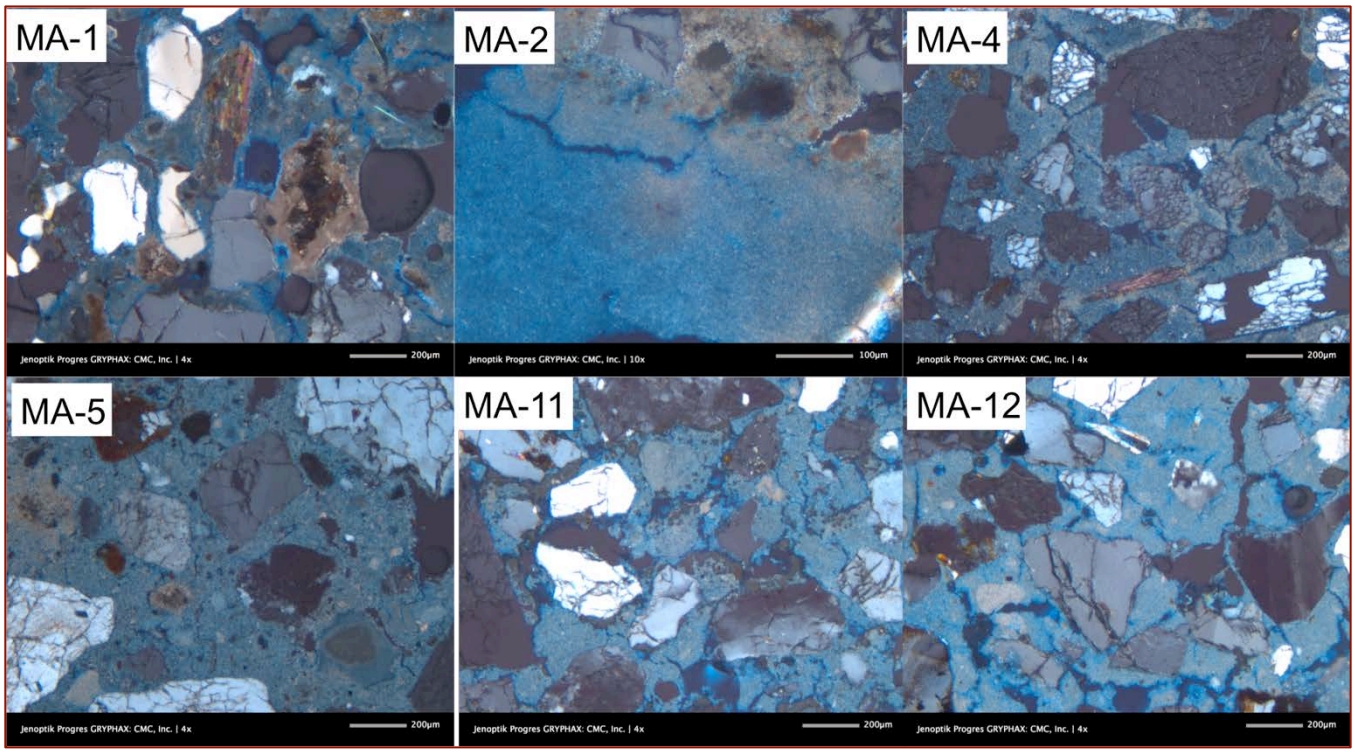

Figure 15: Binder Microstructure 1 of Brick Masonry Mortar: Featureless, uniform, overwhelming, porous, very fine-grained carbonated lime matrix in between sand particles highlighted in plane or crossed polar photomicrographs by the absorbed blue dyed epoxy. This feature constituents the main skeletal microstructure of binder in all mortars.

Figures 15 through 17 show the overwhelming porous, fine-grained, severely carbonated lime matrix in all mortars, having shrinkage microcracks and occasional lumps of unmixed lime, which are the most common and hallmark microstructural features shared by all brick and stone masonry mortars, as also common in many historic lime mortars. The lumps of unmixed lime in Figure 17 shows sharp boundaries from the rest of the carbonated lime matrix and often contain their own internal shrinkage microcracks.

Detection of hydraulic (natural cement) component of binder in a historic mortar requires careful identification of microstructural features above and beyond the above-mentioned typical features that are common mostly in non-

hydraulic historic lime mortars. These 'additional' features, as mentioned before, include: (a) detection and abundance of the remains of ground calcined raw feed particles that have residual textures and mineralogies left from the calcination process (e.g., near-isotropic nature from an amorphous phase from calcination), (b) dense areas in paste from hydration and carbonation of hydraulic (e.g., β-C_2S and other calcium-magnesium-alumino-silicates) components in calcined raw feeds, (c) rims of denser carbonated paste around many calcined raw feed particles that represent hydration of the original hydraulic component of feed (β-C_2S and other calcium-magnesium-alumino-silicates) depositing CSH around the feed, and subsequent carbonation of dense hydration products on the surface of the feed (often occur as golden yellow birefringent rim of carbonation on isotropic calcined feed particle (e.g., MA1 in Figure 15, MA2 in Figure 18, MA10 in Figure 19, Figure 20). Relative abundances of these additional features above and beyond the overall carbonated lime matrix indicates various proportions of limes and natural cements used in the original binders.

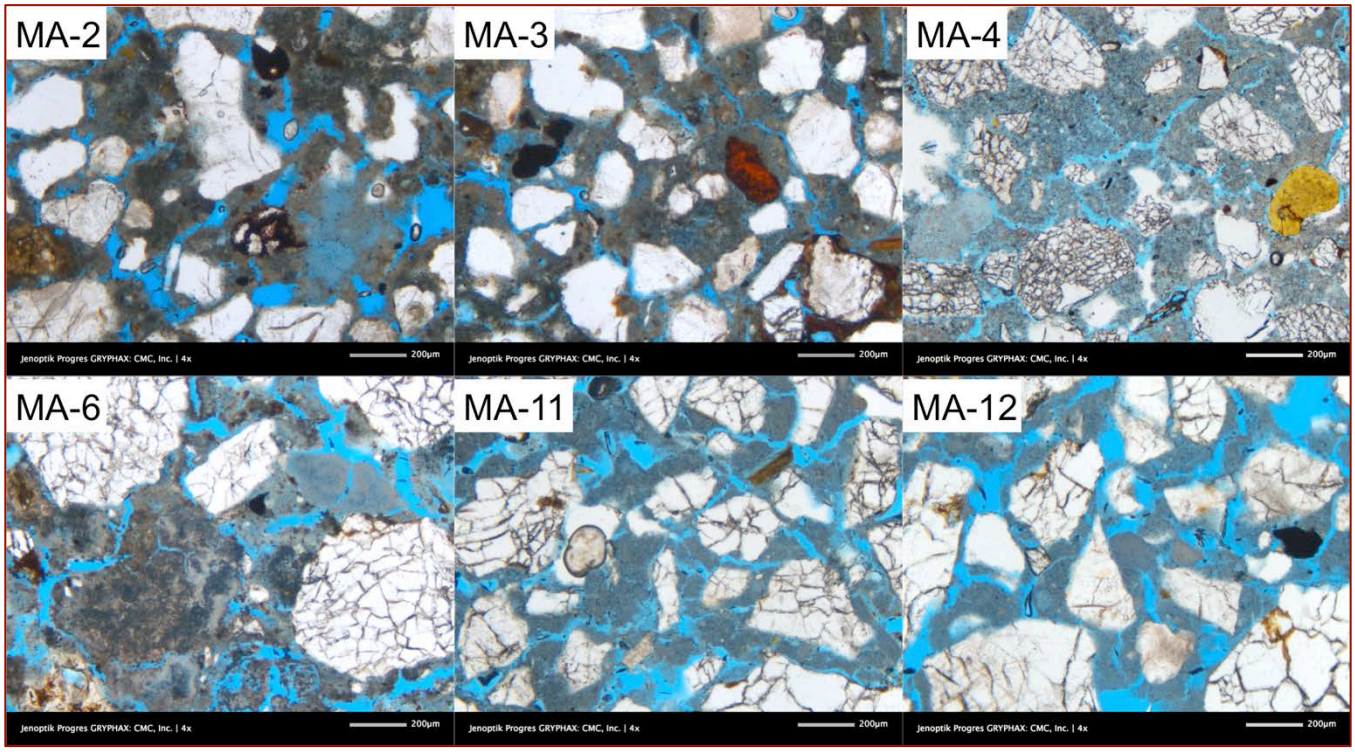

Figure 16: Binder Microstructure 2 of Brick Masonry Mortar: Fine, irregular, discontinuous, elongated separations (highlighted by blue dye-mixed epoxy) with tapered ends as shrinkage microcracks that are hallmark microstructural features of many historic lime mortars.

Figures 16 and 17 show many hallmark microstructural features that are produced almost entirely from the non-hydraulic slaked lime components in the binders. Use of either a non-hydraulic lime or a blended lime-natural cement binder, both containing the slaked lime component (entirely in the non-hydraulic lime and dominantly in the blended mix) produce these features by long-term curing by atmospheric carbonation of slaked lime. The overall paste consists of cryptocrystalline calcite grains with high interstitial porosities, shrinkage microcracks, and lumps or nodules of unmixed lime which are often denser than the surrounding matrix and separated from the rest by sharp boundaries (often contain shrinkage microcracks within the lumps). These features are the most characteristic microstructures of many historic lime mortars.

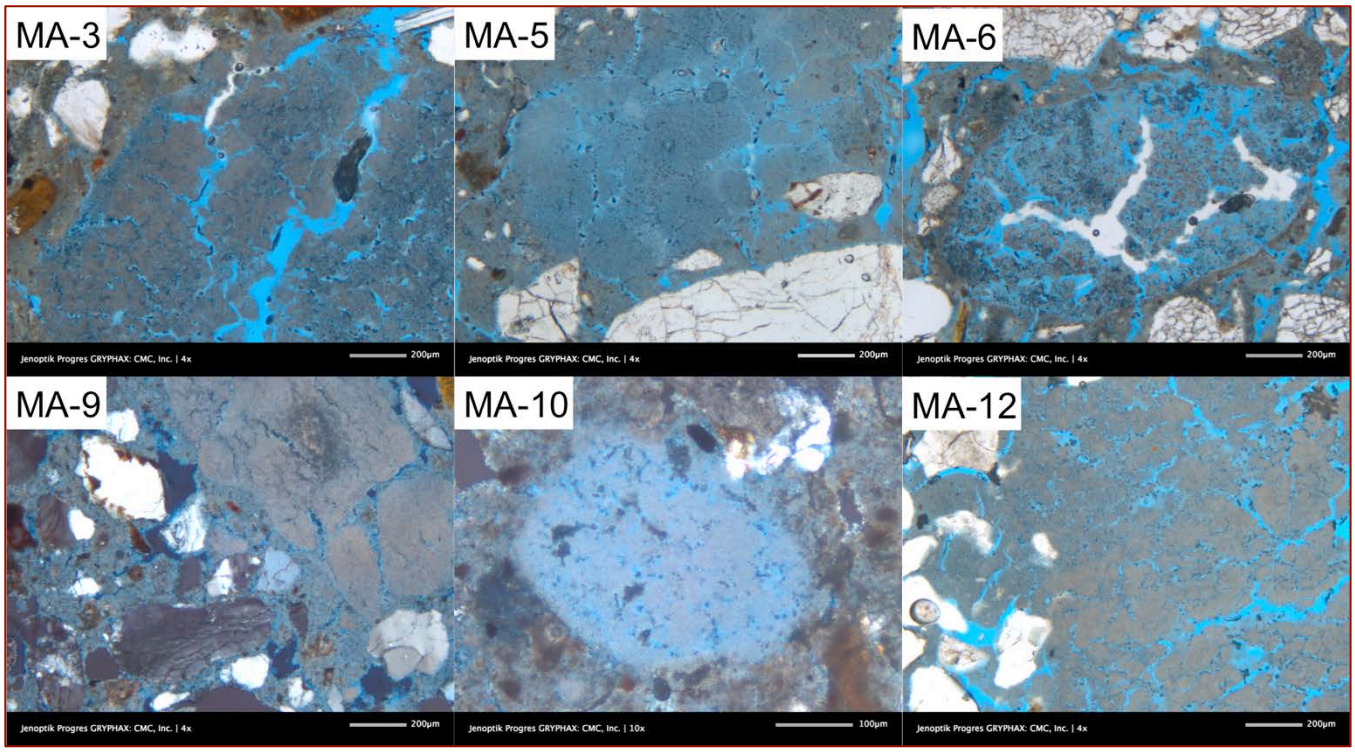

Figure 17: Binder Microstructure 3 of Brick Masonry Mortar: Lumps of unmixed lime, carbonated as well but with distinct boundaries from the surrounding carbonated lime matrix, often containing shrinkage microcracking within the lumps.

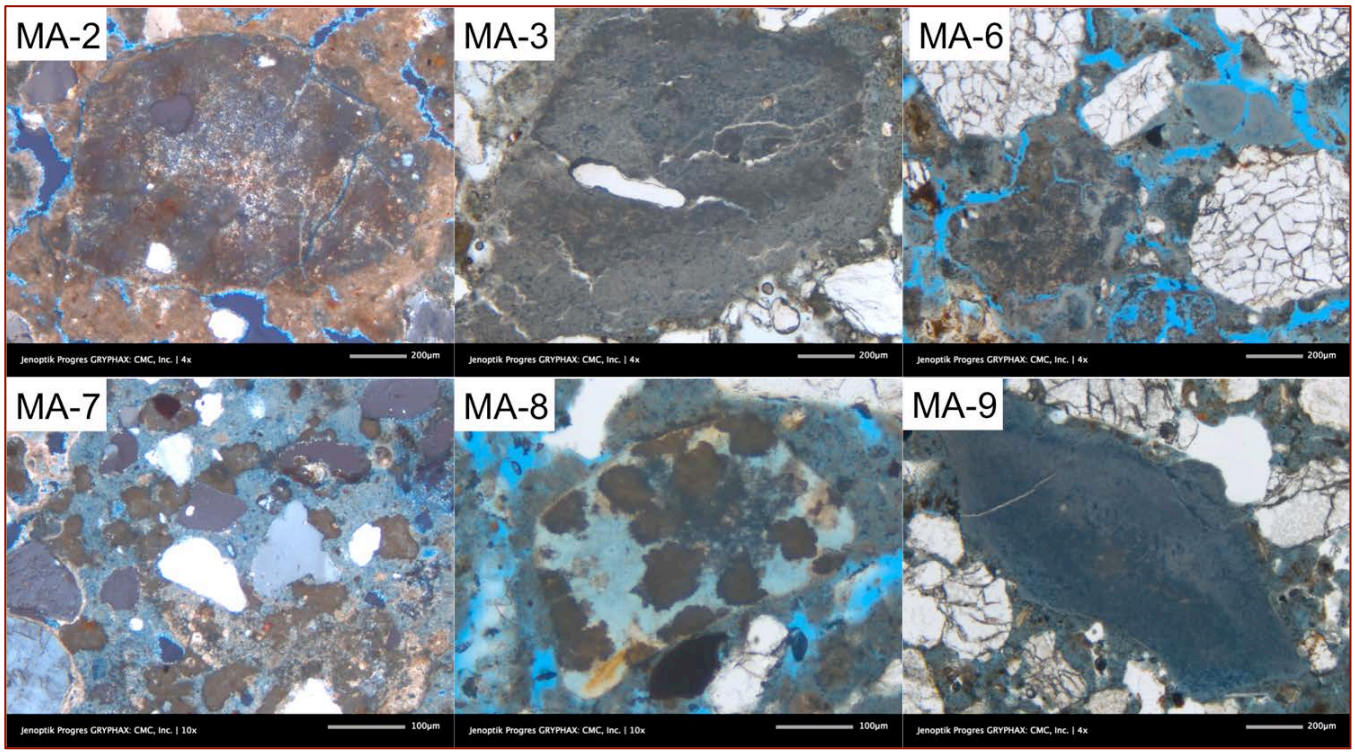

Figure 18: Binder Microstructure 4 of Brick Masonry Mortar: Hard burned lime either occurring as large lumps or as smaller isolated patches having characteristic cloudy appearance in PPL or XPL.

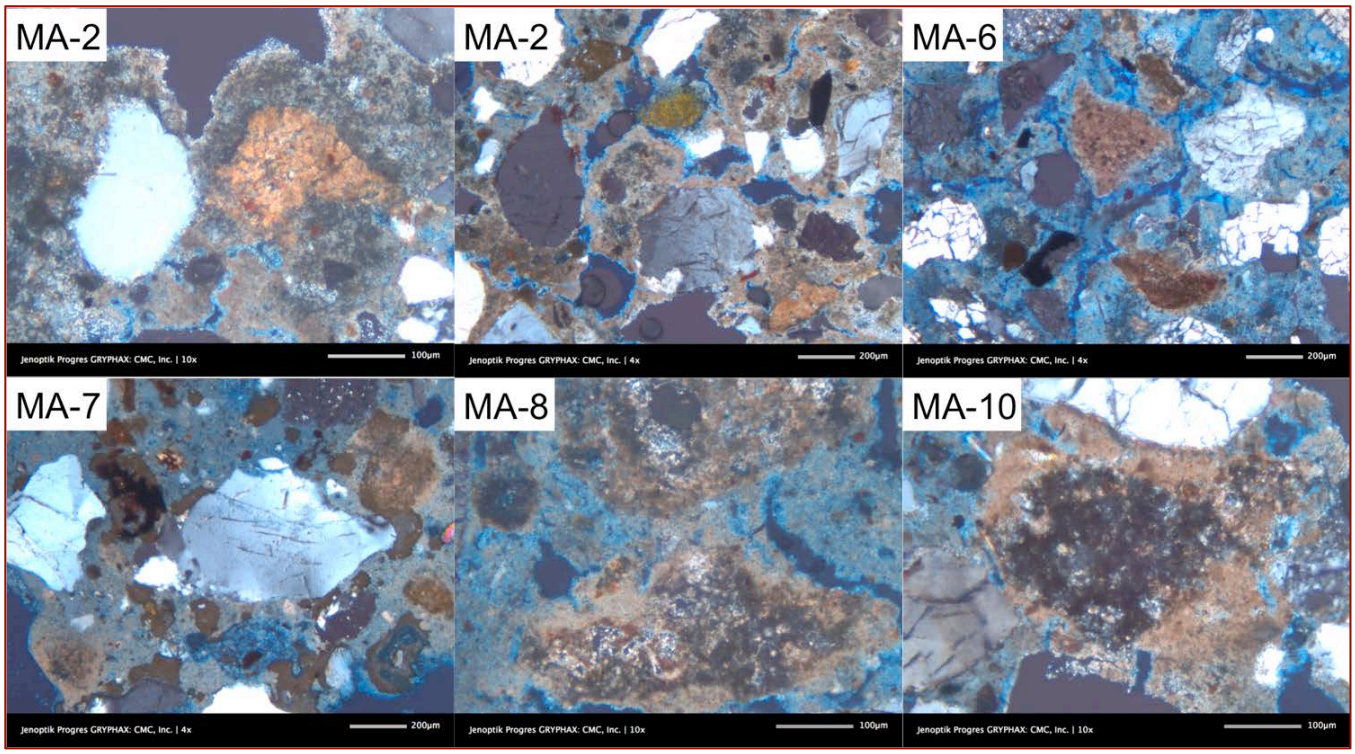

Figure 19: Binder Microstructure 5 of Brick Masonry Mortar: Isolated 'patchy' appearance of denser hydrated phases of paste from the natural cement component of binder distributed in the overwhelming porous more carbonated lime matrix. Notice the near-isotropic nature and golden yellow carbonation rim around a ground calcined raw feed particle in MA10 where the isotropic nature is from a possible amorphous phase formed from calcination and dehydroxylation of clay impurities in the feed.

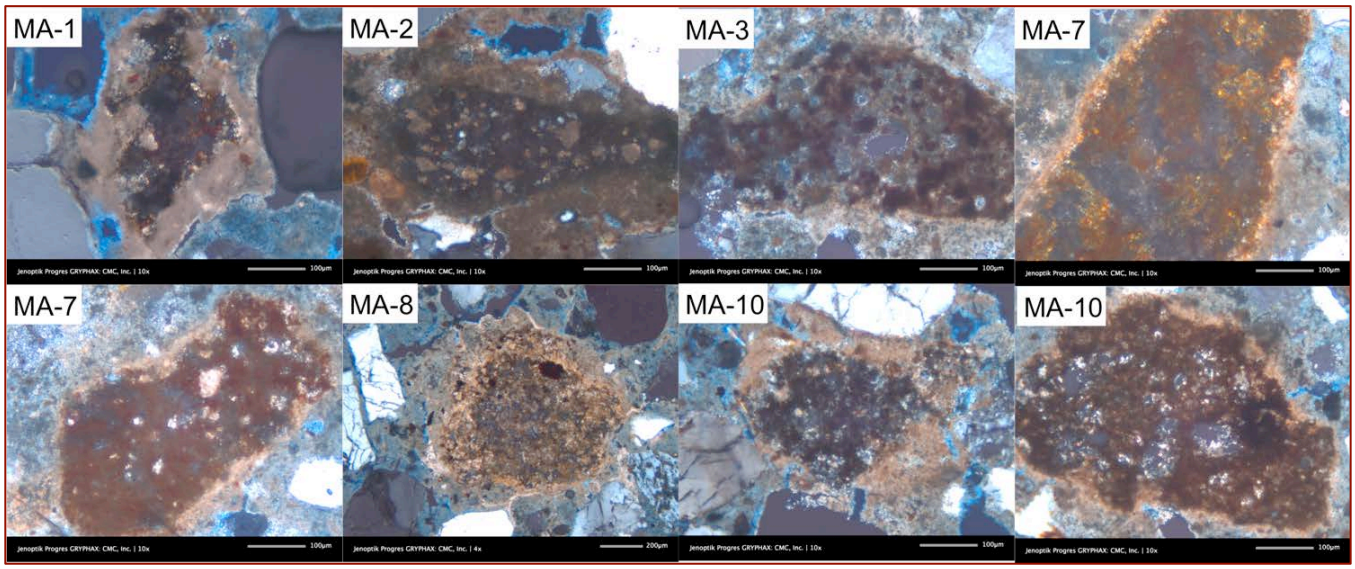

Figure 20: Binder Microstructure 6 of Brick Masonry Mortar: Isolated residual ground calcined limestone raw feed particles (host of β-C_2S and other calcium-magnesium-alumino-silicates) of natural cements, occurring as near-isotropic particles in crossed polars (sometimes containing some fine birefringent quartz inclusions within the dark matrix in XPL). The near-isotropic natures of these natural cement particles are from a possible amorphous phase produced from dehydroxylation of clay (fused clay) during calcination. The particles often contain a denser, less carbonated coat of hydration products (characterized by the golden yellow interference of dense carbonation rims in crossed polars, e.g., in MA1, MA7, MA8, and MA10) compared to the surrounding porous, severely carbonated lime paste.

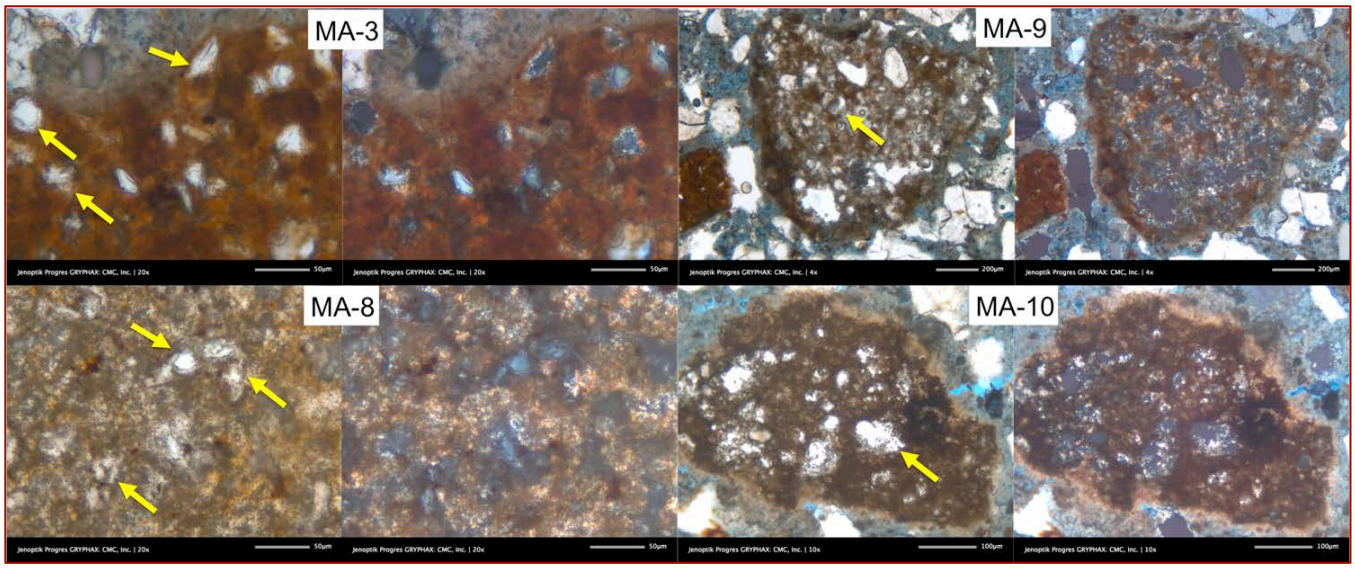

Figure 21: Binder Microstructure 7 of Brick Masonry Mortar: Evidence of development of hydraulicity within the residual ground calcined limestone raw feed particles of natural cement. Relict and residual dicalcium silicate and other calcium-magnesium-alumino-silicate hydraulic phases, cores of unslaked quicklime (sometimes exhibiting radial microcracks within the particle), rims of high temperature form of quartz (tridymite) around quartz inclusions, etc. can be seen within the near-isotropic calcined limestone raw feed particles. Near-isotropic natures of calcined feed particles in MA9 and MA10 are from an interstitial amorphous phase of aluminosilicate composition within the feed, resulted from lime-silica-alumina reactions and dehydroxylation of clay impurities (fused clay) during calcination.

Figures 18 through 22 emphasize importance of positive identifications of remains of ground, variably calcined limestone raw feed particles of natural cements, and distinguishing these grains from any added limestone components in the sand by virtue of various optical characteristics that were developed from the calcination process. Positive identification of such particles is crucial in detection of natural cements used in these mortars.

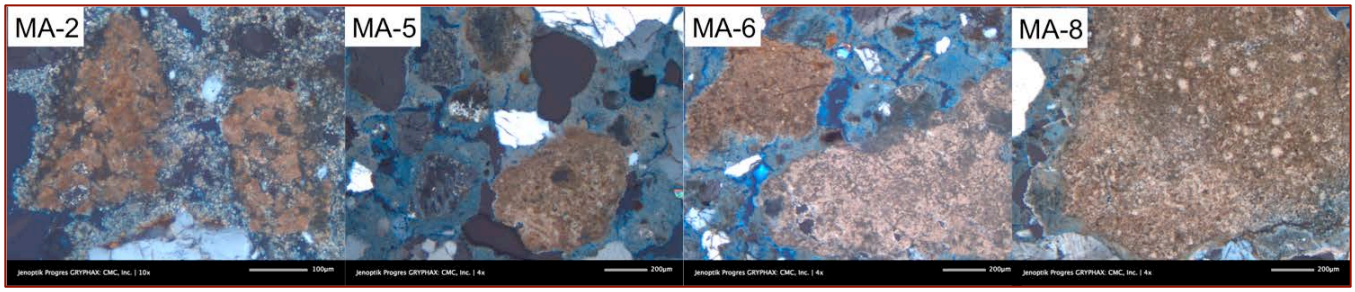

Figure 22: Binder Microstructure 8 of Brick Masonry Mortar: Incompletely calcined limestone raw feed particles in mortars. Their rarity of occurrence, and association with other calcined limestone particles exclude the possibility of their incorporation with sand aggregates.

From Figures 16 through 22, it became apparent that pastes are: (a) more uniform, homogeneous carbonated lime matrix in mortars MA11, MA12, (b) relatively patchier (denser) due to more hydraulic components in MA4, MA5, and MA6, but (c) noticeably patchier due to abundant raw feed and hydraulic components in the other mortars, e.g., MA2, MA3, MA7, MA8, MA9, and MA10 due to increased proportion of the hydraulic (natural cement) component in the binder. Therefore, these three groups of mortars can be produced from varying proportions of non-hydraulic lime and natural cement, where MA11 and MA12 were made with lime only and no natural cement, whereas MA7 and others were made with varying proportions of lime and subordinate amounts of natural cements.

Patchy-Textured Paste – The overall 'patchy' appearance of pastes (e.g., in Figures 18 through 22, and many photomicrographs in Appendixes A26 through A74), therefore, resulted from having mixtures of: (i) the non-hydraulic (high-calcium) lime (i.e. having fine-grained, porous, severely carbonated paste with characteristic shrinkage microcracks and occasional lime lumps), and, (ii) hydraulic (natural cement) components (i.e. having denser, less carbonated, less porous patches). Hydration of the natural cement component generated the denser 'patchy' areas of pastes within the overwhelming skeletal carbonated lime matrix developed from long-term setting by atmospheric carbonation of the original slaked lime component of the lime. This 'patchy' texture is the characteristic of historic blended lime-natural cement mortars, as opposed to featureless, uniform, monotonous, fine-grained, homogeneous appearance of carbonated lime only paste of historic lime mortars.

Ground Calcined Raw Feed (GCRF) – Perhaps, after the 'patchy' texture, the next best evidence is detection of residual or relict grains of ground calcined impure limestone raw feed particles (sometimes described as 'residual natural cements') scattered throughout the paste (Figure 16) that can be positively differentiated from any carbonate component of calcareous sand aggregate by various features that are indicative of their calcined (and hydraulic) natures. For example:

(i) These ground calcined raw feed particles often appear near-isotropic in optical properties when seen in the crossed polarized light (XPL) mode in a petrographic microscope, which is due to the presence of an interstitial amorphous phase of aluminosilicate composition from fused clay;

(ii) These grains are often surrounded by a characteristic golden yellow rim of carbonated paste that is noticeably denser (hence occur as golden yellow birefringence of carbonation) than the surrounding overwhelming more porous and finer-grained carbonated lime paste,

(iii) Sometimes, many relict ground calcined feed particles contain very fine-grained birefringent interstitial quartz grains left-over from the original quartz impurities in feed, which stand up against the overall darker (amorphous) appearance of calcined grains in crossed polars, and sometimes even contain its high-temperature polymorph, tridymite as rims;

(iv) SEM-EDS analyses of calcined feed particles show the characteristic depletion of calcium and enrichment of silica, alumina, magnesia, and iron compared to the surrounding high-calcium (and low silica, alumina, magnesia, iron) carbonated lime matrix (discussed later);

(v) SEM-EDS examinations of calcined feed may show residual β-C_2S phase as rims over silica, and other microstructural features of lime-silica solid-state reactions during calcination (discussed later);

(vi) If the original feed is impure dolomite, calcined particles may contain pseudomorphs of original euhedral rhombic crystals of dolomite often with stained reddish brown oxidized iron rims in individual dolomite rhombs (which are very common in natural cement mortars where cements were manufactured from calcined argillaceous dolostones, as in Rosendale, NY).

Care is needed to differentiate any un-calcined or less calcined raw feed particles of limestone (Figure 18) from any possible calcareous components of sand aggregate, mostly by the above-mentioned features of calcinations, their

rare abundance in the mortar relative to any calcareous component of sand, and detecting if sand is dominantly siliceous, as in the present mortars.

Residual Hydraulic Phases – After detection of ground, calcined raw feed particles, and, the overall 'patchy' appearance of paste, the next most difficult task is to detect any residual hydraulic phases (e.g., beta-dicalcium silicate, other calcium-magnesium-alumino-silicates such as gehlenite and merwinite, and an amorphous phase) which provide the original hydraulic (and cementitious) properties of natural cement. These hydraulic phases in natural cements often consists of: (i) impure form of β-C_2S or belite or larnite, and sometimes associated with α'-C_2S, a high-temperature polymorph (Taylor 1998, found in Roman cements from calcined marlstones by Hughes et al. 2007, Weber et al., 2007), along with (ii) other calcium-magnesium-alumino-silicates in the CaO-MgO-SiO_2-Al_2O_3-Fe_2O_3 system (e.g., gehlenite, merwinite), and (iii) an interstitial amorphous phase, which is more crucial than the silicates at the early age setting and strength development of natural cement, when belite and other silicates are inactive. As mentioned before, natural cements in these mortars have set, hardened, and contributed to strength by combinations of: (i) slow and continuous hydration of β-C_2S and other calcium-magnesium-alumino-silicates, (ii) possible pozzolanic reactions between the amorphous phase and slaked lime to produce hydrates of cementitious properties, (iii) possible cementitious property of the amorphous phase itself to contribute to setting and early age strength development (when β-C_2S and other calcium-magnesium-alumino-silicates are inactive), followed by (iv) atmospheric carbonation of the calcium silicate hydrate (CSH) and hydration/reaction products of β-C_2S and other calcium-magnesium-alumino-silicates, and the interstitial amorphous phase. Detection of these residual hydraulic components (mostly from SEM-EDS studies) in natural cements can, therefore, undoubtedly provide further positive identification of its addition, but, as mentioned, it is often difficult in many historic mortars, and requires detailed SEM-EDS studies.

Despite very slow hydration of β-C_2S compared to tricalcium silicate (C_3S, the main hydraulic component in the Portland cement), β-C_2S in natural cement mortar does not occur in characteristic 'bunch of grapes' texture of belite that is so common in Portland cement pastes. This β-C_2S phase typically occurs as rims over the silica phases (interstitial quartz or silica from fused clay impurities) that provide the seeds for nucleation of β-C_2S (and other calcium-magnesium-alumino-silicates) by solid-state reaction of SiO_2 with the overwhelming calcined lime (free CaO) matrix in the lime kiln below the sintering point of limestone. Similar solid-state reactions between silica and periclase (from calcined dolomite) produces calcium magnesium silicate (merwinite), a common silicate, often occur as second to belite amongst silicates in many Rosendale natural cements. Therefore, in SEM β-C_2S may be found as rims over quartz (or silica from fused clay), or as interstitial phases scattered in the calcined limestone raw feed, or perhaps isolated grains disintegrated from their silica sources. The texture of β-C_2S, therefore, is very different from the 'bunch of grapes' texture in Portland cement paste (where the texture is the result of crystallization of belite from a melt from sintering as opposed to solid-state formation in calcined lime by reactions between lime and silica along the interfaces). Therefore, care is needed for positive identification of any residual β-C_2S and other calcium-magnesium-alumino-silicate components in a historic natural cement mortar, which is often accomplished by

detailed SEM-EDS studies of calcined raw feed remains after positive identifications of the remains by optical microscopy.

Along with β-C_2S, interstitial quartz grains sometimes show high temperature rims of tridymite (arrows in Figure 17), which also requires careful optical identifications for positive confirmations.

Therefore, in summary, based on optical microscopy of brick masonry mortars, it is judged that:

1. A non-hydraulic lime was probably used in the mortars MA11 and MA12 (equivalent to a high-calcium non-hydraulic lime)
2. A more hydraulic binder, e.g., a natural cement was probably used in varying proportions with non-hydraulic lime (subordinate to lime) in the mortars MA1, MA2, MA3, MA4, MA5, MA6, MA8, MA9, and MA10, whereas,
3. A binder consisting of more natural cement than lime was used in the mortar MA7.
4. Remnants of ground calcined raw feeds of natural cements in all mortars are judged to be impure limestone containing siliceous and argillaceous impurities, where silica in the impurity provided the seeds for development of dicalcium silicate and other calcium-magnesium-alumino-silicate hydraulic phases by solid-state calcined lime-silica and calcined magnesia-silica reactions. Some of these silicate phases can be still detectable within the relict calcined raw feed fragments. Fused clay from impurities also formed an interstitial amorphous (aluminosilicate) phase that has imparted the overall near-isotropic nature of the calcined raw feeds.
5. Sands used in all mortars from reportedly different ages, apparently are similar in compositions (crushed quartz sand) though of variable nominal maximum sizes (see Table 2).

Lime Leaching and Paste Alterations in Stone Masonry Mortars

Of the five stone masonry mortars received, Sample SMA3 stands out as the simplest lime mortar having composition and microstructure similar to high-calcium non-hydraulic lime mortars, as found in MA11 and MA12 brick masonry mortars. Sample SMA3, therefore, consists of very fine-grained, porous, severely carbonated lime matrix having shrinkage microcracks, occasional lime lumps, and all other hallmark microstructural features of a non-hydraulic or feebly hydraulic historic lime mortar.

The other four samples, however, are much more complex, somewhat dirty, altered, and weathered (e.g., SMA1 and SMA4) mortars in having: (i) the original ground, calcined impure limestone raw feed particles detected in pastes (indicating use of natural cements), and, also (ii) evidence of severe alterations and leaching of lime at various areas of pastes, having patches of gelatinous or colloidal silica masses in pastes that are enriched in Si, Mg, Al, and Fe relative to Ca for severe leaching of lime.

Samples SMA1, SMA2, and SMA4 show patchy-textured pastes (Figures 23, 24, 26, and 28) having:

1. Denser pastes, occurring as isolated areas or long continuous bands (as in SMA2 and SMA5) that show golden yellow interference color from carbonation in XPL and relatively denser appearance in PPL, and,
2. Porous, leached lime patches or bands that are optically isotropic in appearance (often containing coarsely crystalline calcite grains that are more common in SMA1).
3. SMA5 shows bands of denser pastes and relatively less dense pastes (Figures 27, 28, and 29) having variations in calcium and silica contents that are distinct in PPL and XPL images. Paste does not appear to be as leached or porous as in SMA1, SMA2, and SMA4.

In all these Figures, the condition of the stone masonry mortars, as received, are shown first, followed by large-area thin section images taken from a transmitted-light stereomicroscope (Olympus SZH), then a serious of PPL and corresponding XPL images from various areas of thin sections are shown to highlight various microstructural features.

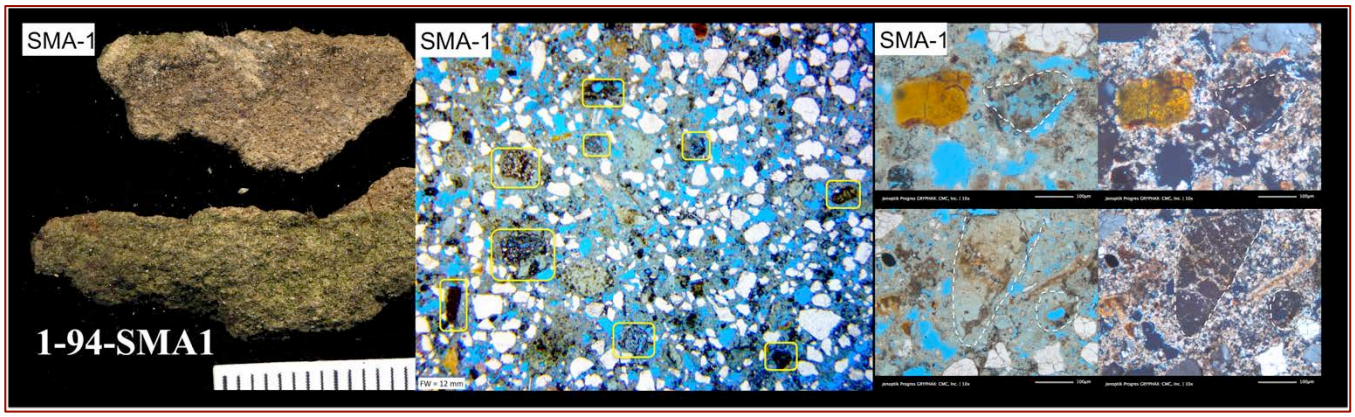

Figure 23: Stone masonry mortar SMA1 received in weathered condition with green algal deposits. Blue dye-mixed epoxy-impregnated thin section photomicrographs show overall porous nature of mortar, an overall coarsely crystalline calcitic carbonated matrix having secondary calcite grains, isolated occurrences of calcined raw feed particles (boxed), and patchy areas of paste having optically isotropic natures (depleted in lime and enriched in Si, Mg, Al, and Fe relative to the surrounding coarsely crystalline calcite carbonated matrix).

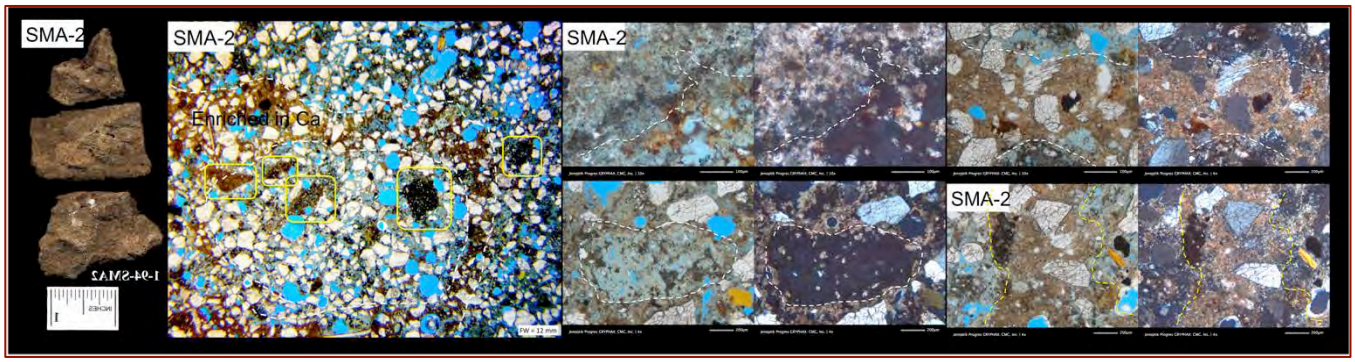

Figure 24: Stone masonry mortar SMA2 received in a weathered condition. Thin section shows a banded nature of paste having denser, golden yellow lesser-carbonated brown bands compared to the surrounding more porous, severely carbonated and/or dark isotropic leached paste (where leached areas of paste have similar depleted Ca and enriched Si, Mg, Al and Fe natures as seen in SMA1 compared to the other areas).

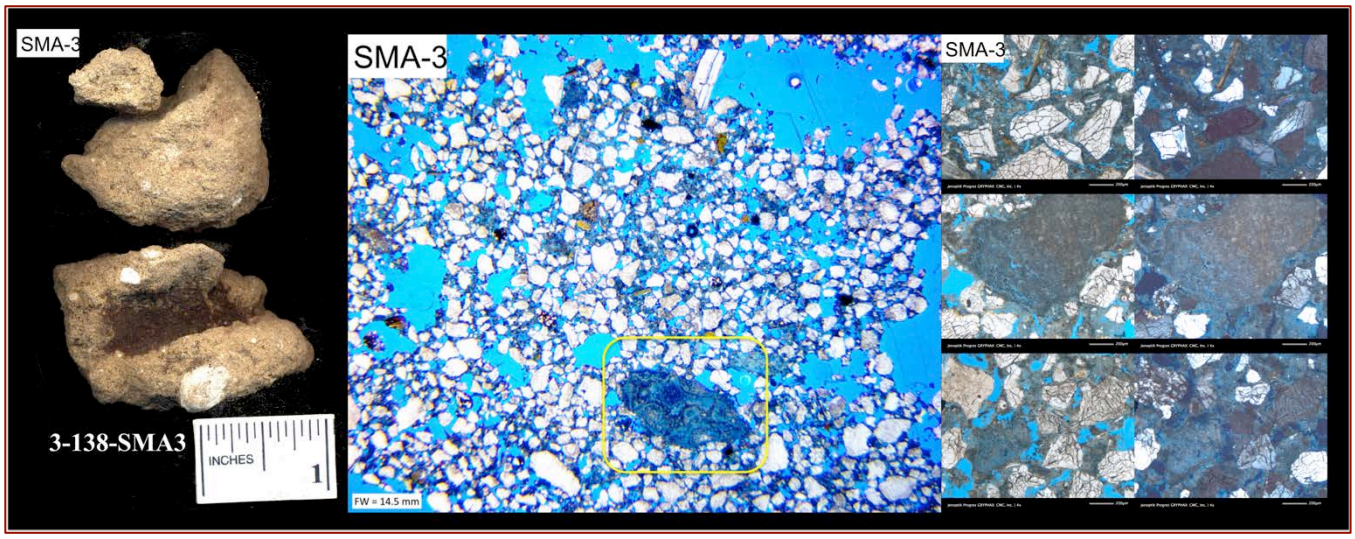

Figure 25: Stone masonry mortar SMA3 resembles typical lime mortars, e.g., MA11 and MA12 in the brick masonry mortars. Blue dye-mixed epoxy-impregnated thin section photomicrographs show an overall porous, very fine-grained severely carbonated lime nature of a typical lime mortar having shrinkage microcracks, lime lumps (boxed in the middle photo), etc.

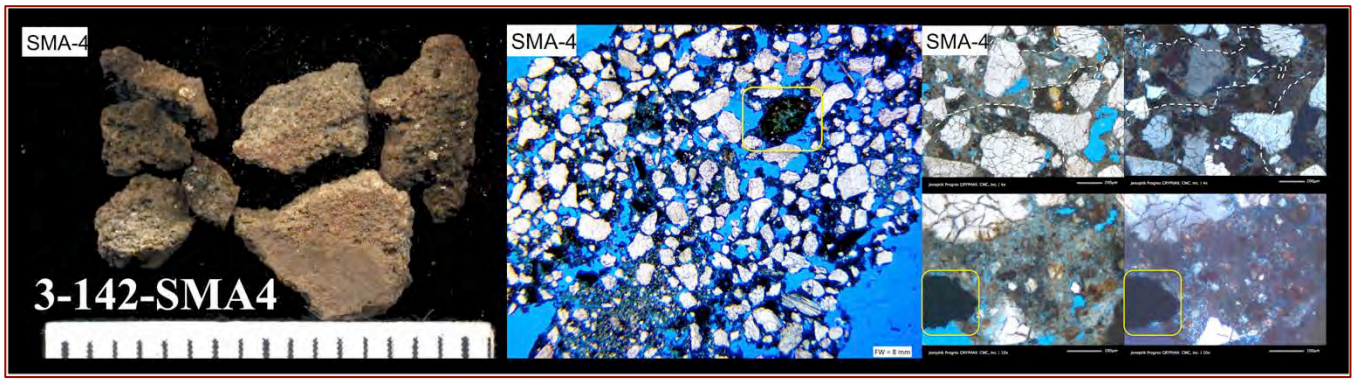

Figure 26: Stone masonry mortar SMA4. Thin section shows 'dirty' appearance and patches of near-isotropic (in XPL) leached lime pastes similar to those found in SMA1 and specially in SMA2.

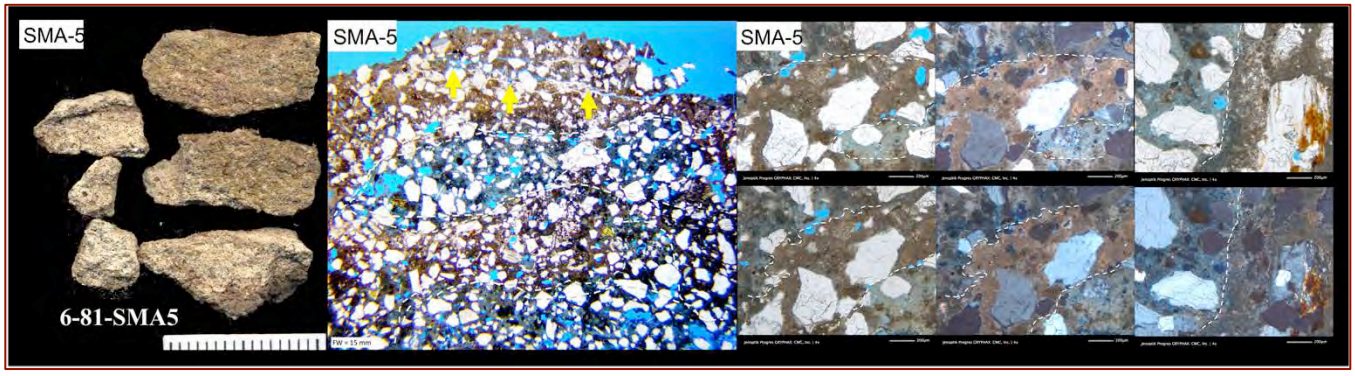

Figure 27: Stone masonry mortar SMA5. Thin section shows banded nature, similar to SMA2, having denser, lesser-carbonated, golden yellow bands of paste (in XPL) alternating with more carbonated, porous lime matrix where denser brown bands are found to have (from further SEM-EDS studies) more Ca and less Si (higher Ca/Si ratio) than the porous carbonated and leached areas (having more Si, lower Ca/Si ratio from lime leaching than the brown bands) in between the denser Ca-rich bands. Some fine surface-parallel microcracks are noticed within the denser brown band at the exposed surface as shown with yellow arrows in the second photo.

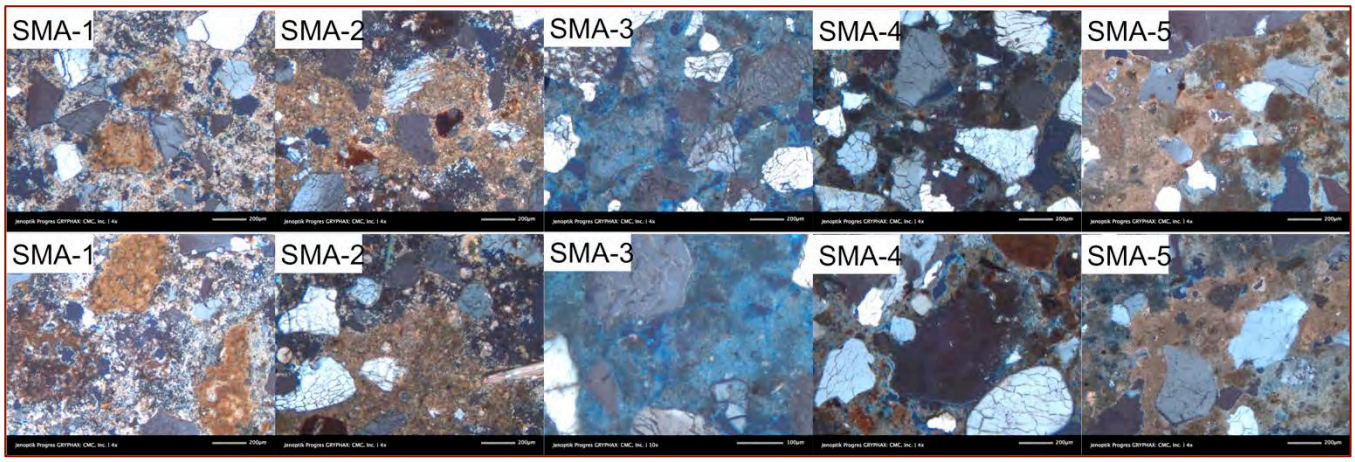

Figure 28: XPL photomicrographs of stone masonry mortars showing coarsely crystalline calcite carbonated matrix and patchy areas of leached (Ca-deficient) paste in SMA1, dense Ca-rich golden yellow bands and dark leached (Ca-deficient) areas in SMA2 and SMA5, overall porous, fine severely carbonated lime matrix of a typical lime mortar in SMA3, and dark (optically isotropic in XPL) leached lime patches of pastes in SMA4. Some residual ground, calcined raw feed particles in SMA1 and other mortars indicate use of natural cement in the original binder.

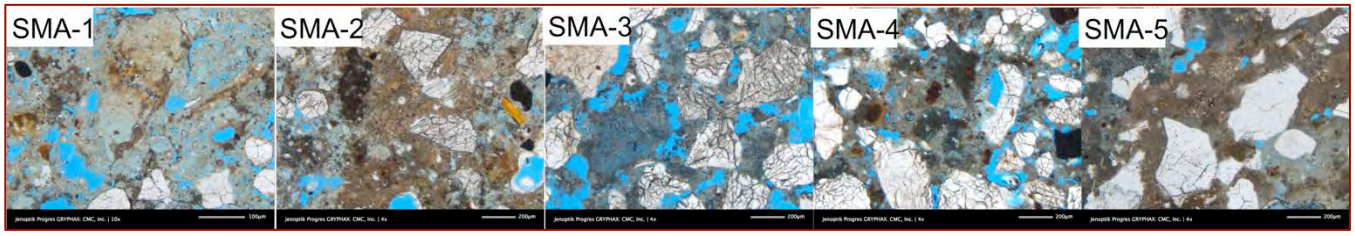

Figure 29: PPL photomicrographs of stone masonry mortars showing leached lime porous areas in SMA1, bands of denser, Ca-rich areas in paste adjacent to leached lime paste in SMA2 and SMA5, shrinkage microcracks in porous fine carbonated lime matrix in SMA3, patchy textured paste of more and less leached-lime areas of paste in SMA4.

Sample SMA1 shows more pervasive leaching of lime from mortar as well as precipitation of leached lime as coarsely crystalline secondary calcite precipitates, thus giving an overall coarse birefringent appearance of paste from secondary calcite precipitates in XPL photos but with interstitial isotropic areas from leaching of the original lime matrix. Leaching, therefore, replaced the original fine-grained porous carbonated lime microstructure of mortar paste to coarsely crystalline calcite mass in a more porous leached matrix. Leaching is observed both in the overall matrix of mortar in SMA1 (Appendixes A54, A55, and A56), in between coarsely crystalline secondary calcite precipitates, as well as from within the original lumps of unmixed lime where the boundary of the original unmixed lime may have somewhat retained, but lime from the entire lump has been leached out from inside, thus leaving a near-isotropic nature of the interior of lump in XPL. Many original calcined feed particles also show leaching of lime from within, retaining pseudomorphs of original shapes and textures.

Sample SMA2, by contrast, shows leaching along a layer or band of paste that is juxtaposed with a denser less-leached layer of paste (Appendixes A57, A58, and A61) where the compositional difference between the leached and less-leached layers (or bands or patches) of pastes are significant, and characterized by severe depletion of Ca and relative enrichment of Si, Mg, Al, and Fe in the leached areas compared to the opposite compositions of the adjacent less-leached areas.

SMA3 is the only sample, which is more pristine i.e. least altered than the rest of the stone masonry mortars, and hence retained its original lime mortar composition (Appendixes A62 and A63), indicating least interaction with moisture during service compared to the other stone masonry mortars.

SMA4 shows an overall 'dirty' appearance containing evidence of lime leaching at isolated patches, leaching of lime from within lumps and calcined feed particles (Appendixes A64 through A68). Compositions and optical properties of leached and less-leached areas of pastes in SMA4 are very similar to the ones found in SMA1 and SMA2.

SMA5 shows banded or patchy nature of paste (Appendixes A69 through A74) with distinct compositional variations (and corresponding variations in appearances in PPL and XPL images) between (i) areas rich in calcium where calcium oxide far outweighs all other oxides (characteristic of a carbonated lime matrix from the original slaked lime component) to (ii) areas rich in calcium and appreciable amounts of silica (i.e. probably representing areas containing hydration products from natural cement component) to (iii) areas that show leaching of lime (Ca-depletion) and corresponding enrichment in Si, Mg, Al, and Fe from the other areas. Further SEM studies thus detected three different types of paste areas in SMA5 some of which, e.g., lime leaching are also found in SMA1, SMA2, and SMA4. The extent of leaching (or depletion of Ca) in SMA5, however, is not as severe as found in the leached patches of pastes in SMA1, SMA2, and SMA4.

Figure 30: PPL and XPL photomicrographs of stone masonry mortar SMA5 showing numerous fine parallel microcracks present along an exposed surface of a fragment within the denser calcium-rich band of paste, which could have formed from salt crystallization, or, freezing-related distress at critically saturated conditions.

The only evidence of physical distress of masonry mortar is found in SMA5 as long, continuous microcracks, as shown in Figure 30, which could have formed from salt crystallization, or, freezing-related distress at critically saturated conditions. These microcracks are parallel to each other and located at a dense band of paste along an exposed surface of a piece in SMA5. Carbonation of paste adjacent to many of these microcracks could have been facilitated by ready migration of atmospheric carbon dioxide through these microcracks.

BINDER MICROSTRUCTURES IN BRICK MASONRY MORTARS FROM SEM

Patchy Versus Uniform Textures of Pastes in Blended (Lime-Natural Cement) versus Non-Hydraulic Lime Binders in Brick Masonry Mortars

The following backscatter electron (BSE) images of pastes from samples MA7 and MA12 in Figure 31 show the two extremes of paste microstructures found in the brick masonry mortars –

1. An overall patchy appearance of paste in MA7 consisting of mixtures of denser (and darker) patches of hydrated pastes, and, less dense, lighter, porous carbonated lime pastes, resulted from the original natural cement and lime components of the binders, respectively, whereas,
2. More or less uniform, monotonous porous appearance of paste in non-hydraulic lime mortar in MA12 that have many characteristic carbonation shrinkage microcracks as seen in many historic lime mortars.

These are two end-member paste microstructures; all other mortars fall in between these two extremes.

It is interesting to note that carbonation shrinkage microcracks are more common (rather characteristic) in predominantly lime mortars as seen in MA12 (and also common in many historic non-hydraulic lime mortars) but are less common in the denser pastes of lime-natural cement mortars containing patches of hydrated phases from the natural cement component of the binders; shrinkage microcracks are absent in MA7 as seen in the BSE image.

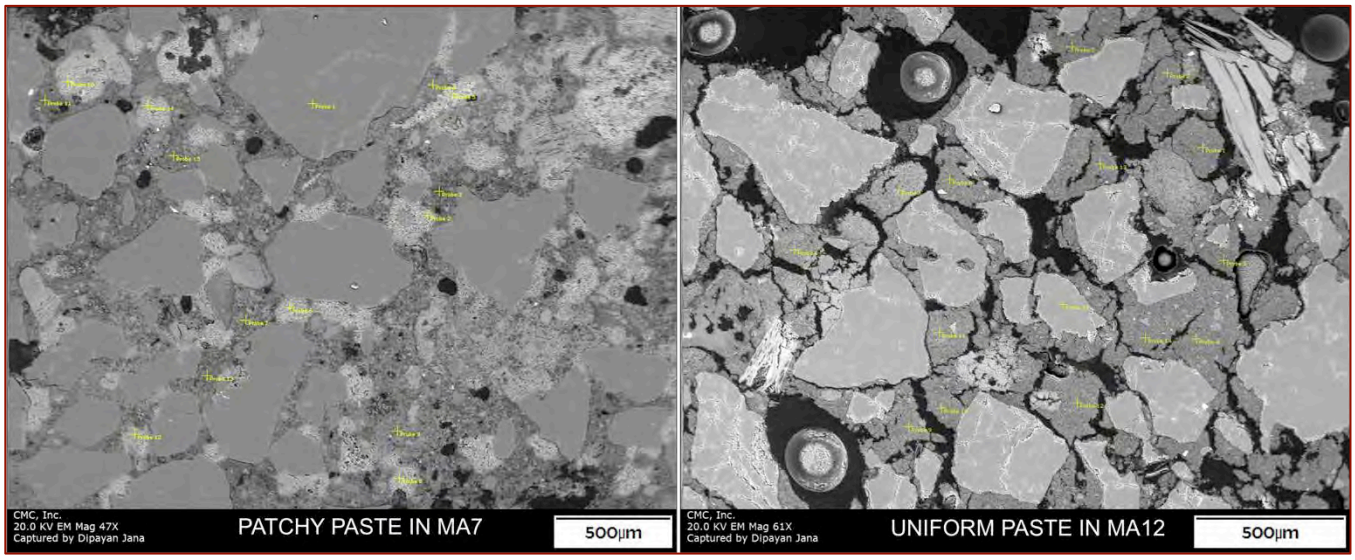

Figure 31: Binder Microstructure 9: Patchy versus uniform appearance of pastes containing hydraulic (natural cement-lime) binder in the patchy paste in MA7 as opposed to non-hydraulic lime binder in the uniform paste in MA12. Notice severe shrinkage cracking in MA12 as opposed to none in MA7.

A detailed investigation of compositional variations between the lighter-toned versus darker-toned patchy areas of pastes in the BSE image of MA7 (Figure 31, left photo) revealed some interesting and systematic differences in paste compositions between these two shades. The lighter-toned paste areas are consistently higher in silica and lower in calcium (high paste-CI) resulted from the natural cement component than the darker toned areas (darker patches are higher in CaO, lower in SiO_2 i.e. lower paste-CI than the lighter patches) resulted from the lime components.

The following graph in Figure 32 shows a systematic variation in compositions of paste in these two patchy areas of paste with a region of overlap (the so-called gray area) in the graph of the ratio of calcium to silica in paste plotted against paste-CI (hydraulicity). Hydraulicity of paste is defined as Eckel's cementation index (CI), which is calculated from compositions of pastes across these different shades of areas as, $CI = [(2.8\times SiO_2)+(1.1\times Al_2O_3)+(0.7\times FeO)] / [(CaO) + (1.4\times MgO)]$.

Clearly, patches of more and less hydraulic areas of paste correspond to respective contributions from the original hydraulic (natural cement) and non-hydraulic (slaked lime) components of the binder. Areas having higher silica, lower calcium, lower CaO/SiO_2 ratio, higher paste-CI (lighter toned in BSE image) are contributed from the hydraulic (natural cement) component of binder, whereas, the adjacent paste patches having more porous and opposite chemical characteristics are contributed from the slaked lime component of the original binder. The intimate mixture of two as patchy-textured paste is indicative of an intimate mixture of the original hydraulic (natural cement) and non-hydraulic (slaked lime) components of the binder.

Such scenario, however, can also arise when the original raw feed has limestone and clay components thoroughly mixed together either manually i.e. from separate mixtures of ground limestone and clay components, as in manufacturing of many 'hydraulic limes', or, from calcination of a naturally occurring argillaceous limestone, where clay impurities are uniformly distributed throughout the limestone matrix, as in manufacturing of natural hydraulic lime (NHL), or natural cements. The extent of patchiness in the final mortar provides clues to the proportions of the slaked lime and hydraulic (e.g., natural cement) components contributed from the respective raw feeds.

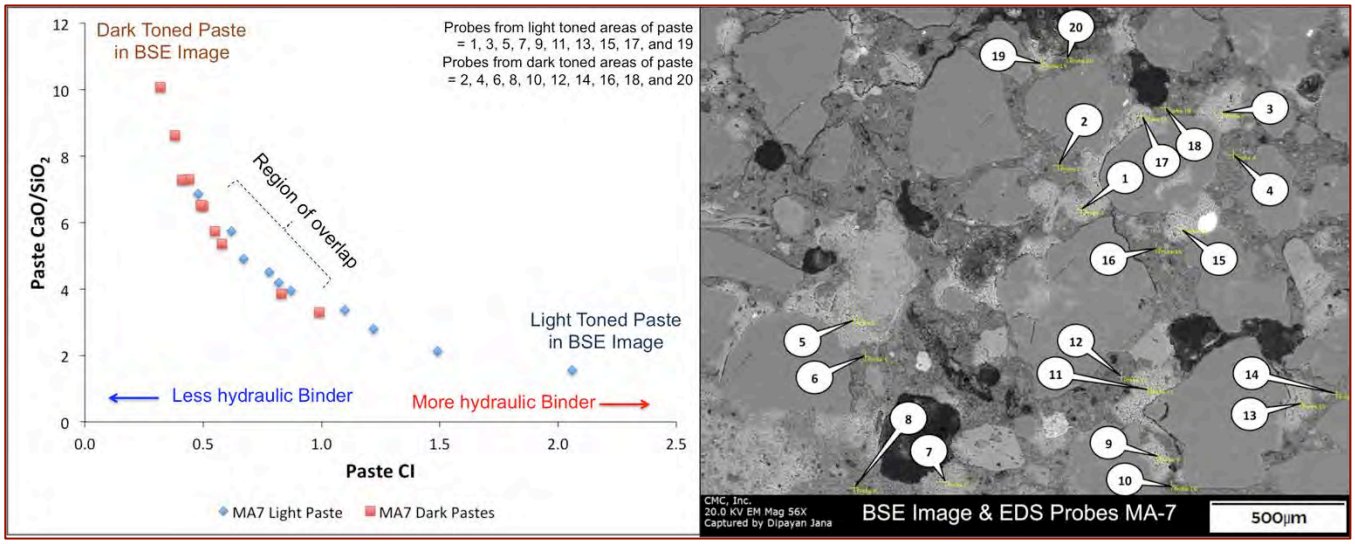

Figure 32: Higher calcium, lower silica, and lower paste-CI compositions of the darker patches of pastes (from slaked lime component), as opposed to the opposite chemical compositions of the lighter areas of pastes in the BSE image of the brick mortar MA7 having higher silica and lower calcium (from natural cement component). Probes in BSE image point to the individual measurement points in paste areas that are given in Appendix A94.

Since natural cements are produced from calcination (without slaking) of naturally occurring argillaceous limestone or dolomite (dolostone), natural cements can also share similar textural characteristics of patchy-textured pastes of high-Ca/low-Si and low-Ca/high-Si patches, if calcined from a limestone having higher calcite than dolomite to produce some excess free lime (CaO) from calcination that can hydrate during subsequent hydration to act similar to slaked lime from lime additions i.e. in having: (i) characteristics of hydration of hydraulic components of natural cement in having denser, less carbonated, higher silica and lower calcium contents (higher paste-CI), and, (ii) adjacent patchy areas of carbonated lime matrix of higher porosity, higher calcium and lower silica (lower paste-CI) contents from the hydrated lime component of natural cement.

The following optical and electron micrographs, and X-ray elemental mapping of a remnant, ground, calcined raw feed particle of natural cement in the brick masonry mortar MA7 show relative enrichment in silica, magnesium, aluminum, and iron, and depletion of calcium within the calcined feed relative to the carbonated lime surrounding that have resulted from the calcination of natural cement raw feed. Most calcined raw feed particles (or residual natural cements) show such characteristic Si-Mg-Al-Fe enrichments and Ca-depletions compared to the surrounding matrix. Free lime and magnesia, from calcination of calcite and dolomite, respectively reacted with silica from interstitial quartz and fused de-hydroxylated clay impurities in feed and formed β-C_2S and other calcium-magnesium-alumino-silicates as rims over the silica nuclei. Detection of rims of β-C_2S over interstitial silica nuclei, however, is more common in a freshly cured hardened paste of natural cement (for slow hydration of β-C_2S) than in a historic mortar as MA7.

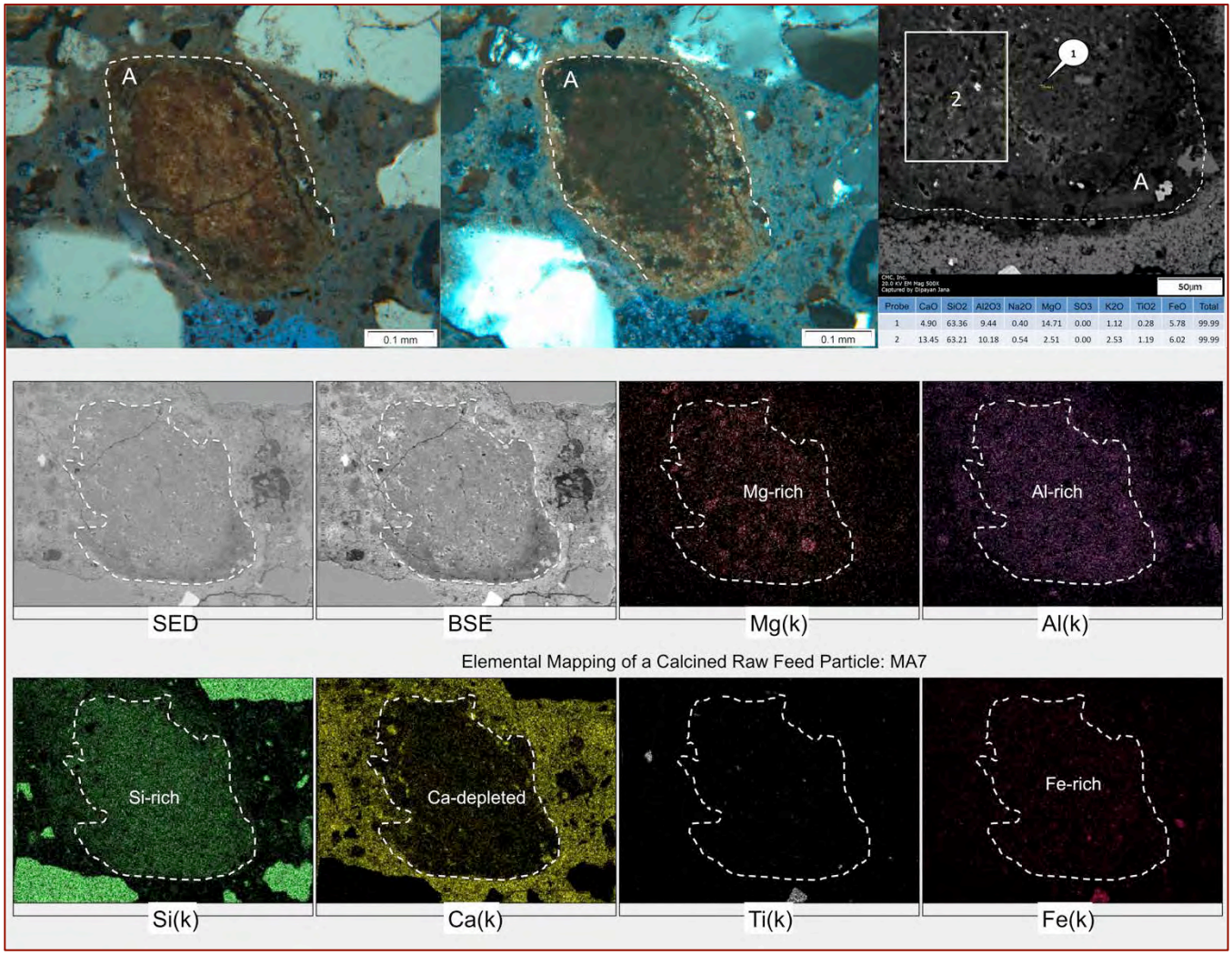

Figure 33: Optical micrographs (in PPL and XPL at top left and middle), backscatter electron image (top right), x-ray elemental analyses of a point '1' and area '2' on BSE image (analyses shown beneath the BSE image), and x-ray elemental mapping of a calcined raw feed particle (residual natural cement) in the brick mortar MA7 showing the characteristic optically isotropic nature of the particle in XPL (and dark gray to black in BSE image), and relative enrichment in Si, Mg, Al, and Fe and depletion in Ca in the particle from the surrounding carbonated lime matrix. Appendix A97 provides larger views of these images.

Depletion of Ca within the feed is due to hydration and loss of rims of β-C_2S and other calcium-magnesium-alumino-silicates over silica from the feed, leaving a skeletal particle rich in Si, Mg, Al, and Fe and depleted in Ca relative to the surrounding lime matrix. Enrichment in silica and alumina in the feed is possibly from an aluminosilicate amorphous phase formed from dehydroxylation of the clay impurities that has imparted the near-isotropic nature of raw feeds in XPL. The magnesium spots as islands within the feed represent locations of dolomite grains in the original dolomitic limestone feed.

Figure 34 shows similarity in overall chemistry and microstructure of calcined raw feed particles in natural cement-lime mortar in MA7 as seen in Figure 33, and, in a laboratory-cured modern Rosendale natural cement mortar. The dicalcium silicate hydraulic component of Rosendale natural cement shows spectacular development: (i) as rims over silica grains (along with limited hydration to CSH after 90 days of laboratory cure, both left and right images), (ii) or at isolated interstitial areas within a calcined feed (enclosed by dashed line in the right image), or, (iii) in detached silica (as quartz) grains (in left image). Calcined dolomite pseudomorph, dicalcium silicate hydraulic component, fused clay (amorphous aluminosilicate phase), and interstitial quartz – all within a calcined feed show their characteristic shades of gray tones in BSE image, as well as characteristic elemental compositions in SEM-EDS.

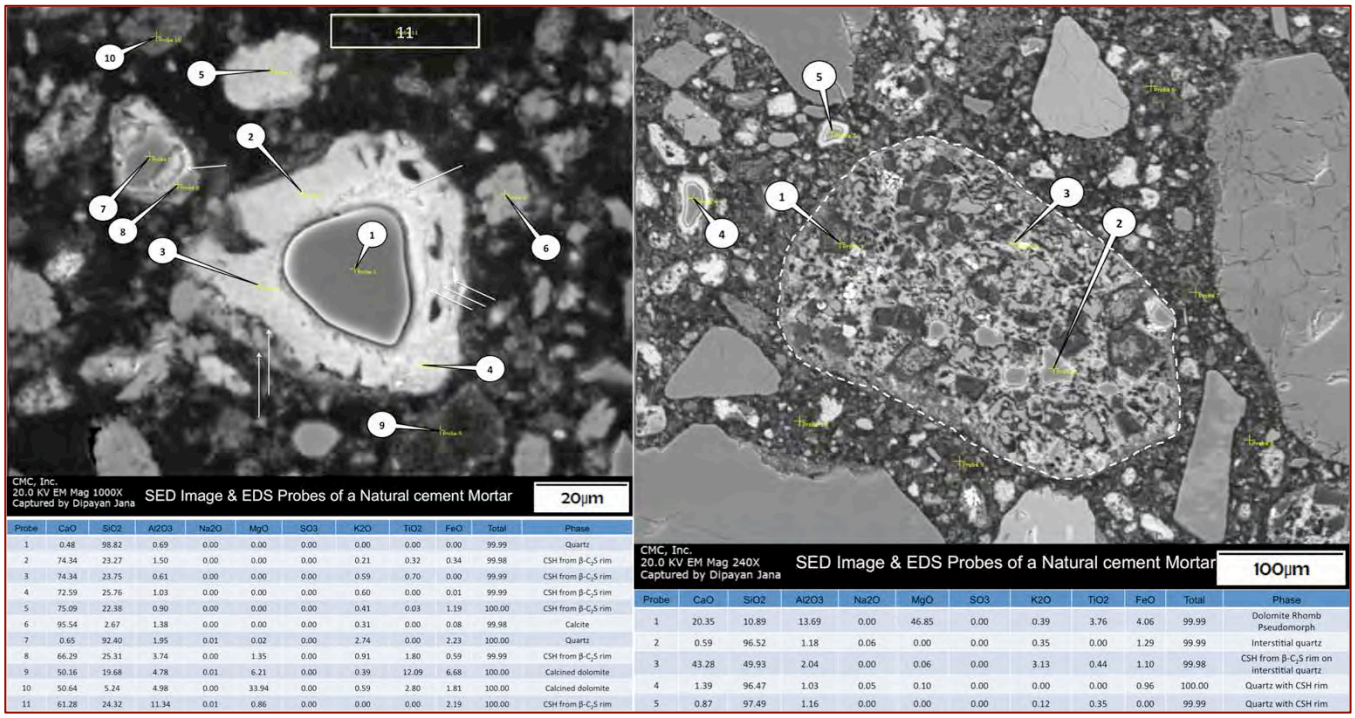

Probe	CaO	SiO2	Al2O3	Na2O	MgO	SO3	K2O	TiO2	FeO	Total	Phase
1	0.48	98.82	0.69	0.00	0.00	0.00	0.00	0.00	0.00	99.99	Quartz
2	74.34	23.27	1.50	0.00	0.00	0.00	0.21	0.32	0.34	99.98	CSH from β-C_2S rim
3	74.34	23.75	0.61	0.00	0.00	0.00	0.59	0.70	0.00	99.99	CSH from β-C_2S rim
4	72.59	25.76	1.03	0.00	0.00	0.00	0.60	0.00	0.01	99.99	CSH from β-C_2S rim
5	75.09	22.38	0.90	0.00	0.00	0.00	0.41	0.03	1.19	100.00	CSH from β-C_2S rim
6	95.54	2.67	1.38	0.00	0.00	0.00	0.31	0.00	0.08	99.98	Calcite
7	0.65	92.40	1.95	0.01	0.02	0.00	2.74	0.00	2.23	100.00	Quartz
8	66.29	25.31	3.74	0.00	1.35	0.00	0.91	1.80	0.59	99.99	CSH from β-C_2S rim
9	50.16	19.68	4.78	0.01	6.21	0.00	0.39	12.09	6.68	100.00	Calcined dolomite
10	50.64	5.24	4.98	0.00	33.94	0.00	0.59	2.80	1.81	100.00	Calcined dolomite
11	61.28	24.32	11.34	0.01	0.86	0.00	0.00	0.00	2.19	100.00	CSH from β-C_2S rim

Probe	CaO	SiO2	Al2O3	Na2O	MgO	SO3	K2O	TiO2	FeO	Total	Phase
1	20.35	10.89	13.69	0.00	46.85	0.00	0.39	3.76	4.06	99.99	Dolomite Rhomb Pseudomorph
2	0.59	96.52	1.18	0.06	0.00	0.00	0.35	0.00	1.29	99.99	Interstitial quartz
3	43.28	49.93	2.04	0.00	0.06	0.00	3.13	0.44	1.10	99.98	CSH from β-C_2S rim on interstitial quartz
4	1.39	96.47	1.03	0.05	0.10	0.00	0.00	0.00	0.96	100.00	Quartz with CSH rim
5	0.87	97.49	1.16	0.00	0.00	0.00	0.12	0.35	0.00	99.99	Quartz with CSH rim

Figure 34: BSE image and X-ray elemental analyses of a hardened modern Rosendale natural cement mortar (cured in the laboratory for 90 days, prepared by mixing a pre-packaged natural cement mortar with water, at a water-to-dry mortar powder mass ratio of 0.25, not from this study) showing layer-by-layer development of calcium silicate hydrate (CSH) from the original β-C_2S rims over interstitial quartz and silica from fused clay impurities in a calcined argillaceous dolostone raw feed. Left photo shows spectacular CSH rim formation (as layers that are marked with arrows) over a large and a small quartz grain that have been detached from their raw feeds. Right photo shows a calcined argillaceous dolostone raw feed of natural cement in the paste, that has the characteristic internal textures of: (i) dark grey to black rhombs of dolomite pseudomorphs rich in Mg, Al, Si and depleted in Ca (probe 1), (ii) interstitial silica in medium grey tones (probes 2, 4, and 5 all having bright white rims of β-C_2S), and (iii) β-C_2S formation as rims over silica (partially hydrated to CSH from 90 days of hydration) as bright white rims on medium grey silica areas (probe 3, 4, and 5). See Appendixes A97 and A98 for larger views of images and the oxide analyses tables for the probes.

BINDER COMPOSITIONS IN BRICK MASONRY MORTARS FROM SEM-EDS: BINDER HYDRAULICITY FROM CEMENTATION INDICES

Appendixes A86 through A105 provide results of detailed compositional analyses of binder fractions of brick masonry mortars in SEM-EDS. Several points (probes) were carefully selected in the interstitial binder areas between sand grains across a backscatter electron image or a secondary electron image, after examining pastes that are free from interference of any particulate matters so that a true representative composition of the paste can be obtained. Point-mode analyses, therefore, were preferred in most cases over area (raster)-mode to avoid any potential interference of sand or other non-binder particles. Major element oxide compositions of Si, Al, Ca, Mg, Fe (total), Na, K, and S were determined in point modes in several areas of pastes from multiple locations for each mortar.

Overall, carbonated lime pastes in brick masonry mortars are characterized by very high CaO, and, little or no SiO_2 whereas, denser patchy areas of pastes containing hydration products of natural cements (such as adjacent to ground calcined raw feeds or residual natural cements) show noticeably higher silica and lower calcium than the areas away from dense patches, or in the non-hydraulic lime mortars. These systematic compositional variations between two extremes of lime only-paste versus hydrated (lime-silica) lime-natural cement pastes are common in small scales within the mortars that showed patchy-textured paste in optical microscopy.

Table 7 summarizes results of 'average' chemical compositions of pastes determined from several areas of pastes for each brick masonry mortar by SEM-EDS (detailed compositions of each mortar are given in the Appendixes A86 through A105)

Mortar Paste	CaO	SiO_2	Al_2O_3	Na_2O	MgO	SO_3	K_2O	TiO_2	FeO	Total	Paste CI
MA1	84.54	9.23	1.86	0.09	2.93	0.08	0.20	0.07	1.00	100.00	0.33
MA2	70.89	15.77	3.94	0.14	3.96	0.00	0.88	0.28	4.13	100.00	0.70
MA3	67.72	17.16	5.11	0.01	3.10	0.00	1.06	0.64	5.19	100.00	0.86
MA4	88.17	7.10	1.65	0.00	0.09	0.00	0.44	1.34	1.21	99.99	0.26
MA5	81.15	11.40	2.80	0.00	0.29	0.00	0.57	0.39	3.38	99.99	0.55
MA6	82.96	9.63	2.65	0.02	0.40	0.11	0.98	0.44	2.79	99.99	0.40
MA7	62.54	16.63	8.95	3.53	1.04	0.01	3.53	0.70	3.08	100.00	1.08
MA8	74.86	10.08	5.53	0.11	1.05	0.00	0.53	0.79	7.06	100.00	0.61
MA9	72.88	13.37	4.10	0.04	2.81	0.30	0.75	1.28	4.46	100.00	0.61
MA10	72.46	12.61	3.01	0.10	2.73	0.00	0.57	4.25	4.27	99.99	0.59
MA11	89.51	5.87	2.24	0.00	0.01	0.00	0.45	0.22	1.69	99.99	0.24
MA12	90.22	5.64	1.82	0.03	0.07	0.00	0.52	0.05	1.66	99.99	0.21

Table 7: Results of 'average' chemical compositions of paste fractions of brick masonry mortars determined by SEM-EDS. Paste CI is calculated from: CI =$[(2.8\times SiO_2)+(1.1\times Al_2O_3)+(0.7\times FeO)]$ / $[(CaO) + (1.4\times MgO)]$. MA7 provides an 'average' composition from the darker and lighter paste patches of different compositions. It shows the highest paste-CI of 1.08 amongst all brick mortars, indicating highest proportion of natural cement component added to this mortar amongst the 12 brick mortars examined.

Eckel's Cementation Index (CI)

Since the 19th century, various authors have proposed many chemical parameters to define 'hydraulic activity' of lime i.e. its ability to harden under water through hydration rather than carbonation (Bartos et al. 2000, Callebaut et al 2000, 2001, Elsen et al. 2012). For example, hydraulic index (HI) has been proposed as the ratio between the percentage of silica and alumina to the percentage of lime. This parameter, however, is criticized for not subdividing alumina and silica within the lime sample and assuming these two to have similar reactivities, which is not the case. Cementation index (CI) includes percentages of lime, silica, alumina, iron, and magnesia. Vicat (1837) proposed feebly hydraulic, hydraulic, and eminently hydraulic limes having CI of 0.10-0.16, 0.16-0.31, and 0.32-0.42, respectively. Eckel (1922) proposed feebly and eminently hydraulic lime having CI 0.3-0.7 and 0.7-1.1, respectively. Boynton (1980) proposed feebly hydraulic, hydraulic, and eminently hydraulic lime having CIs 0.3-0.5, 0.5-0.7, and 0.7-1.1, respectively. Like HI, this CI method of calculation for defining lime hydraulicity has also been criticized because not all silicates and aluminates are necessarily reactive, and if a certain amount of clay impurities is necessary to achieve hydraulicity, its degree will also be subjected to the manufacturing process and to the uniformity of raw materials. Eckel (1922) proposed CI with assumption that silica and lime combine to form C_3S, but this only forms at higher firing temperatures (i.e. in Portland cement manufacturing) than normally associated with lime calcination (where silica and lime combines to form β-C_2S). Eckel believed that C_2A forms with the combination of lime and silica, but instead C_2AS is usually formed in a calcined impure limestone, which is a non-hydraulic component of hydraulic lime, and cannot therefore be added to the strength development of lime mortar.

Despite such criticisms of using HIs and CIs in the past to define and classify various hydraulic binders, however, extension of such calculations for pastes (i.e. after the manifestation of hydraulicity and strength development in mortars) may not be all meaningless, specially if such parameter separates mortars having different hydraulic natures due to different proportions of lime and natural cement components in the original binders, especially if such classification scheme from CI is also confirmed by microscopy.

The twelve brick masonry mortars represent a good set to show how effective this CI classification/parameterization scheme is for pastes having different hydraulic characteristics that are also confirmed from optical and scanning electron microscopy. Stone masonry mortars are excluded for various degrees of leaching and alterations of pastes, where the original binder composition is more difficult to ascertain due to lime leaching. Lime leaching, however, showed abnormally high CIs, and thus still helped to differentiate leached versus less-leached areas of pastes from the respective CI values. Figure 35 shows results of elemental analysis of various points (probes) across the pastes in different brick masonry mortars in SEM-EDS, plotted in Eckel's cementation index (Eckel, 1922) calculated for each analysis point against paste-SiO_2 and paste-CaO, and plot of paste-SiO_2 versus paste-CaO. Eckel's cementation index (CI) is calculated from bulk compositions of various lime and cement binders (dry powders) as:

$$CI = [(2.8\times SiO_2)+(1.1\times Al_2O_3)+(0.7\times FeO)] / [(CaO) + (1.4\times MgO)].$$

A non-hydraulic (e.g., high-calcium) lime has the lowest CI, and, CI increases for various hydraulic binders with increasing hydraulicity, e.g., with increasing addition of natural cement to a lime-only binder, and, continue to further increase for natural cement, slag cement, Portland cement, etc. with increasing hydraulic components.

Although originally devised by Eckel as a chemical classification scheme for various hydraulic cement types, the concept is extended here for the 'pastes' of various hydraulic lime mortars that are encountered in the project to determine whether or not there are similar variations in CI's, hence hydraulicities of various mortar binders across the samples analyzed, and, if variations in microstructural properties of pastes determined in optical microscopical examinations from homogeneous carbonated lime mortar type to patchy-textured lime-natural cement mortars can be further reproduced in terms of similar variations in chemical compositions (CIs) across the types as well. Hence, major element oxide compositions of pastes determined from various areas of the binders in between sand grains in SEM-EDS (expressed as oxides) are used here in the calculation of CIs of pastes, instead of dry powders used by Eckel (1922) for classification of hydraulicities of various lime and cement binders.

Despite many criticisms, extension of CI as a parameter for expressing the overall chemical composition of pastes has several advantages.

1. First, since any phase other than paste *per se* has very different CI (e.g., quartz grains show abnormally high CI for lack of CaO and MgO in quartz) any interference in the paste data in SEM-EDS from any microscopical grains of quartz can be easily detected by off-the-chart high CI values compared to the 'normal' range of CI's of hydraulic binders that for dry powders usually vary from 0.1 to 1.5, or maximum 2.0 (that too for natural or Portland cements only). Therefore, analyses that have produced 'reasonable' values of CIs were selected for representative compositions of pastes that are free from any aggregate interference.
2. Secondly, CI can conveniently differentiate a non-hydraulic lime binder (CIs < 0.5) from a natural cement one (CIs >0.5), and show a systematic range of values from varying proportions of lime and natural cements.
3. Thirdly, the extent of local variations in compositions of paste in a patchy-textured paste of blended lime-natural cement binder can be readily determined from large variations in CIs over a small area in the binder.
4. Additionally, extension of CI for weathered stone masonry mortars show effective determination of lime leached areas in pastes from very high CIs (from very high silica and low calcium contents of leached areas, Table 8, Figure 40).

Plots in the left column in Figure 35 incorporated all 'screened' data points from pastes for each brick masonry mortar (excluding any interference from aggregates having abnormally high CI data) where all data points fall within a maximum CI of 1.6. Plots in the right column in Figure 35 cleaned out the data by having similar plots of 'average' compositions of binder for each mortar.

Both sets of data points show a vey systematic trend of variations in paste-CaO, SiO_2 contents with paste-CIs, as well as negative correlations between calcium and silica. Most importantly, such plots clearly differentiate the most hydraulic lime-natural cement mortar MA7 from non-hydraulic lime mortars MA11 and MA12 in having very high

and very low CIs, respectively. All other brick masonry mortars fall in between these two extreme CIs, as anticipated from optical microscopical examinations.

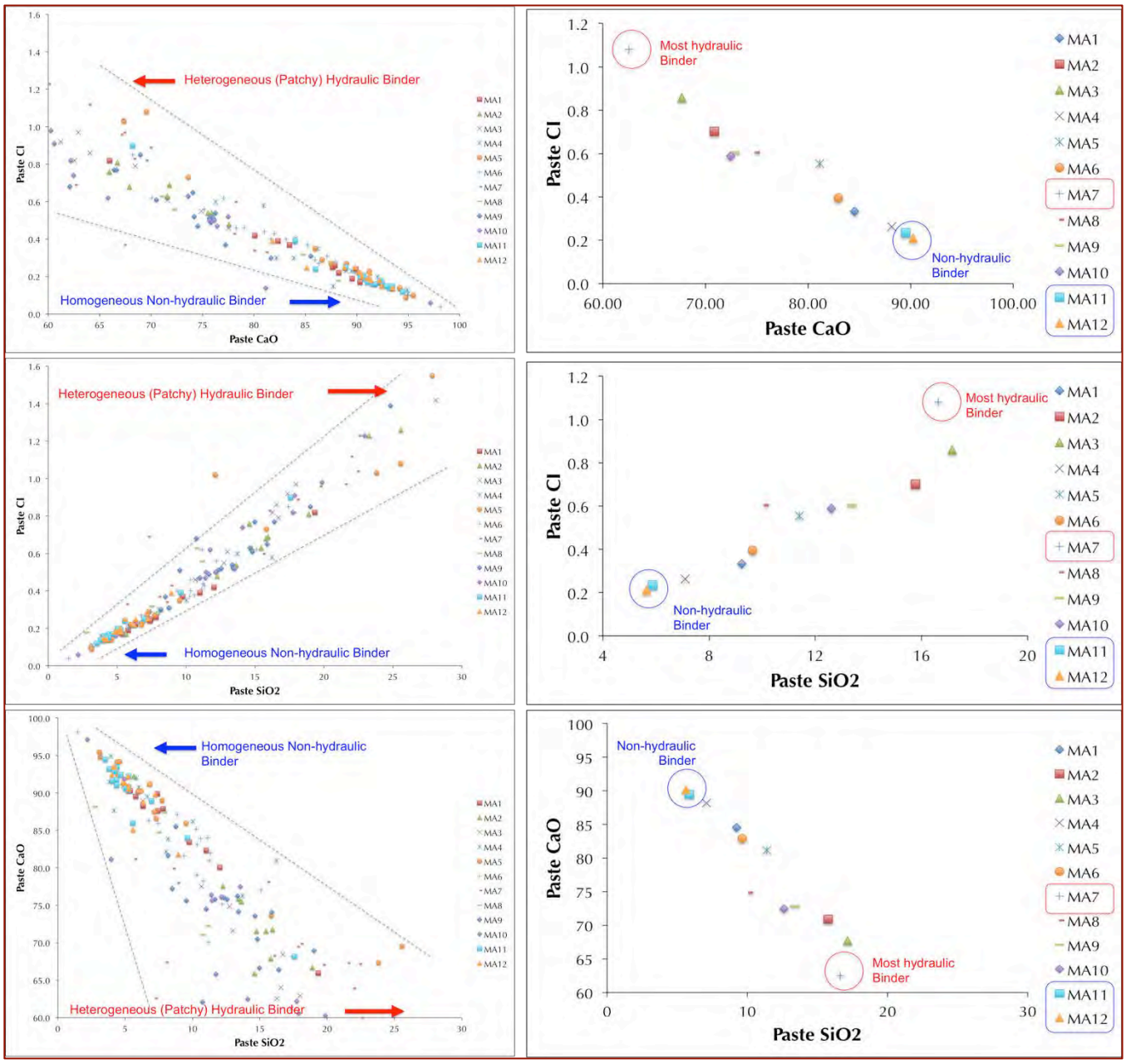

Figure 35: Left column shows results of elemental analyses of various points across the paste in different brick masonry mortars in SEM-EDS, plotted in Eckel's cementation index (CI) calculated for each analysis point against SiO_2 and CaO, and paste-SiO_2 versus paste-CaO. Right column shows similar plots but average of all analysis points for each mortar, where each data point represents average composition of binder for each mortar. The most hydraulic mortar, MA7 is marked in red and the least hydraulic ones (MA11 and MA12) are marked in blue.

Results show some startling similarities (as anticipated) to the conclusions derived from optical microscopy of brick masonry mortars from non-hydraulic hydraulic mortar types in MA11 and MA12 at one extreme to most hydraulic patchy-textured lime-natural cement mortar (having the highest proportion of natural cement amongst all brick mortars) in MA7 at the opposite extreme, and all other mortar types fall in between these two extremes. This differentiation of mortar types based on their CIs is clear in the right column in Figure 35, i.e. after averaging out all

data obtained across the paste areas for each mortar. Left column (incorporating all data from pastes having CIs up to 1.6) shows another interesting feature i.e. less noise in the non-hydraulic end where paste is more texturally homogeneous, chemically and texturally uniform, featureless, non-patchy, and, more noise (fanning out of data) towards the hydraulic ends of binders where paste is more patchy i.e. having small-scale chemical heterogeneities and having mixtures of both low-CI (less-hydraulic, slaked lime) and high-CI (more-hydraulic, natural cement hydrates) areas. Therefore, such fanning out of data towards the hydraulic end in the left column clearly shows increasing local heterogeneities introduced from increased hydraulicity of lime-natural cement blended paste, as opposed to more uniform composition of high-calcium, non-hydraulic lime-only paste.

BINDER MICROSTRUCTURES IN STONE MASONRY MORTARS FROM SEM

Dense (Ca-Si-rich) Versus Carbonated Lime (Ca-rich) Versus Leached Lime (Si-Mg-Al-Fe rich and Ca-poor) Patches of Pastes

PPL and XPL thin section photomicrographs in Figures 23 through 29 (and also in Appendixes A54 through A74) detected three types of pastes having various degrees of leaching, alternation, and carbonation in the stone masonry mortars SMA1, SMA2, SMA4, and SMA5. Further SEM-EDS analyses of these paste areas revealed their characteristic compositional differences, classified as Types 1, 2, and 3 pastes:

1. Type 1: A dense, carbonated paste having both calcium and silica in most unaltered condition (Ca > to slightly < Si > rest of the elements) that was originally formed from hydration and carbonation of hydraulic and non-hydraulic components of the lime-natural cement binder;
2. Type 2: A severely carbonated lime-rich matrix of paste, where Ca far outweigh all other elements, similar to a typical carbonated non-hydraulic lime matrix, as also found in SMA3; and,
3. Type 3: Optically isotropic bands or areas or patches of highly altered paste that are severely leached in calcium (and hence relatively enriched in Si, Mg, Al, Fe) relative to the surrounding or adjacent Ca-rich paste areas, mostly occurring as gelatinous Si, Mg, Al, Fe-rich patches. These paste areas are associated with Type 1 paste areas in mostly SMA1, SMA2, SMA4, and not so severely as the other three in SMA5. Coarsely crystalline secondary calcite grains are detected as 'floated' in the overall optically isotropic leached lime patches in SMA1, SMA2, and SMA4.

The following sets of photographs in Figures 36 through 38 are condensed from far more detailed figures and analyses of all three types of pastes that are provided in Appendixes A108 through A133. In all these photomicrographs, leached areas or patches of pastes are identified by dark areas in BSE images, whereas less leached and carbonated areas are characteristically lighter toned. Corresponding X-ray elemental analysis of silica (Si), calcium (Ca), aluminum (Al), magnesium (Mg), Titatium (Ti), and iron (Fe) show depletion of Ca and relative enrichment of Si, Mg, Al, and Fe in the leached areas of pastes compared to those values in the adjacent less-leached or carbonated areas.

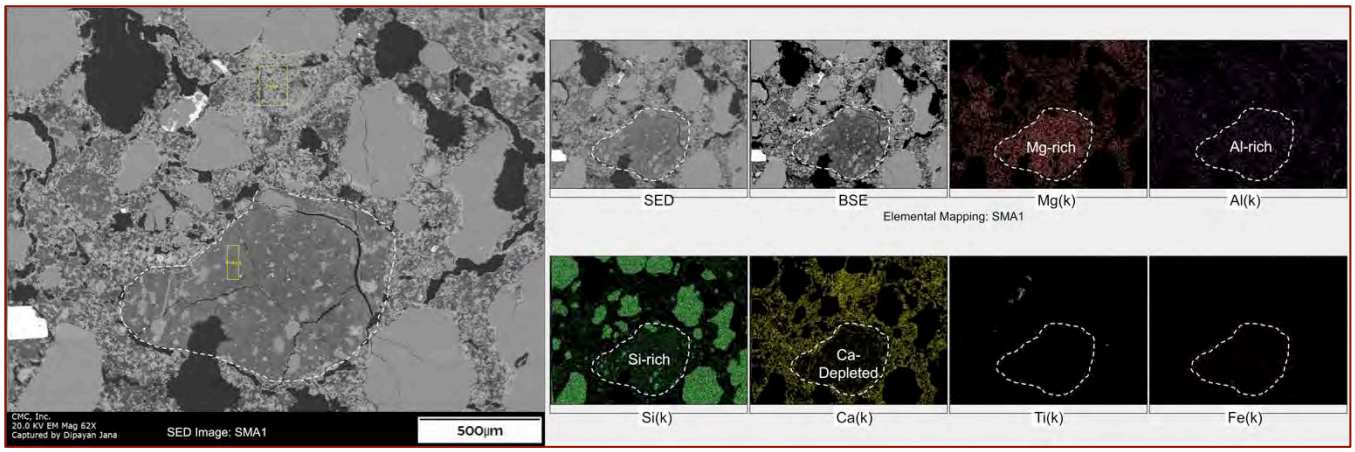

Figure 36: Secondary electron detector (SED) image (left) and corresponding X-ray elemental mapping of an isolated patch of paste (Type 3 paste, marked in dashed line) in the stone masonry mortar SMA1 that is depleted in Ca from lime leaching and hence relatively enriched in Si, Mg, Al, and Fe from the Ca-rich carbonated lime matrix surrounding (Type 2 paste).

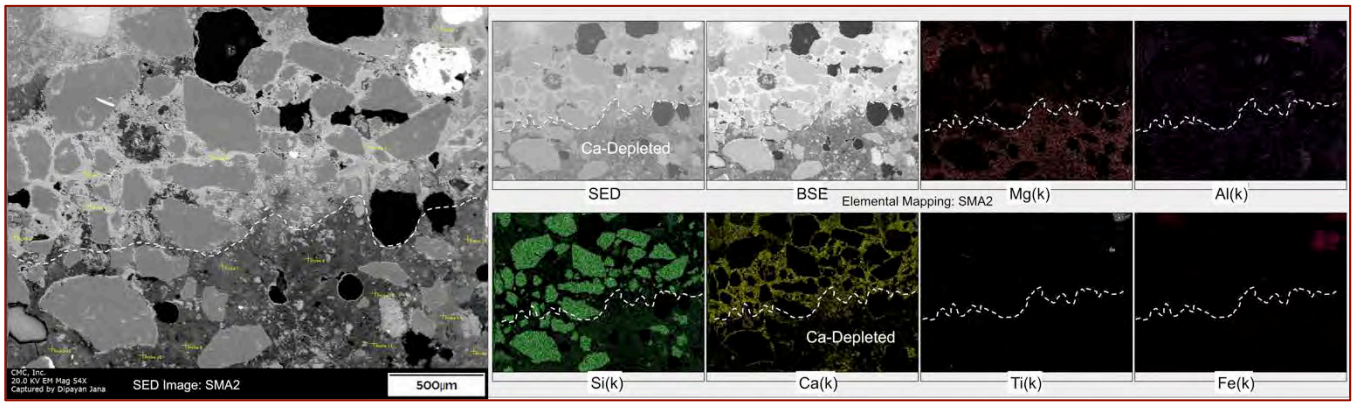

Figure 37: Secondary electron detector (SED) image (left) and corresponding X-ray elemental mapping of lighter and darker areas of pastes (separated by dashed line) in the stone masonry mortar SMA2 that are depleted in Ca from lime leaching and hence relatively enriched in Si, Mg, Al, and Fe in the dark areas at the bottom half (Type 3 paste) compared to the Ca-rich carbonated lime matrix in the brighter areas at top half (Type 2 paste).

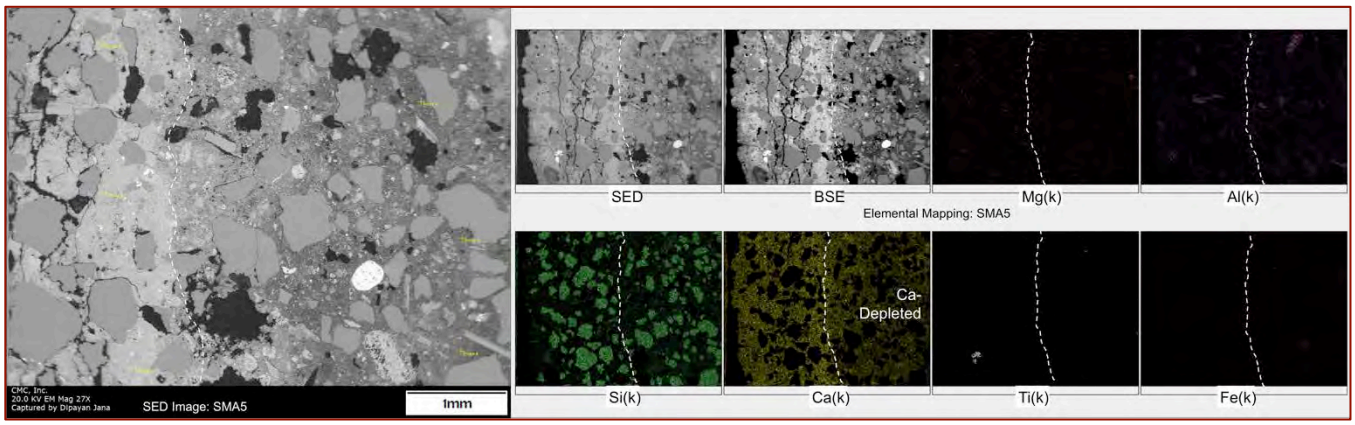

Figure 38: Secondary electron detector (SED) image (left) and corresponding X-ray elemental mapping of lighter and darker areas of pastes (separated by dashed line) in the stone masonry mortar SMA5 that has intermediate Ca-Si composition in the dark areas at the right half (Type 1 paste) compared to the Ca-rich carbonated lime matrix in the brighter areas at the left half (Type 2 paste, which contains parallel microcracks).

The next series of plots in Figures 39 and 40 show compositional variations of these three broad types of pastes as detected in the SEM-EDS studies of stone masonry mortar.

The figures classified the salient compositional variations in three types of pastes from: (i) severely carbonated lime matrix of a typical non-hydraulic lime mortar, as detected in SMA3 and as patches in other mortars (Type 2) to (ii) severely leached lime paste patches and areas detected in SMA1, SMA2, SMA4 (Type 3), to (iii) somewhat intermediate in composition of calcium and silica where paste is carbonated but not leached, at least not as severely as in the Type 3 leached pastes (Type 1).

The plots in Figure 39 show systematic trends of paste compositions in the three chosen chemical parameters of CaO, SiO_2, and CaO/SiO_2, as anticipated for the three types of paste with a gradation between the three types.

1. The severely carbonated lime matrices in Type 2 pastes are characterized by very high CaO (>70 percent), where CaO contents far outweighed all other oxides.
2. On the other hand, the severely leached Type 3 pastes are characterized by very low CaO contents (as low as <10 percent), where SiO_2 contents approached to far exceed CaO contents (along with higher MgO, Al_2O_3, and FeO contents) compared to the surrounding lime matrix.
3. Pastes that are neither severely carbonated nor leached (Type 1) show somewhat intermediate values of these parameters, which are more representative of the original pastes from lime-natural cement binders.

Appendix A108 through A133 show detailed compositional variations of pastes in all stone mortars as determined from extensive SEM-EDS studies.

Data points in Figure 39 are actual compositional plots, not the average of each paste type that are shown in Figure 40.

Notice the systematic variations in calcium and silica contents across the three paste types from very high calcium and lowest silica carbonated lime pastes towards the lowest calcium highest silica leached paste end.

Figure 39 and Table 8 summarize all compositional variations between these three broad paste compositions as encountered in Appendix A108 through A133 for five stone masonry mortars as the average compositions for each paste Type so that the characteristic compositions for each paste type can be seen.

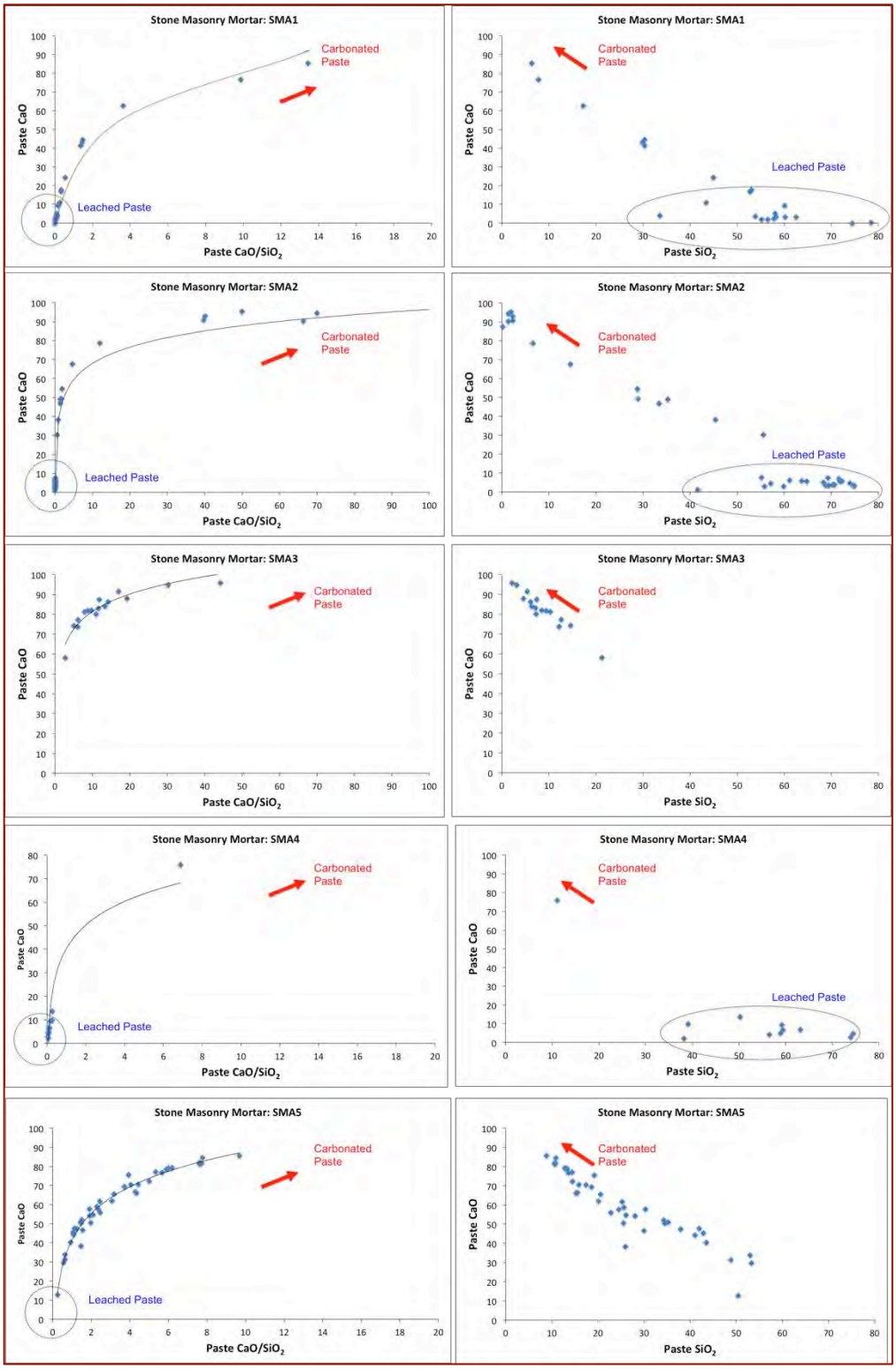

Figure 39: Plots of CaO, SiO_2, and CaO/SiO_2 of pastes of five stone masonry mortars determined from SEM-EDS showing systematic compositional variations in pastes from: (a) severe carbonation of pastes producing CaO contents far outweighing SiO_2 (Type 2 paste, in red), to (b) less carbonated, more pristine pastes having intermediate CaO and SiO_2 contents (Type 1 paste) to (c) leached lime paste (in blue, Type 3 paste) having low to very low CaO contents, SiO_2 contents approaching to far exceeding CaO (also enriched in MgO, Al_2O_3, and FeO), and, corresponding variations in CaO/SiO_2 ratios from very high to low, respectively, with lowest ratios for severely leached paste having gelatinous silica formation (ellipses in right column plots). Notice SMA3 does not have leached lime patches in paste as noticed in its absence in optical and electron microscopy. Also SMA5 does not have as leached areas in paste as those found as optically isotropic patches in SMA1, SMA2, and SMA4.

Leached areas of pastes are characterized by abnormally high CIs (>5.00) due to loss of calcium and enrichment of silica. In these areas, such very high CIs are simple artifacts of lime leaching and not related to the hydraulicity of pastes. Carbonated areas, i.e. the other extremes show very low CIs (<0.60). Pastes having both carbonation and silica from hydration of hydraulic components of lime have intermediate CIs around 1.00 to 2.00.

SMA1, SMA2, and SMA4 show a lot of data towards the leached paste ends (circled in the left column graphs), SMA5 shows limited data, whereas SMA3 shows no data at all. Therefore, these plots are helpful to determine the proportions of leached areas in paste and the degree of lime leaching.

BINDER COMPOSITIONS IN STONE MASONRY MORTARS FROM SEM-EDS: LEACHED VERSUS CARBONATED PASTES

Table 8 and Figure 39 summarize the difference in chemical compositions of three broad types of pastes encountered in stone masonry mortars i.e.: (i) Type 1 paste having intermediate calcium and silica contents, versus (ii) Type 2 typical carbonated lime pastes having calcium as the dominant element (>70% CaO), versus (iii) Type 3 paste severely leached in lime (<10% CaO) and enriched in silica. Results given in Table 8 are 'average' taken from multiple analyses across the mortars for each paste type.

	Probe	CaO	SiO_2	Al_2O_3	Na_2O	MgO	SO_3	K_2O	TiO_2	FeO	Total	Paste CI
SMA1	Leached Paste, Dark in BSE, Type 3	4.82	59.33	9.49	2.57	15.48	0.23	0.67	0.93	6.48	100.00	5.34
SMA1	Carbonated Paste, Light in BSE, Type 2	74.92	10.48	2.15	0.05	2.04	0.01	5.92	0.01	4.42	100.00	0.47
SMA2	Leached Paste, Dark in BSE, Type 3	5.03	67.64	7.79	0.49	11.50	0.00	0.36	0.31	6.88	100.00	10.37
SMA2	Carbonated Paste, Light in BSE, Type 2	90.44	2.63	0.42	0.00	0.07	0.00	0.27	5.36	0.81	100.00	0.10
SMA3	Carbonated Paste, Type 2	84.16	7.81	3.78	0.02	0.75	0.00	0.73	0.29	2.47	100.00	0.34
SMA4	Leached Paste, Dark in BSE, Type 3	6.58	57.31	13.31	0.29	8.27	0.00	0.69	0.85	12.70	100.00	-
SMA4	Carbonated Paste, Type 2	75.91	11.04	3.15	0.05	6.38	0.00	0.52	0.49	2.46	100.00	0.43
SMA5	Carbonated Paste, Light in BSE, Type 3	76.36	13.86	3.52	0.10	0.89	0.22	1.44	0.52	3.08	100.00	0.59
SMA5	Ca-Si Paste, Type 1	47.39	34.86	7.08	0.67	1.37	0.72	2.04	2.09	3.79	100.00	2.14

Table 8: SEM-EDS analyses of pastes in stone masonry mortars showing 'average' compositions of: (i) lime-leached pastes (Type 3) having very low calcium and very high silica (along with noticeable alumina, magnesia, and iron), (ii) typical carbonated lime matrix having calcium as the dominant constituent (Type 2), and (iii) paste having intermediate calcium and silica (Type 1). High Paste-CIs in leached pastes are simple artifacts of lime leaching, and not indicative of paste hydraulicity.

Enrichment of silica in the leached paste areas (Type 3) also enriched alumina, magnesia and iron compared to the other paste types.

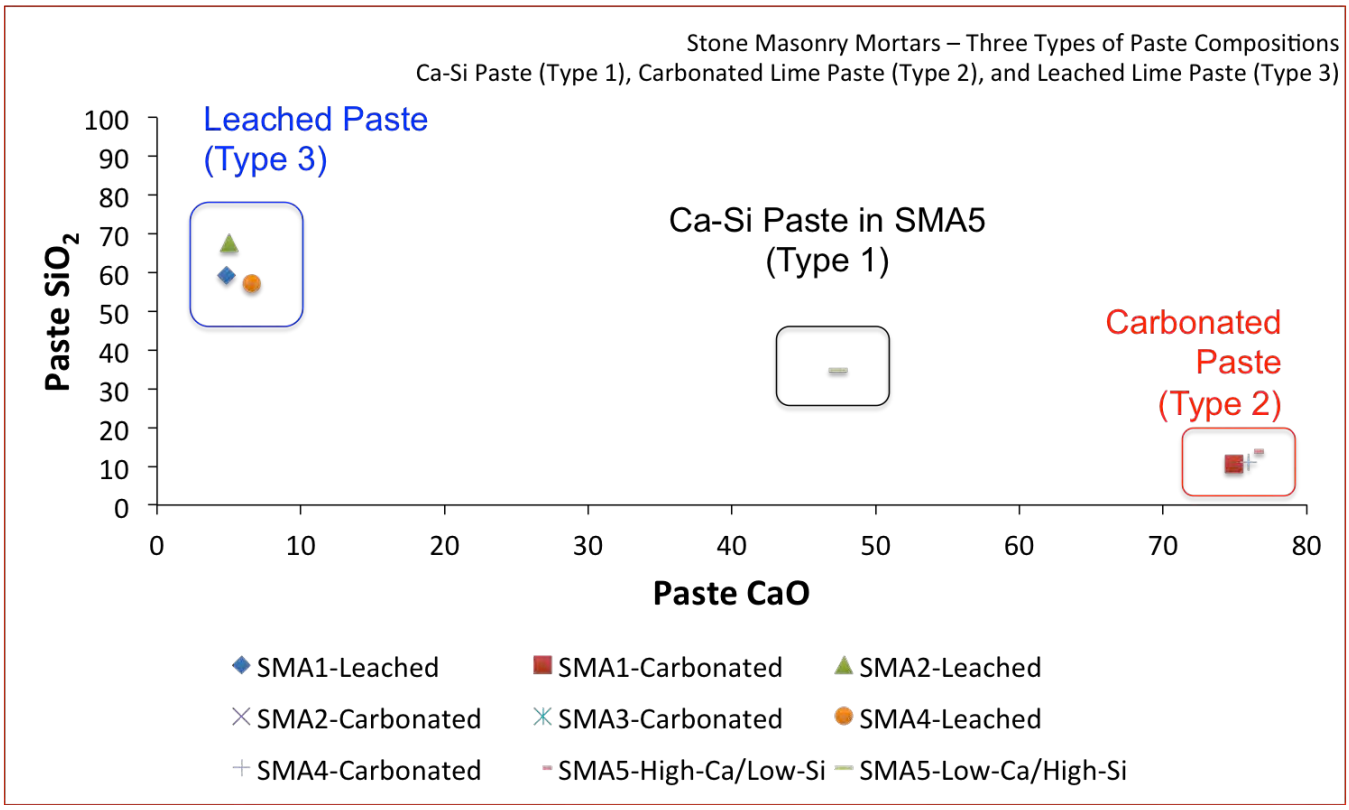

Figure 40: SEM-EDS analyses of pastes in stone masonry mortars showing 'average' compositions of: (i) lime-leached (optically isotropic) pastes (Type 3) having very low calcium and very high silica (probably of silica gel, along with noticeable alumina, magnesia, and iron), (ii) typical carbonated lime matrix (highly birefringent) having calcium as the dominant constituent (Type 2), and (iii) paste having intermediate calcium and silica (Type 1). Detailed compositions of pastes are given in Appendixes A108 through A133.

MINERALOGICAL COMPOSITIONS OF MORTARS FROM X-RAY DIFFRACTION

The following Tables 9 and 10 summarize results of semi-quantitative mineralogical compositions of bulk mortars from X-ray diffraction, and, sources of major minerals as suspected or determined from optical microscopy.

Sample ID	Quartz	Calcite	Gypsum	Biotite	Illite	Vaterite
Brick Masonry Mortars						
8-69-MA1	82.1	13.0	-	4.9	-	-
4-85-MA2	78.2	16.2	2.7	3.0	-	-
1/2-121-MA3	66.3	20.2	3.4	-	10.1	-
3-142-MA4	72.8	19.5	-	7.8	-	-
5-1-MA5	74.0	22.6	-	3.4	-	-
5-5-MA6	75.9	21.9	-	2.2	-	-
3-16-MA7	63.2	29.5	7.3	-	-	-
2-31-MA8	69.1	26.5	4.4	-	-	-
1-34-MA9	85.2	14.8	-	-	-	-
4-41-MA10	65.3	23.1	7.7	3.9	-	-
6-56-MA11	51.1	20.6	6.9	5.8	12.2	3.4
6-64-MA12	66.9	15.7	2.9	3.4	11.0	-

Stone Masonry Mortars						
1-94-SMA1	68.5	28.3	3.1	-	-	-
1-94-SMA2	74.7	9.9	-	3.0	12.4	-
3-138-SMA3	81.3	15.1	-	3.6	-	-
3-142-SMA4	97.3	2.7	-	-	-	-
6-81-SMA5	57.9	28.1	2.1	2.6	9.3	-

Table 9: Mineralogical compositions of mortars from X-ray diffraction. Semi-quantitative results are obtained from search/match module of MDI's Jade software using ICDD's mineral database.

X-ray diffraction patterns of bulk brick and stone masonry mortars are shown in Appendixes A75 through A83.

Sample ID	Quartz	Calcite	Gypsum	Biotite	Illite	Vaterite
Brick Masonry Mortars						
8-69-MA1	Aggregate	Binder	-	Sand, Feed	-	-
4-85-MA2	Aggregate	Binder	Acid Rain, Plaster	Sand, Feed	-	-
$^{1}/_{2}$-121-MA3	Aggregate	Binder	Acid Rain, Plaster	-	Sand, Feed	-
3-142-MA4	Aggregate	Binder	-	Sand, Feed	-	-
5-1-MA5	Aggregate	Binder	-	Sand, Feed	-	-
5-5-MA6	Aggregate	Binder	-	Sand, Feed	-	-
3-16-MA7	Aggregate	Binder	Acid Rain, Plaster	-	-	-
2-31-MA8	Aggregate	Binder	Acid Rain, Plaster	-	-	-
1-34-MA9	Aggregate	Binder	-	-	-	-
4-41-MA10	Aggregate	Binder	Acid Rain, Plaster	Sand, Feed	-	-
6-56-MA11	Aggregate	Binder	Acid Rain, Plaster	Sand, Feed	Sand, Feed	Binder
6-64-MA12	Aggregate	Binder	Acid Rain, Plaster	Sand, Feed	Sand, Feed	-
Stone Masonry Mortars						
1-94-SMA1	Aggregate	Binder	Acid Rain, Plaster	-	-	-
1-94-SMA2	Aggregate	Binder	-	Sand, Feed	Sand, Feed	-
3-138-SMA3	Aggregate	Binder	-	Sand, Feed	-	-
3-142-SMA4	Aggregate	Binder	-	-	-	-
6-81-SMA5	Aggregate	Binder	Acid Rain, Plaster	Sand, Feed	Sand, Feed	-

Table 10: Sources of different minerals detected in XRD studies. Gypsum could come from acid rain, or a plaster component added with lime binders. Biotite and illite could come from sand or, more plausibly, from argillaceous impurities of un-calcined (or under-calcined) raw feeds.

Role of Gypsum – Detection of gypsum in seven out of twelve brick masonry mortars and two out of five stone masonry mortars indicate possible introduction of dissolved sulfate ions from the environment (e.g., acid rain weathering) and/or from the adjacent brick or stone masonry units, and precipitation of secondary calcium sulfate salts (Hughes and Bargh 1982, Lubell et al. 2004, Charola and Lazzarin 2009). Gypsum crystallization in pore spaces can develop pressures to exert stresses, which can potentially cause distress in masonry units or mortars, such as spalling of exposed surfaces of brick and stone masonries from cryptoflorescence (by pressures of gypsum crystallizations beneath the surfaces). Present mortars containing gypsum, however, do not show any evidence of distress or cracking (except perhaps parallel microcracking seen in one stone masonry mortar, SMA5) to suspect such mechanism in the field. Microcracking in SMA5 could form from either or a combination of freezing at moist conditions, and, secondary gypsum crystallization.

Gypsum, however, could have been added as a separate plaster component along with lime in those mortars, in which case, its presence does not necessarily warrant any potential distress. Field evidence of the conditions of brick

and stone masonry units adjacent to these mortars containing gypsum are needed to evaluate any potentially deleterious role of gypsum in the performance of masonry units and mortars.

CHEMICAL ANALYSES

SAND CONTENTS FROM ACID-INSOLUBLE RESIDUES AND WATER CONTENTS PLUS CARBONATION FROM LOSS ON IGNITION

Tables 11 and 12 summarize results of acid-insoluble residue contents of brick and stone masonry mortars, respectively, after digesting pulverized (US No. 50) portions of bulk mortar fragments in hydrochloric acid, and loss on ignition of separate aliquots of pulverized mortars to 110°C, 550°C, and 950°C, which correspond to free water, combined (hydrated) water, and degree of carbonation, respectively. Due to the presence of siliceous sand only and no calcareous components in sands, the determined acid-insoluble residue contents correspond to the sand contents of the mortars.

Components	MA1	MA2	MA3	MA4	MA5	MA6	MA7	MA8	MA9	MA10	MA11	MA12
Acid-Insoluble Residue (%)	79.5	69.0	67.9	73.8	75.0	72.9	62.5	77.1	77.8	71.3	73.2	74.4
Loss on Ignition: From 0°C to 110°C (Free Water) (%)	0.80	1.60	1.00	0.20	0.30	1.40	1.90	0.80	0.49	0.50	0.50	0.39
Loss on Ignition: From 110-550°C (Combined Water) (%)	3.00	7.10	5.00	2.80	2.40	4.40	4.10	2.50	3.60	3.00	2.30	2.00
Loss on Ignition: From 550-950°C (Carbonation, CO_2) (%)	7.30	6.90	7.70	9.60	9.70	8.50	7.40	7.40	7.60	7.90	7.50	7.20

Table 11: Hydrochloric acid-insoluble residue contents and loss on ignition to 110°C, 550°C and 950°C for brick masonry mortars.

Components	SMA1	SMA2	SMA3	SMA4	SMA5
Acid-Insoluble Residue (%)	53.9	72.0	76.6	-	59.3
Loss on Ignition: From 0°C to 110°C (Free Water) (%)	2.60	3.30	1.10	-	1.70
Loss on Ignition: From 110-550°C (Combined Water) (%)	4.00	3.40	2.30	-	3.70
Loss on Ignition: From 550-950°C (Carbonation, CO_2) (%)	10.70	5.10	7.20	-	11.70

Table 12: Hydrochloric acid-insoluble residue contents and loss on ignition to 110°C, 550°C and 950°C for stone masonry mortars. There wasn't enough sample left for SMA4 to do chemical analysis.

A plot of hydrate water contents in the brick masonry mortars i.e. loss on ignition from 110°C to 550°C, with their corresponding average CI of paste did not produce a strong positive correlation, as anticipated, since both parameters follow the overall hydraulicity of paste (the higher the hydraulic component in a binder, the higher would be the hydrate water content of paste).

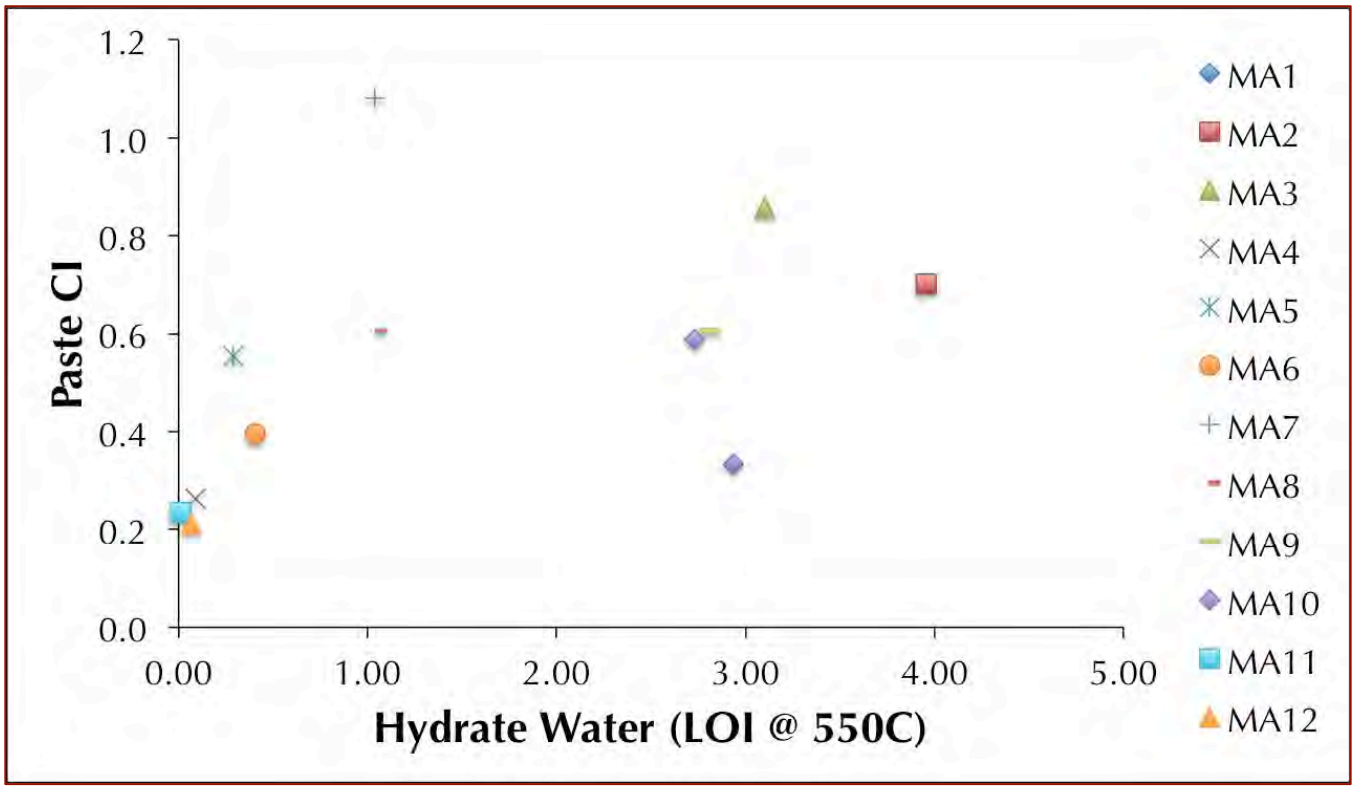

Figure 41: Plot of paste-CI versus loss on ignition from 110°C to 550°C (corresponding to the amount of hydrate water) for brick masonry mortars. Both parameters are commonly considered for defining hydraulicity of a hydraulic mortar, as their values increase with increasing hydraulicity of paste.

Overall trend of all data points, except MA7 is broadly positive; MA7 fell off the trend by having intermediate hydrate water content despite having the higher CI-paste amongst all brick mortars.

A plot of quartz contents of mortars from X-ray diffraction to acid-insoluble residue contents is shown in Figure 42. Figure 42 shows a broad positive correlation between the two, as would be expected from quartz contributing to the bulk of the insoluble residue, with some mortars fall off the tread. Despite finding an appreciate amounts of clay and mica in the insoluble residues in many brick and stone masonry mortars (Table 6), such positive correlation between quartz and insoluble residue contents indicates that clay and mica in the residue are probably derived from the un-calcined feed than from the sand.

Two mortars that fall off the trend are MA11 from brick and SMA1 from stone masonry mortars. MA11 has the lowest quartz content detected for all brick masonry mortars, and also contained clay, gypsum, biotite, and vaterite that are detected along with quartz in XRD. Except vaterite, all other minerals are mostly insoluble in acid, hence they all together with quartz showed a high total insoluble residue content despite having a relatively lower quartz content than the other mortars on the trend of similar insoluble contents but higher quartz contents. Therefore, sand having an appreciable amount of clay, mica, and similar constituents that are insoluble in acid can deviate from an ideal positive correlation of the two parameters. The off-the-trend position of the stone masonry mortar SMA1, however, could not be explained since the mortar was re-analyzed for insoluble residue content for an additional time, when it produced 55.7 percent residue i.e. not very different from the original value of 53.9. Its quartz content from XRD

also is consistent at 68.5, irrespective of number of times it was analyzed. The only way SMA1 data can be explained is if some of the quartz became solubilized in acid, which seemed unlikely.

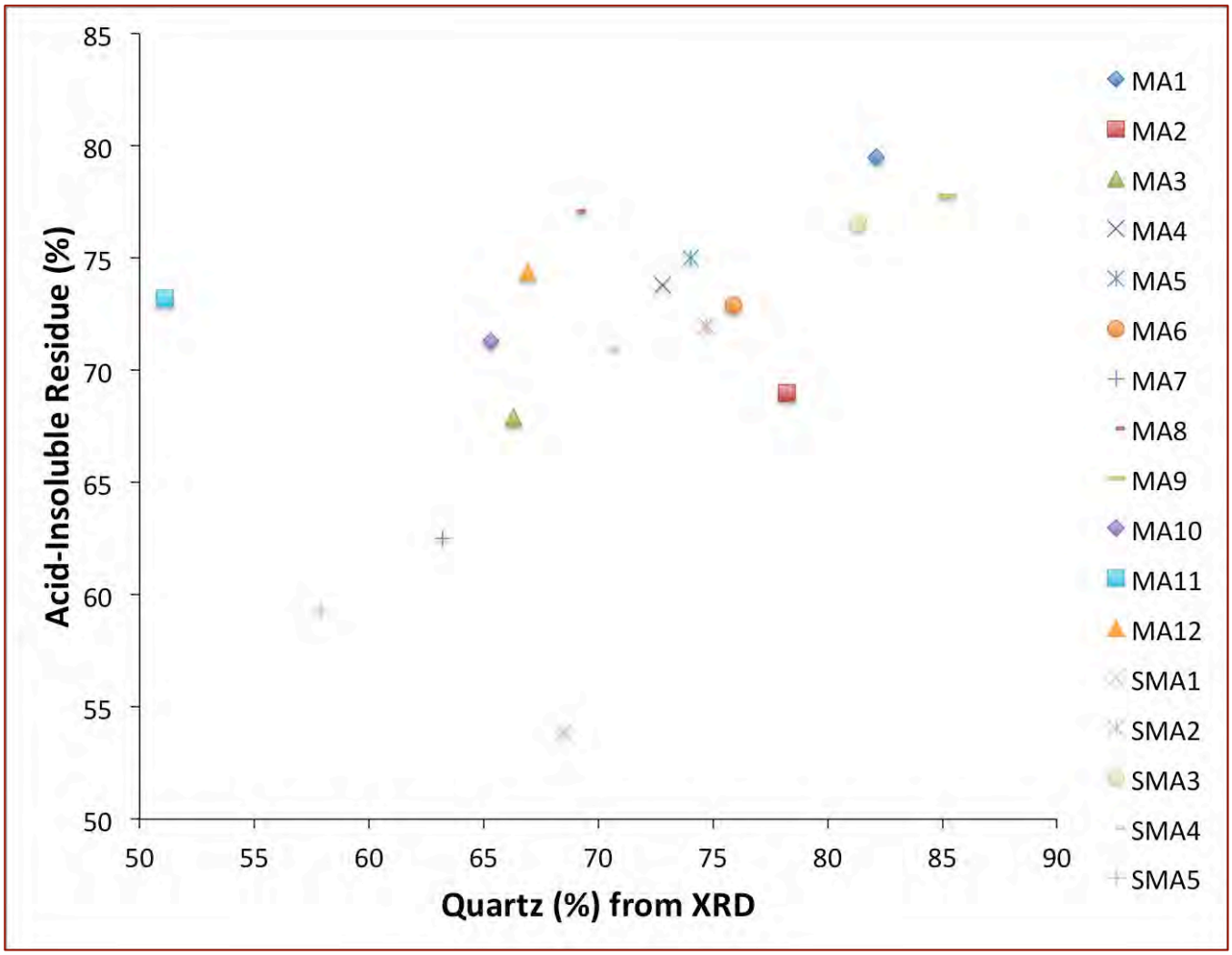

Figure 42: Overall positive correlation between quartz contents from X-ray diffraction and acid-insoluble residue contents of all mortars, except a brick masonry mortar, MA11, and a stone masonry mortar, SMA1.

CALCITIC VERSUS DOLOMITIC LIME FROM BRUCITE CONTENTS IN BULK MORTARS OR MAGNESIUM OXIDE CONTENTS IN BINDERS

XRD studies did not detect any brucite in the mortars, which is indicative of use of a high-calcium lime as opposed to a dolomitic lime, produced from calcination of an impure high-calcium limestone.

SEM-EDS analyses of binders, however, show variable amounts of magnesium oxide across the matrices of hydraulic lime mortars, but the amounts determined are still negligible compared to a dolomitic lime binder. Figure 43 shows plot of average compositions of paste from various areas for each brick masonry mortar plotted as cementation index (CI) versus MgO. The non-hydraulic lime mortars (MA11 and MA12) show the lowest MgO in paste, indicating their derivation from high-calcium limestones, whereas the most hydraulic mortar MA7,

along with all other types show variable MgO contents up to 4.0 percent, indicating their possible derivation from magnesian limestone or dolomite raw feeds of natural cements.

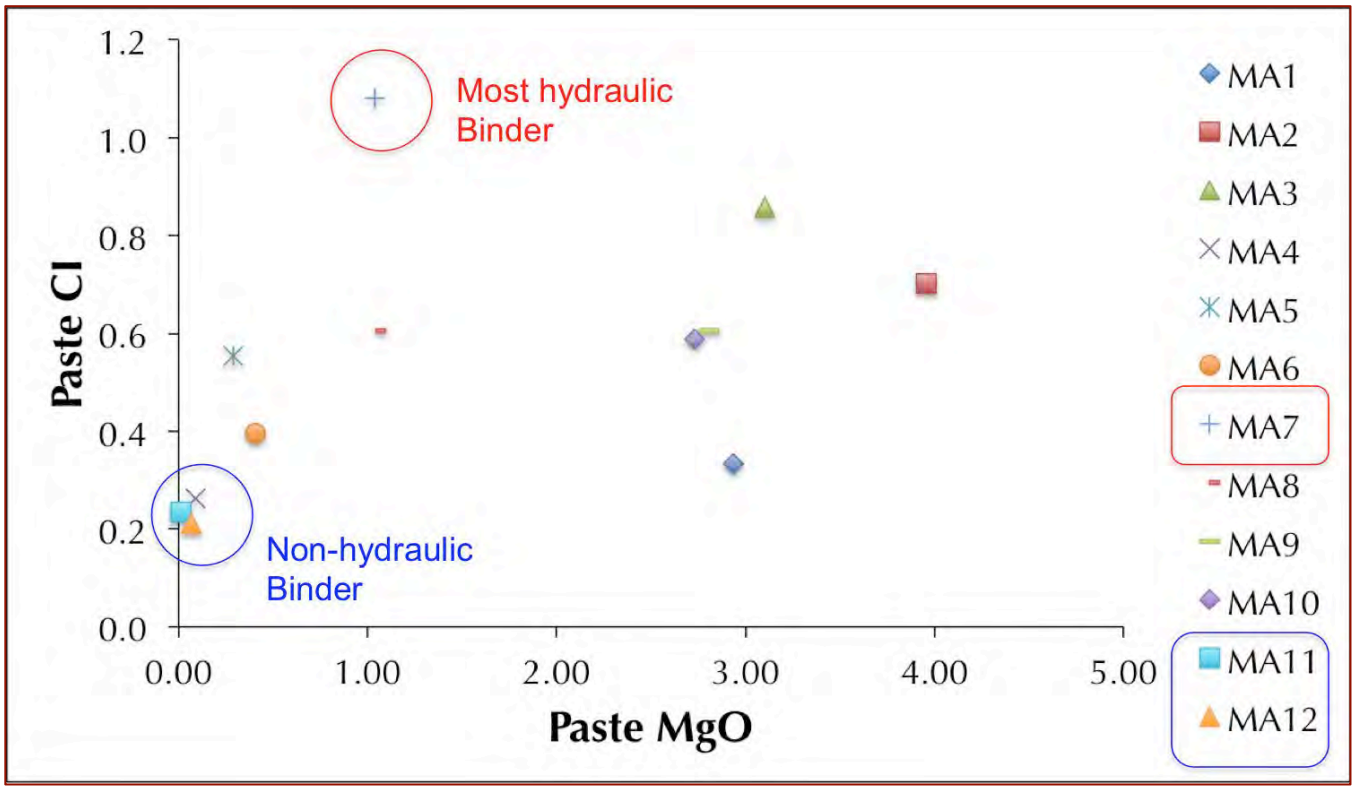

Figure 43: Plot of average compositions of pastes from various areas for each mortar plotted against cementation index (CI, Eckel) versus MgO. The non-hydraulic lime mortars show lowest MgO in paste, indicating their derivation from high-calcium limestones, whereas the most hydraulic mortar MA7, along with all other types show variable MgO contents up to 4.0 percent MgO indicating their possible derivation from natural cements.

SOLUBLE SILICA FROM BINDERS, & CALCIUM AND MAGNESIUM OXIDES IN BRICK MASONRY MORTARS

Components	MA1	MA2	MA3	MA4	MA5	MA6	MA7	MA8	MA9	MA10	MA11	MA12
Soluble Silica Content (%)	1.89	4.89	5.51	1.86	2.85	2.61	6.24	2.31	2.97	3.62	1.57	1.44
Calcium Oxide, CaO (%)	17.33	21.98	21.74	23.10	20.29	22.48	23.45	17.14	16.18	20.80	23.99	23.10
Magnesium Oxide, MgO (%)	0.60	1.23	1.00	0.02	0.07	0.11	0.39	0.24	0.62	0.78	0.00	0.02

Table 13: Soluble silica, calcium and magnesium oxides in brick masonry mortars.

Figure 44 shows a positive correlation between soluble silica and Paste CI, confirming characterization of hydraulic natures of mortars by using either Paste CI and/or soluble silica content parameters in mortars that were contributed solely (mostly) from binders. Despite the absence of a strong positive correlation of paste-CI with hydrate water contents (loss on ignition from 110°C to 550°C), the soluble silica content, which is the other parameter of hydraulicity showed a better correlation with paste-CI. Due to various degrees of alterations and lime leaching of paste (where paste-CIs show some unusually high values for very low-Ca and high-Si leached areas), stone masonry mortars are excluded from this plot, and soluble silica analyses.

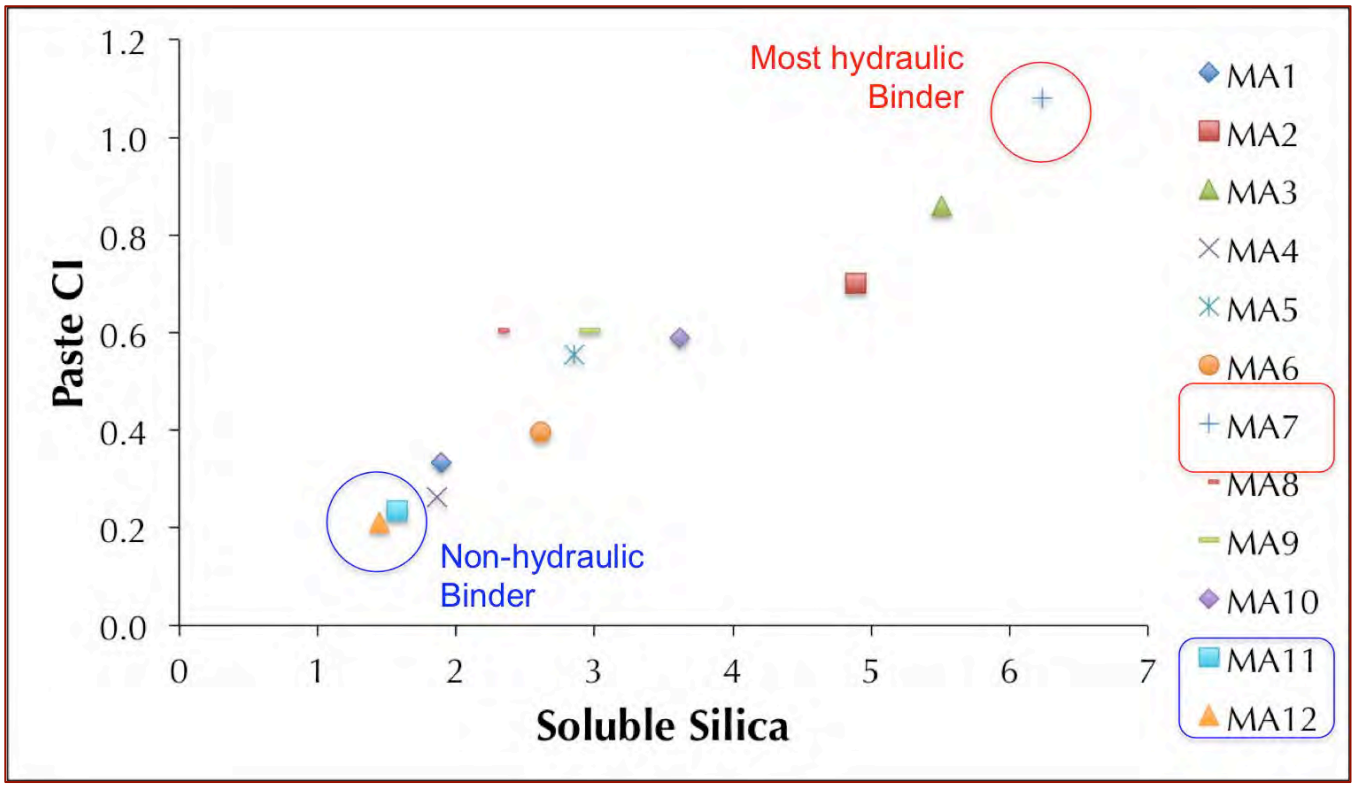

Figure 44: Correlation between soluble silica content of brick masonry mortars and their paste-CIs.

CALCULATIONS OF MIX PROPORTIONS OF MORTARS

High-Calcium (Non-Hydraulic) Lime Mortars in Brick Masonry: Assumptions & Calculations

For non-hydraulic lime mortars MA11 and MA12: (a) lime contents are determined from their respective carbonation (CO_2) data, by dividing the CO_2 data by a factor 0.594, where the factor is derived from molecular ratios of CO_2 to $Ca(OH)_2$ = 44/74.09 = 0.594, and, lime volumes are determined by assuming a bulk density of high-calcium lime to be 40 lbs./ft^3, and, (b) sand contents are determined from the acid-insoluble residue contents, and sand volumes by assuming a bulk density of high-calcium lime to be 80 lbs./ft^3.

Components	MA11	MA12
Non-Hydraulic Lime Content from CO_2 Data	7.50/0.594 = 12.62	7.20/0.594 = 12.12
Non-Hydraulic Lime Volume from Lime Bulk density of 40 lbs./ft^3	12.62/40 = 0.315	12.12/40 = 0.303
Sand Content from Acid-Insoluble Residue (Siliceous Sand)	73.2	74.4
Sand Volume from Sand Bulk density of 80 lbs./ft^3	73.2/80 = 0.915	74.4/80 = 0.930
Volumetric Proportions of Lime to Sand	1 : 2.90	1 : 3.07

Table 14: Volumetric Proportions of lime to sand in the non-hydraulic (high-calcium) lime mortars, MA11 and MA12.

Both mortars show mixes of 1 part lime to approximately 3 parts of sand, which are not outside the commonly recommended dosage of sand (up to 3 parts of sand to sum of separate volumes of cement and lime) specified for cement-lime or masonry cement mortars *a la* ASTM C 270.

The above calculations, however, assumed these mortars to be made using lime and sand only, and excluded gypsum that was detected in X-ray diffraction studies on these mortars and showed 6.9 and 2.9 percent gypsum in MA11 and MA12, respectively. If these gypsum contents represent an added plaster component with lime in the original mixes of these mortars, then volumetric proportions of plaster can be calculated from gypsum contents multiplied by a factor of 0.843 (mol. wt. of plaster i.e. 145 divided by mol. wt. of gypsum i.e. 172 = 0.843), and dividing the plaster contents by an assumed bulk density of plaster to be 70 lbs./ft^3:

Components	MA11	MA12
Non-Hydraulic Lime Content from CO_2 Data	7.50/0.594 = 12.62	7.20/0.594 = 12.12
Non-Hydraulic Lime Volume from Lime Bulk density of 40 lbs./ft^3	12.62/40 = 0.315	12.12/40 = 0.303
Plaster Content from Gypsum Content data in XRD	6.9 x 0.843 = 5.81	2.9 x 0.843 = 2.44
Plaster Volume from Plaster Bulk Density of 70 lbs./ft^3	5.81/70 = 0.083	2.44/70 = 0.034
Sand Content from Acid-Insoluble Residue (Siliceous Sand)	73.2	74.4
Sand Volume from Sand Bulk density of 80 lbs./ft^3	73.2/80 = 0.915	74.4/80 = 0.930
Volumetric Proportions of Plaster to Lime to Sand	1 : 3.79 : 11.02 (2.30 times sum of separate volumes of plaster and lime)	1 : 8.91 : 27.35 (2.76 times sum of separate volumes of plaster and lime)

Table 15: Volumetric proportions of gypsum plaster to lime to sand in the non-hydraulic lime mortars, MA11 and MA12.

Therefore, incorporation of gypsum plaster along with lime in the above calculations does not change the total proportions of binder components (whether just lime or lime plus plaster) to sand too much from approximate 1 part of sum of separate volumes of binder components to 2.3 to 3 parts of sand.

Proportions of Lime and Natural Cements in Brick Masonry Mortars: Assumptions & Calculations

Proportions of lime and natural cements can be determined from the following assumptions:

(i) Natural cement contents can be determined by assuming a fixed composition of natural cement, e.g., containing 20 percent soluble silica and using the *soluble silica data* of mortars in Table 13 to calculate natural cement contents [i.e. = (soluble silica in mortar divided by 20) × 100];

(ii) Lime contents can be determined from the calcium oxide data in Table 13 after assigning calcium oxide for natural cement, assuming 40 percent CaO in natural cement, which represents a median value in Eckel's compilation of compositions of 88 natural cements (see Figure 45), and converting the remaining CaO to lime, $Ca(OH)_2$, by multiplying the remaining CaO with the factor 1.322 (ratio of molecular weights of $Ca(OH)_2$ to CaO is 1.322), so high-calcium lime content = 1.322 × [CaO content in mortar – (0.40 × the determined natural cement content)]; and

(iii) Sand contents from acid-insoluble residue contents in Table 11, since sands from petrographic examinations are determined to contain no acid-soluble (calcareous) components.

(iv) Finally, volumes of cement, lime, and sand components can be determined by assigning bulk densities of 75, 40, and 80-lbs./ft^3 for natural cement, lime, and sand, respectively.

Components	MA1	MA2	MA3	MA4	MA5	MA6	MA7	MA8	MA9	MA10
Natural Cement Content from Soluble Silica Data i.e. (soluble silica in mortar divided by 20) × 100	9.45	24.45	27.55	9.3	14.25	13.05	31.20	11.55	14.85	18.10
Hydraulic Lime Content from CaO Data i.e. 1.322 × [CaO content in mortar – (0.40 × the determined natural cement content)]	17.91	16.12	14.17	25.62	19.28	22.81	14.50	16.55	13.53	17.92
Natural Cement Volume from Bulk density of 75 lbs./ft^3	0.126	0.326	0.367	0.124	0.190	0.174	0.416	0.154	0.198	0.241
Hydraulic Lime Volume from Lime Bulk density of 40 lbs./ft^3	0.447	0.403	0.354	0.640	0.482	0.570	0.362	0.413	0.338	0.448
Sand Content from Acid-Insoluble Residue (Siliceous Sand)	79.5	69.0	67.9	73.8	75.0	72.9	62.5	77.1	77.8	71.3
Sand Volume from Sand Bulk density of 80 lbs./ft^3	0.993	0.862	0.848	0.922	0.937	0.911	0.781	0.963	0.972	0.891
Volumetric Proportions of Cement to Lime to Sand	1: 3.5: 7.8	1: 1.2: 2.6	1: 0.9: 2.3	1: 5.1: 7.4	1: 2.5: 4.9	1: 3.2: 5.2	1: 0.8: 1.9	1: 2.7: 6.2	1: 1.7: 4.9	1: 1.8: 3.7
Ratios of sand to sums of separate volumes of cement and lime	1.73	1.18	1.17	1.20	1.39	1.22	1.00	1.69	1.81	1.29

Table 16: Volumetric proportions of natural cement to lime to sand in the brick masonry mortars.

The mix proportions thus determined for natural cement, lime, and sand in brick masonry mortars are similar to calculation of proportions of portland cement and lime in a cement-lime mortar from an assumed composition of Portland cement (21% SiO_2, 63.5% CaO) as described in ASTM C 1324. The estimated proportions here are in 'gross agreements' to the information obtained from microscopy, e.g., higher proportion of lime than natural cement (as judged from higher areas of carbonated lime matrix in the pastes than the denser cement hydrate areas), and, the highest proportion of natural cement to lime in MA7 compared to other mortars (having, in fact, more natural cement than lime in MA7).

However, the ratios of sand volumes to sums of separate volumes of cement and lime in MA1 through MA10 are all less than 2, which are less than the minimum requirement of at least 2½ times sand than total cement plus lime in ASTM C 270 specifications for cement-lime masonry mortars, indicating these historic mortars are probably under-sanded compared to the requirements of higher sand volumes in the modern masonry mortars. For the non-hydraulic lime mortars MA11 and MA12, however, these ratios of sand to lime volumes are around 3 as found in Table 14 (as opposed to all less than 2 for the hydraulic types). Sand 'contents' of MA1 through MA10 as determined from the acid-insoluble residue contents in Table 11, or sand 'volumes' of MA1 through MA10 as estimated from optical microcopy in Figures 7 through 9, however, are not very different from the non-hydraulic lime mortars, MA11 and MA12. From optical microscopy, XRD studies to acid-insoluble residue contents, all brick masonry mortars, from non-hydraulic to hydraulic types, showed more or less similar 'sand' volumes (e.g., in Table 2 from image analyses)

or 'sand' contents, e.g., an average 72.7 percent acid-insoluble residue content for hydraulic types (MA1 through MA10) in Table 11, compared to an average 73.8 percent residue for the non-hydraulic types (MA11 and MA12). However, the same is not true for the quant content, which constituents the sand. Quartz contents (from XRD results in Tables 6 and 9) of hydraulic types (MA1 to MA10), however, are systematically higher than the non-hydraulic types (MA11 and MA12). For example, the 'average' quartz contents (from XRD results in Table 9) in the bulk mortars of the hydraulic types are 73.2 percent, as opposed to only 59.0 percent quartz for the non-hydraulic ones. For acid-insoluble residues, quant contents in the residues (from XRD results in Table 6) are 93.3 percent in the hydraulic types as opposed to 82.2 percent in the non-hydraulic ones. In both bulk mortars and acid-insoluble residues, the lower quartz contents in the non-hydraulic types (despite similar total acid-insoluble residue contents) are found to be due to the presence of a significant amount (> 10 percent) of acid-insoluble illitic clay in the non-hydraulic mortars (MA11 and MA12) that are detected in XRD studies in both Tables 6 and 9, and not found in most of the hydraulic types. Sand added in the non-hydraulic types (MA11 and MA12) were 'dirty' river sand i.e. containing a significant portion of illitic clay, which has increased the acid-insoluble residue content in these two mortars and thus provided an over-estimation of sand volumes in mix calculations.

Therefore, the systematically lower sand proportions relative to sums of separate volumes of natural cement and lime calculated for the hydraulic types MA1 through MA10 (all <2 in Table 16), or, rather the higher sand proportions relative to lime (around 3 in Table 14) in the non-hydraulic mortars MA11 and MA12 is found out to be due to inclusion of the illitic clay component of acid-insoluble residue in MA11 and MA12 into the calculations of sand contents (and hence volumes) that has over-estimated the sand contents (and volumes) in MA11 and MA12 compared to the hydraulic-types that do not have increased residue content from clay. Therefore, it is important to take consideration of information obtained from optical microscopy and XRD into the calculations of mix proportions without necessarily relying on the chemical data. A mix proportion calculated only from the chemical data can be incorrect if it does not incorporate the results from microcopy and XRD.

Furthermore, absolute volumetric proportions calculated here are strongly dependent on the assumed chemical composition of natural cement i.e. assuming the cement contains 20 percent SiO_2 and 40 percent CaO. Although these values are not unrealistic for natural cements, however, compared to strict chemical compositions of portland cements natural cement show significant variations in chemical compositions since the naturally occurring argillaceous limestone/dolomite raw feeds for natural cements are not as strictly controlled carefully proportioned limestone-shale mixture in portland cement manufacturing.

To show large compositional variations of natural cements, Figure 45 shows compilations of chemical analyses of 88 natural cements along with 79 Portland cements, 35 high-calcium limes, 12 magnesian limes, 3 eminently hydraulic limes, and 11 slag cements from Eckel (1922). Natural cements are shown by green triangles. Large compositional variations of natural cements are seen from the spread of data points across the plots. Figures 46 and 47 show just the natural cements data in CaO and MgO vs. SiO_2 and SiO_2 and Al_2O_3 vs. CI plots, respectively from Eckel (1922) and many other sources, including present author's unpublished data on three modern Rosendale natural cements from Edison Coatings, Inc.

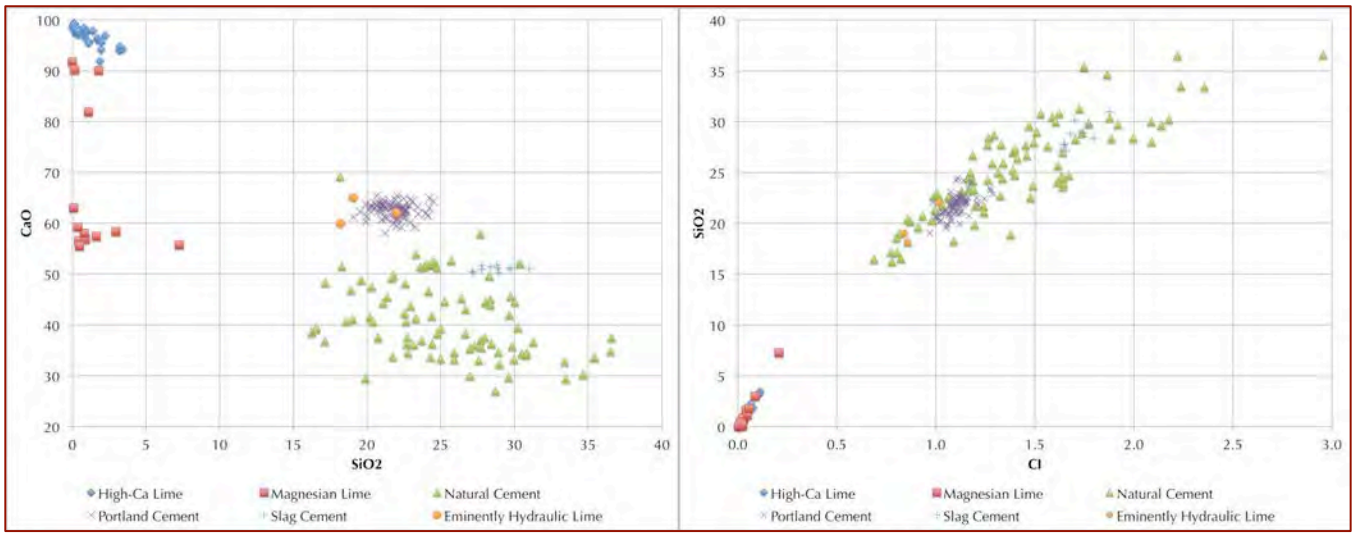

Figure 45: Compositional variations of Cementation Index (CI). CaO, and SiO_2 amongst various lime and cement from Eckel (1922) showing: high-calcium lime (35 analyses in Page 118, Table 40 of Eckel 1922), magnesian lime (12 analyses in Page 121, Table 42), eminently hydraulic lime (3 analyses in Page 186, Table 81), natural cements (88 analyses in Pages 244-251, Tables 116-127), Portland cements (79 analyses in Pages 521-523, Table 222), and slag cements (11 analyses in Page 610, Table 249). Notice large compositional variations of natural cements (shown by green triangles) compared to far more restricted chemical compositions of Portland cements, limes, and slag cements (all data are from Eckel 1922).

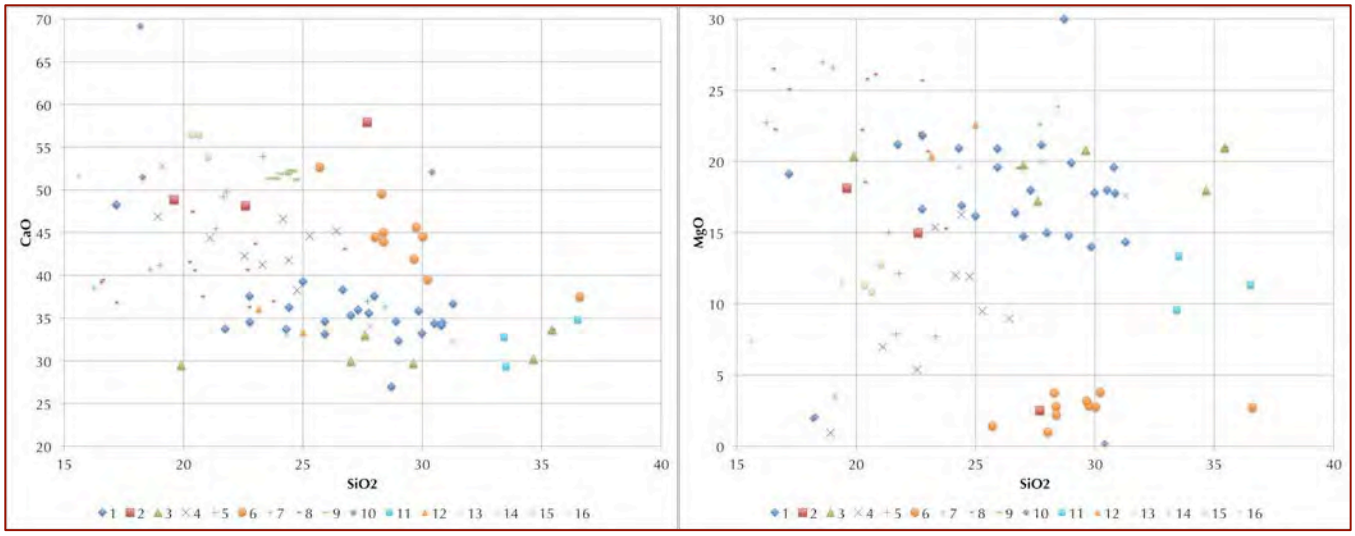

Figure 46: Compositional variations of natural cements from various sources, from 88 analyses of natural cements in Eckel (1922, data legends '1' through '12') to present author's unpublished chemical analyses of modern Rosendale cements (three batches of Rosendale 10C from Edison Coatings, Inc.). Legend captions are for different natural cement plants/states in the US: 1 = Rosendale, NY (Eckel), 2 = Howard and Dixie, GA (Eckel); 3 = Illinois (Eckel); 4 = Indiana-Kentucky (Eckel); 5 = Kansas (Eckel); 6 = Hancock and Cumberland, MD (Eckel); 7 = Mankato, Minnesota (Eckel); 8 = Utica, Buffalo, Akron and other plants in NY (Eckel); 9 = North Dakota (Eckel); 10 = Lehigh District, PA (Eckel); 11 = West Virginia (Eckel); 12 = Wisconsin (Eckel); 13 = Two samples of Rosendale natural cements from Vyskocilova et al. 2007; 14 = Prompt natural cement from Vyskocilova et al. 2007; 15 = three samples of Rosendale natural cements from Brosnan (2012); and 16 = three samples of Rosendale 10C natural cements from Edison Coatings, Inc. analyzed by ICP-AES by the present author.

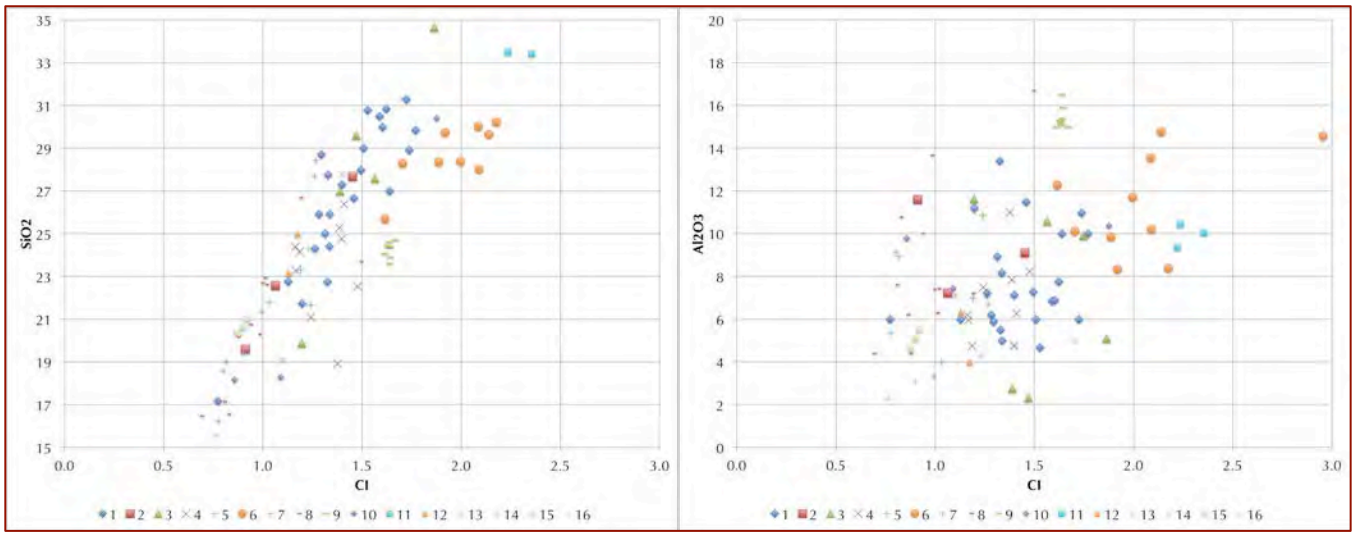

Figure 47: Compositional variations of natural cements from various sources, from 88 analyses of natural cements in Eckel (1922, data legends '1' through '12') to present author's unpublished chemical analyses of modern Rosendale cements (three batches of Rosendale 10C from Edison Coatings, Inc.). Legend captions are for different natural cement plants/states in the US: 1 = Rosendale, NY (Eckel), 2 = Howard and Dixie, GA (Eckel); 3 = Illinois (Eckel); 4 = Indiana-Kentucky (Eckel); 5 = Kansas (Eckel); 6 = Hancock and Cumberland, MD (Eckel); 7 = Mankato, Minnesota (Eckel); 8 = Utica, Buffalo, Akron and other plants in NY (Eckel); 9 = North Dakota (Eckel); 10 = Lehigh District, PA (Eckel); 11 = West Virginia (Eckel); 12 = Wisconsin (Eckel); 13 = Two samples of Rosendale natural cements from Vyskocilova et al. 2007; 14 = Prompt natural cement from Vyskocilova et al. 2007; 15 = three samples of Rosendale natural cements from Brosnan (2012); and 16 = three samples of Rosendale 10C natural cements from Edison Coatings, Inc. analyzed by ICP-AES by the present author.

Large compositional variations of natural cements revealed in these above plots demonstrate limitation in calculations of mix proportions of natural cement-based binders, where the calculated proportion of natural cement is dependent on its assumed chemical composition.

Stone Masonry Mortars

Due to various degrees of alterations and lime leaching, it is far more difficult to calculate proportions of lime and sand used in the stone masonry mortars than the corresponding brick mortars. Due to simple non-hydraulic character of SMA3, it can be treated relatively easily, similar to MA11 and MA12 brick masonry mortars. Based on similar calculations from carbonation data, SMA3 shows a lime content of 12.1 percent (i.e. 7.9 percent carbonation divided by 0.594), and a sand content of 76.6 percent (from insoluble residue content). Assuming bulk densities of lime and sand to be 40 and 80 lbs./ft^3, respectively, relative volume of lime to sand is determined to be 1-part of lime to 3.17-part of sand.

For the other stone masonry mortars, however, the calculation is complicated for various degrees of alterations and lime leaching that did not provide a meaningful soluble silica data to calculate natural cement contents. Moreover, two stone masonry mortars SMA2 and SMA5 showed significant amounts of illitic clay (in Table 9), which would overestimate the sand contents and volumes. Therefore, as a rough approximation i.e. from information obtained from petrographic examinations of least altered portions of the other mortars (e.g., in Type 1 paste areas) and seeing their overall similarities to the brick masonry mortars it can be assumed that the proportions of natural cements, lime,

and sands used in stone masonry mortars are not significantly different from that obtained for the brick masonry mortars.

Components	SMA3
Hydraulic Lime Content from CO_2 Data for SMA3	12.1
Hydraulic Lime Volume from Lime Bulk density of 40 lbs./ft^3	0.302
Sand Content from Acid-Insoluble Residue (Siliceous Sand)	76.6
Sand Volume from Sand Bulk density of 80 lbs./ft^3	0.957
Volumetric Proportions of Lime to Sand	1 : 3.17

Table 17: Volumetric Proportions of lime to sand in the stone masonry mortar, SMA3.

CONCLUSIONS

AGGREGATES

Sand extracted from mortars showed quartz as the dominant mineral, as anticipated for siliceous quartz sands. X-ray diffraction studies on extracted sand showed that 8 out of 12 brick masonry mortars have 3 to 9 percent biotitic mica and as much as 10 to 15 percent illitic clay (Table 6). Sands extracted from two stone masonry mortars (SMA2 and SMA3) showed 1 to 3 percent biotitic mica and as high as 31.2 percent illitic clay in SMA2 (Table 6). Sample SMA5 also showed 9.3 percent illitic clay in the bulk mortar (Table 6). Such high amounts of mica and clay in sand are detrimental for properties and performance of mortar as mica and especially clay increase the water requirements in mortar at a given workability, and introduce many deleterious issues during performance of mortar, e.g., volume instability during wetting and drying, inadequate bond to the paste, excessive shrinkage, etc. Many brick and stone mortars in the project, therefore, used sand that weren't cleaned or washed off mica and clay prior to the incorporation into the mortar mixes.

ORIGINAL BINDERS

Brick Masonry Mortars

Blended lime and natural cement were the original binders in most of the brick masonry mortars examined here (except MA11 and MA12, where the binders are mostly non-hydraulic i.e. high-calcium lime). Absence of brucite in all mortars indicates dolomitic lime was not used. Natural cement was produced by calcination of impure dolomitic limestones containing argillaceous (clay) impurities. Slaked lime was produced by calcination of relatively pure limestone with little or no clay impurities, followed by conventional slaking of the quicklime. The magnesium enriched spots within the ground calcined raw feed particles of natural cement in MA7 indicates dolomite pseudomorphs of the original dolomitic limestone raw feed of natural cement, where MA7 being the most hydraulic mortar of all, contain the maximum proportion of natural cement to lime amongst the brick masonry mortars. The near-isotropic character (in XPL) of ground calcined raw feed particles of residual natural cements in MA7 and in other hydraulic brick masonry mortars (throughout MA1 through MA10) is judged to be due to formation of an amorphous phase from lime-silica-alumina reactions and dehydroxylation of clay impurities within the feed that has

resulted in enrichment of silica and alumina and depletion of calcium within the residual calcined feed particles relative to the surrounding high-calcium carbonated lime matrix of slaked lime.

Therefore, after calcinations of respective raw feeds the original constituents of natural cement and lime binders consisted of: (i) calcium silicates (mostly beta-dicalcium silicate, β-C_2S, may also had a high-temperature polymorph, α'-C_2S), (ii) other calcium-magnesium-alumino-silicates of CaO-MgO-SiO_2-Al_2O_3-Fe_2O_3 system (gehlenite, merwinite), (iii) calcium oxide (free lime or quicklime, CaO, which was subsequently slaked in the high-calcium slaked lime component), (iv) an amorphous aluminosilicate phase that is characteristically depleted in calcium and enriched in alumina and silica than the surrounding lime matrix, probably formed from fused clay or lime-silica-alumina reactions), and (v) some un-calcined calcium carbonate (as well as some hard burnt lime) in the ground, calcined raw feed particles. The primary 'hydraulic' component responsible for hydration, calcium-silicate-hydrate (CSH) formation and strength development was C_2S (with possible minor amounts of C_4AF from the reddish brown stains of many calcined feed particles, and gehlenite C_2AS, although gehlenite is not hydraulic). The amorphous phase (responsible for imparting an overall near-isotropic character in the ground calcined raw feed particles of natural cement) is judged to have played an important role in not only providing some pozzolanic characters to the binders by reactions with the slaked lime component but may also have provided some cementitious properties by itself. This interstitial amorphous phase may have played an important role in the early age setting, hardening, and strength development of natural cement hydrates, since belite is mostly inactive during the early ages. Reactions of such amorphous phases with slaked lime in the presence of moisture can develop additional calcium silicate (± aluminate) hydrates to improve the strength and durability of mortars. Unlike Portland cement, alite (impure-C_3S) was not formed due to the lower calcination temperatures (below sintering) of natural cement feeds in the kiln. Initial setting of lime mortars were mostly achieved by atmospheric carbonation of slaked lime [$Ca(OH)_2$], whereas long-term setting was achieved by combined carbonation of slaked lime and hydration/pozzolanic reactions of C_2S/ amorphous phase. The primary hydration product of natural cement, CSH (or perhaps CASH, or even CMASH), occurred as a featureless dense material of fibers, flakes, honey combs and tightly packed grains, initially intermixed with two types of $Ca(OH)_2$, one from hydration of C_2S (coarser, patchy, short prismatic) and other from slaked lime component (cryptocrystalline) that has not been carbonated. As in Portland cement hydration, where C_2S hydrates very slowly and provides late stage (long-term) strength development of cement, strength development from C_2S hydration in natural cement hydrates were also very slow, originally derived from the growth of CSH and $Ca(OH)_2$ crystals, probably from a significantly contribution from the amorphous phase, and, partial carbonation of the slaked lime component (along with possible pozzolanic reactions between the amorphous phases in calcined raw feed and slaked lime).

For mortars MA11 and MA12, however, the original binders were non-hydraulic lime, produced by calcination of high-calcium limestone that had very little, if any, clay impurities. Hence, the lime formed from calcination was almost entirely free lime (with some possible un-calcined limestone), which was subsequently slaked to form fine powders (with controlled water), or more likely as lime putty (with excess water) of non-hydraulic lime. These two mortars have gained strength very slowly, primarily by atmospheric carbonation of slaked lime to form the skeleton of very fine-grained calcium carbonate paste (thus completed the lime cycle).

Stone Masonry Mortars

Non-hydraulic lime was the binder in SMA3, which was similar in composition to the binders used in the brick masonry mortars MA11 and MA12. For other samples, due to various degrees of alterations and lime leaching, determinations of compositions of original binders are difficult. Nevertheless, from textural and mineralogical compositions of pastes and residual ground calcined feed particles it is suspected that the binders are similar to the lime and natural cement binders detected in the hydraulic brick masonry mortars MA1 through MA10. For SMA and SMA5 areas of pastes rich in silica and calcium (as opposed to just calcium e.g., for carbonated lime matrix in SMA3) indicates use of blended lime-natural cement binder where the silica component in the paste was derived from hydration of natural cement.

TYPES OF MORTARS

Based on optical and scanning electron microscopy, X-ray elemental analyses of binder fractions, and chemical analyses, the twelve (12) brick masonry mortars and five (5) stone masonry mortars can be classified into three (or perhaps four) groups, as follows:

1. Non-hydraulic high-calcium lime mortars, e.g., MA11 and MA12 brick masonry mortars and SMA3 stone masonry mortar, all of which have very uniform featureless, monotonous very fine-grained, porous, severely carbonated lime matrices and well-graded crushed quartz sand.
2. Blended lime and natural cement mortar having more natural cement than lime in MA7 brick masonry mortar that has patchy-textured heterogeneous paste consisting of isolated denser patches of paste constituting the hydrated product of the original hydraulic components of lime that has also been carbonated like rest of the overwhelming severely carbonated lime matrix but at lower degrees, has overall distinctly much higher percentages of silica, alumina, and iron in the pastes (all contributed from fused clay impurities) and lower lime than the non-hydraulic mortars (MA11 and MA12). The overall patchy-texture and silica-rich chemistry of paste in this mortar resemble many natural cement mortars, only differentiated by virtue of having more carbonated slaked lime components for having a greater portion of slaked lime in the binder than commonly found in historic natural cement pastes.
3. Rest of the brick masonry mortars (MA1 through MA10 except MA7) having variable silica, lime, alumina, iron contents and textures that fall in between the above two extremes, e.g., having blended lime and natural cement mortars but more lime than natural cement.
4. Stone masonry mortars SMA1, SMA2, and SMA4 that show various degrees of weathering, alteration, and leaching of lime due to moisture percolations. As a result, pastes in these mortars show various degrees of lime leaching to almost gelatinous silica formation in patches of pastes where lime contents approached very low compared to silica (and are also enriched in alumina, magnesia, and iron) compared to the unaltered or less altered paste areas. Such leaching of lime is not noticed in the brick masonry mortars, probably due to lack of such moisture percolations through the mortars.

SUGGESTED TUCKPOINTING MORTARS

Based on the determined compositions of mortars, Table 18 provides possible tuckpointing mortars that could be used with the existing ones. The following suggestion is just a recommendation from the present study, which provides no guarantee to the overall match in appearance and properties to the existing mortars. Many other mortars could also be used as long as the mortars chosen match closely to the existing mortars in color and properties of aggregates, appearance of the hardened mortar, and in physical and mechanical properties to the existing mortars to reduce any undue stresses from any such incompatibilities. The final tuckpointing mortars must be verified with the project engineer/architect to confirm their suitability with the existing mortars.

Sample ID	Determined Mortar Compositions			Possible Tuckpointing Mortars		
	Aggregate	Binder	Proportions	Aggregate	Binder	Cement-to-Lime Proportion
Brick Masonry Mortars						
8-69-MA1	100	Lime > Natural Cement	1: 3.5:7.8	100	Natural Cement (ASTM C 10), Hydrated Lime (ASTM C 207)	1:2
4-85-MA2	100	Lime > Natural Cement	1:1.2:2.6	100		1:2
1/2-121-MA3	100	Lime > Natural Cement	1:0.9:2.3	100		1:1
3-142-MA4	100	Lime > Natural Cement	1:5.1:7.4	100		1:2
5-1-MA5	94.4	Lime > Natural Cement	1:2.5:4.9	100		1:2
5-5-MA6	100	Lime > Natural Cement	1:3.2:5.2	100		1:2
3-16-MA7	100	Natural Cement > Lime	1:0.8:1.9	100		1:1
2-31-MA8	100	Lime > Natural Cement	1:2.7:6.2	100		1:2
1-34-MA9	100	Lime > Natural Cement	1:1.7:4.9	100		1:2
4-41-MA10	100	Lime > Natural Cement	1:1.8:3.7	100		1:2
6-56-MA11	100	Non-Hydraulic Lime	1: 2.90	100		1:3
6-64-MA12	100	Non-Hydraulic Lime	1: 3.07	100		1:3
Stone Masonry Mortars						
1-94-SMA1	100	Lime > Natural Cement	-	100	Natural Cement (ASTM C 10), Hydrated Lime (ASTM C 207)	1:2
1-94-SMA2	100	Lime > Natural Cement	-	100		1:2
3-138-SMA3	100	Non-Hydraulic Lime	1: 3.17	100		1:3
3-142-SMA4	100	Lime > Natural Cement	-	100		1:2
6-81-SMA5	100	Lime ~ Natural Cement	-	100		1:1

Table 18: Possible tuckpointing mortars for the examined mortars. Aggregate values represent percent passing through US No. 4 sieve (4.75-mm opening, either determined from Tables 3, 4, and 5, or recommended). Sand proportions in the final recommended column at the right should be 2½ to 3 times the sum of separate volumes of lime and natural cement.

Aggregates to use should be close to the grading requirements of ASTM C 144, and should be clean, free of any clay or mica or other contaminants, e.g., sound, well-graded, siliceous (quartz) sand.

Other alternative binders include: (i) high-calcium, magnesian, or dolomitic non-hydraulic limes, (ii) regular hydraulic lime or natural hydraulic lime (NHL), (iii) natural cement only, and (iv) any of these binders with or without pozzolans (e.g., fly ash, pfa, ground slag, etc.) for added strength, if needed, etc. Use of Portland cement/lime or masonry cement mortars of ASTM C 270 should be avoided since those mortars do not match as closely in physical and mechanical properties and breathability to the existing lime and lime-natural cement mortars.

Finally, the following section provides some additional information to consider during selection of an appropriate tuckpointing mortar:

1. It is more important for a tuckpointing mortar to be as close in physical, chemical, and mechanical properties to the existing mortar as possible than to conform to the ASTM C 270 specification for cement-lime or masonry/mortar cement mortars for unit masonry, which are for modern mortars to use for modern structural applications, and not necessarily applicable to renovation of historic lime mortars.
2. Aggregate to use in the tuckpointing mortar should be similar in color, gradation, appearance, mineralogy, and composition to the sand used in the existing mortar. Masonry sands should conform to the grading requirements of ASTM C 144. Avoid using sand that contains appreciable amounts of potentially alkali-silica reactive particles (e.g., chert).
3. Binder for tuckpointing mortar should be as close to the binder of the existing mortar in composition and properties as possible. For historic lime mortars, possible choices of binders are many: (i) non-hydraulic high-calcium lime, or magnesian lime, or dolomitic lime (ASTM C 51) either in dry hydrate (hydrated lime) form, or as slurry or putty form, (ii) hydraulic lime, (iii) natural hydraulic lime (i.e. NHL 2, NHL 3.5, and NHL 5 with increasing strengths), (iv) natural cements (conforming to ASTM C 10), or (v) a combination of these, (vi) with or without a pozzolan (fly ash, slag, etc. if an added strength and durability are needed). Portland cement, if used must be added at lesser proportions than lime, having proportions tested to find the best match in properties to the existing mortar. For breathability of the masonry wall, least stress to the exiting mortar, accommodation of building movements, and good bond to masonry units, the binder of choice should be durable and similar in properties and performance to the existing binder.
4. During applications of modern masonry mortars: (i) a job-mixed cement-lime mortar is commonly preferred by the architects than a masonry cement mortar, due to the better quality control of the former mortar; (ii) a masonry cement mortar is characteristically air-entrained, which may interfere with the bond to the adjacent masonry units, whereas, a non-air-entrained cement-lime mortar provides a better bond to the adjacent masonry units than an air-entrained masonry cement mortar, (iii) air entrainment usually provides better workability and freeze-thaw durability to a mortar, however, as mentioned, it reduces the bond to the adjacent masonry units (depending on air content); (iv) for Portland cement-lime mortars, a Type M or S mortar (i.e. having a higher cement content than lime and hence a higher strength) is preferred for load-bearing applications than a Type N mortar (having a higher lime content than cement, hence provides better workability and water retention than a Type S or M mortar); (v) Portland cement to use in a mortar should conform to the specification of ASTM C 150; hydrated lime should conform to ASTM C 207, masonry/mortar cement, if used, should conform to ASTM C 91/C 1329; blended hydraulic cement, if used, should conform to ASTM C 595; (vi) relative proportions of portland cement and lime will control the overall strength, workability, and bond properties of the repointing mortar.
5. Mineral oxides or carbon-based pigments, if used and positively detected in an examined mortar, should be carefully replicated in the tuckpointing process to reproduce the color, texture and appearance similar to the existing mortar (including the effects of atmospheric weathering on pigments). Dosage of pigment in the

tuckpointing mortars should be estimated from trial mixes of various dosages. If the original mortar contains a polymer component as suspected from microscopy, characterization of polymer could be difficult without perhaps use of FTIR-microscopy.

6. To have an optimum bond of a mortar to the adjacent masonry unit, relative proportions of cementitious materials and lime contents in the mortar should be carefully controlled. Lime provides the necessary workability and water retention, which are important in a mortar when used with a masonry unit of high suction). Therefore, the initial rate of absorption (or suction property) of the adjacent masonry units should also be carefully determined to match with the appropriate lime content in the mortar.
7. The final tuckpointing mortar should match in color and appearance to the existing mortars, and the closest match should be determined by trial and error on small test areas of the masonry wall to be tuck-pointed.

REFERENCES

ASTM C 10, "Standard Specification for Natural Cement," In Annual Book of ASTM Standards, Section Four Construction, Vol. 04.01 Cement; Lime; Gypsum; ASTM Committee C01 on Cement, 2007.

ASTM C 1324, "Standard Test Method for Examination and Analysis of Hardened Masonry Mortar," In Annual Book of ASTM Standards, Section Four Construction, Vol. 04.05 Chemical-Resistant Nonmetallic Materials; Vitrified Clay Pipe; Concrete Pipe; Fiber-Reinforced Cement Products; Mortars and Grouts; Masonry; Precast Concrete; ASTM Committee C12 on Mortars for Unit Masonry, 2005.

ASTM C 270, "Standard Specification for Mortar for Unit Masonry," In Annual Book of ASTM Standards, Section Four Construction, Vol. 04.05 Chemical-Resistant Nonmetallic Materials; Vitrified Clay Pipe; Concrete Pipe; Fiber-Reinforced Cement Products; Mortars and Grouts; Masonry; Precast Concrete; ASTM Committee C12 on Mortars and Grouts for Unit Masonry, 2007.

ASTM C 51, "Standard Terminology Relating to Lime and Limestone (as used by the Industry)'" In Annual Book of ASTM Standards, Section Four Construction, Vol. 04.01 Cement; Lime; Gypsum; ASTM Committee C07 on Lime, 2007.

ASTM C 1723, Standard Guide for Examination of Hardened Concrete Using Scanning Electron Microscopy, In Annual Book of ASTM Standards, Section Four Construction, Vol. 04.02; ASTM Subcommittee C 9.65, 2010.

Bartos, P. Groot, C., and Hughes, J.J. (eds.), Historic Mortars: Characteristics and Tests, Proceedings PRO12, RILEM Publications, 2000.

Boynton, R., Chemistry and Technology of Lime and Limestone, 2nd edition, John Wiley & Sons, Inc. 1980.

Brosnan, Denis, A., Characterization of Rosendale Mortars For Fort Sumter National Monument and Degradation of Mortars by Sea Water and Frost Action, Final Report, April 19, 2012.

Callebaut, K., Elsen, J., Van Balen, K., and Viaene, W., "Nineteenth century hydraulic restoration mortars in the Saint Michael's Church (Leuven, Belgium) Natural hydraulic lime or cement?" Cement and Concrete Research, V 31, pp 397-403, 2001.

Callebaut, K., Elsen, J., Van Balen, K., and Viaene, W., Historical and scientific study of hydraulic mortars from the 19th century. In International RILEM workshop on historic mortars: Characterization and Tests; Paisley, Scotland, 12th to 14th May 1999, Edited by Barton, P., Groot, C., and Hughes, J.J., Cachan, France, RILEM Publications, 2000.

Charloa, A.E., "Mortar analysis: A comparison of European procedures." US/ICOMOS Scientific Journal: Historic Mortars & Acidic Deposition on Stone, 3 (1), pp. 2-5, 2001.

Charola, A.E., and Lazzarin, L., Deterioration of Brick Masonry Caused by Acid Rain, ACS Symposium Series, Vol. 318, pp. 250-258, 2009.

Chiari, G., Torraca, G., and Santarelli, M.L., Recommendations for Systematic Instrumental Analysis of Ancient Mortars: The Italian Experience, Standards for Preservation and Rehabilitation, ASTM STP 1258, S.J. Kelley, ed., American Society for Testing and Materials, pp. 275-284, 1996.

Doebley, C.E., and Spitzer, D., Guidelines and Standards for Testing Historic Mortars, Standards for Preservation and Rehabilitation, ASTM STP 1258, S.J. Kelley, ed., American Society for Testing and Materials, pp. 285-293, 1996.

Eckel, Edwin, C., Cements, Limes, and Plasters, John Wiley & Sons, Inc. 655 pp., 1922.

Edison, M.P. (Editor), *Natural Cement*, ASTM STP 1494, American Society for Testing and Materials, 2008.

Elsen, J., Microscopy of historic mortars – a review, Cement and Concrete Research 36, 1416-1424, 2006.

Elsen, J., Van Balen, K., and Mertens, G., Hydraulicity in Historic Lime Mortars: A Review, In, Valek, J, Hughes, J.J., and Groot, W.P. (Eds.), Historic Mortars Characterisation, Assessment and Repair, RILEM Book series, Volume 7, pp. 125-139, Springer, 2012.

Erlin, B., and Hime, W.G., Evaluating Mortar Deterioration, APT Bulletin, Vol. 19, No. 4, pp. 8-10+54, 1987.

Goins E.S., "Standard Practice for Determining the Components of Historic Cementitious Materials," National Center for Preservation Technology and Training, Materials Research Series, NCPTT 2004.

Goins, E.S., "A standard method for the characterization of historic cementitious materials." US/ICOMOS Scientific Journal: Historic Mortars & Acidic Deposition on Stone, # (1), pp. 6-7, 2001.

Hughes, D.C., Jaglin, D., Kozlowski, R., Mayr, N., Mucha, D., and Weber, J., Calcination of Marls to Produce Roman Cement, pp. 84-95, In, Edison, M.P. (Editor), *Natural Cement*, ASTM STP 1494, American Society for Testing and Materials, 2007.

Hughes, J.J., Cuthbert, S., and, Bartos, P., Alteration textures in historic Scottish lime mortars and the implications for practical mortar analysis, Proceedings of the 7th Euroseminar on Microscopy Applied to Building Materials, Delft, pp. 417-426, 1999.

Hughes, R.E., and Bargh, B.L., The weathering of brick: Causes, Assessment and Measurement, A Report of the Joint Agreement between the U.S. Geological Survey and the Illinois State Geological Survey, 1982.

J. Weber, N. Gadermayr, K. Buyar et al., "Roman cement mortars in Europe's architectural heritage of the 19th century," *Journal of ASTM International*, vol. 4, pp. 69–83, 2007.

Jana, D., Application of Petrography In Restoration of Historic Masonry Structures, In: Hughes, J.J., Lesie, A.B. and Walsh, J.A., eds. Proceedings of 10th Euroseminar on Microscopy Applied to Building Materials, Paisley, 2005.

Jana, D., Sample Preparation Techniques in Petrographic Examinations of Construction Materials: A State-of-the-art Review, Proceedings of the 28th Conference on Cement Microscopy, International Cement Microcopy Association, Denver, Colorado, pp. 23-70, 2006.

Leslie, A.B., and Hughes, J.J., Binder microstructure in lime mortars: implications for the interpretation of analysis results, Quarterly Journal of Engineering Geology & Hydrogeology, V. 35, No. 3, pp. 257-263, 2001.

Lubell, B., van Hees, Rob. P.J., and Groot, Casper J.W.P., The role of sea salts in the occurrence of different damage mechanisms and decay on brick masonry, Construction and Building Materials, Vol. 18, pp. 119-124, 2004.

Middendorf, B., Hughes, J.J., Callebaut, K., Baronio, G., and Papayanni, I., "Investigative methods for the characterization of historic mortars – Part 2: Chemical characterization," Materials and Structures, Vol. 38, pp 771-780, 2005a.

Middendorf, B., Hughes, J.J., Callebaut, K., Baronio, G., and Papayanni, I., "Investigative methods for the characterization of historic mortars – Part 1: Mineralogical characterization," Materials and Structures, Vol. 38, 2005b.

Otto, T.J., St. Elizabeths Hospital: A History, United States General Services Administration, National Capital Region, May 2013.

Taylor, H.F.W., Cement Chemistry, 2nd Edition, Thomas Telford, 459pp, 1998.

Valek, J, Hughes, J.J., and Groot, W.P. (Eds.), "*Historic Mortars Characterisation, Assessment and Repair*," RILEM Book series, Volume 7, Springer, pp. 464, 2012.

Valek, J, Hughes, J.J., and Groot, W.P. Historic Mortars: Characterisation, Assessment and Repair. A State-of-the-Art Summary, In, Valek, J, Hughes, J.J., and Groot, W.P. (Eds.), Historic Mortars Characterisation, Assessment and Repair, RILEM Book series, Volume 7, pp. 1-14, Springer, 2012.

Valek, J., Hughes, J.J., and Groot, C. (eds.), Historic Mortars: Characterisation, Assessment and Repair, Springer, RILEM Book series Vol. 7, 2012.

Van Balen, K., Toumbakari, E.E., Blanco, M.T., Aguilera, J., Puertas, F., Sabbioni, C., Zappia, G., Riontino, C., and Gobbi, G., "Procedures for mortar type identification: A proposal." In International RILEM workshop on historic mortars: Characteristics and Tests; Paisley, Scotland, 13th to 14th May 1999, edited by Barton, P., Groot, C., and Hughes, J.J., Cachan, France: RILEM Publications, 2000.

Vyskocilova, R., W. Schwarz, D. Mucha, D. Hughes, R. Kozlowski, and J. Weber, "Hydration processes in pastes of roman and American natural cements," *ASTM STP*, vol. 4, no. 2, 2007.

Weber, J., Gadermayr, N., Kozlowski, R., Mucha, D., Hughes, D., Jaglin, D., and Schwarz, W., Microstructure and mineral composition of Roman cements produced at defined calcination conditions, Materials Characterization, Vol. 58, pp. 1217-1228, 2007.

ACKNOWEDGMENTS

Sincere thanks are due to Jennifer Hall for setting up the project, coordinating with the client and CMC personnel during various stages of the project, and formatting and finalizing the report; Mitzi Casper for doing preliminary petrographic examinations, chemical analysis, and X-ray diffraction, and collecting photographs and photomicrographs; Jeffery Brown for preparing thin sections and polished thin sections and solid sections of mortars for optical and electron microscopy; and finally our client for engaging our services for the renovation project of this national historic landmark. Discussions with Professor Denis A. Brosnan of Clemson University, SC, Rick Dorrance of Fort Sumter National Monument, SC, Michael F. Pistilli, IL, and Michael P. Edison of Edison Coatings, Inc., CT on various aspects of natural cement are appreciated.